

EPA

U.S. Environmental Protection Agency
Office of Research and Development

Industrial Environmental Research
Laboratory

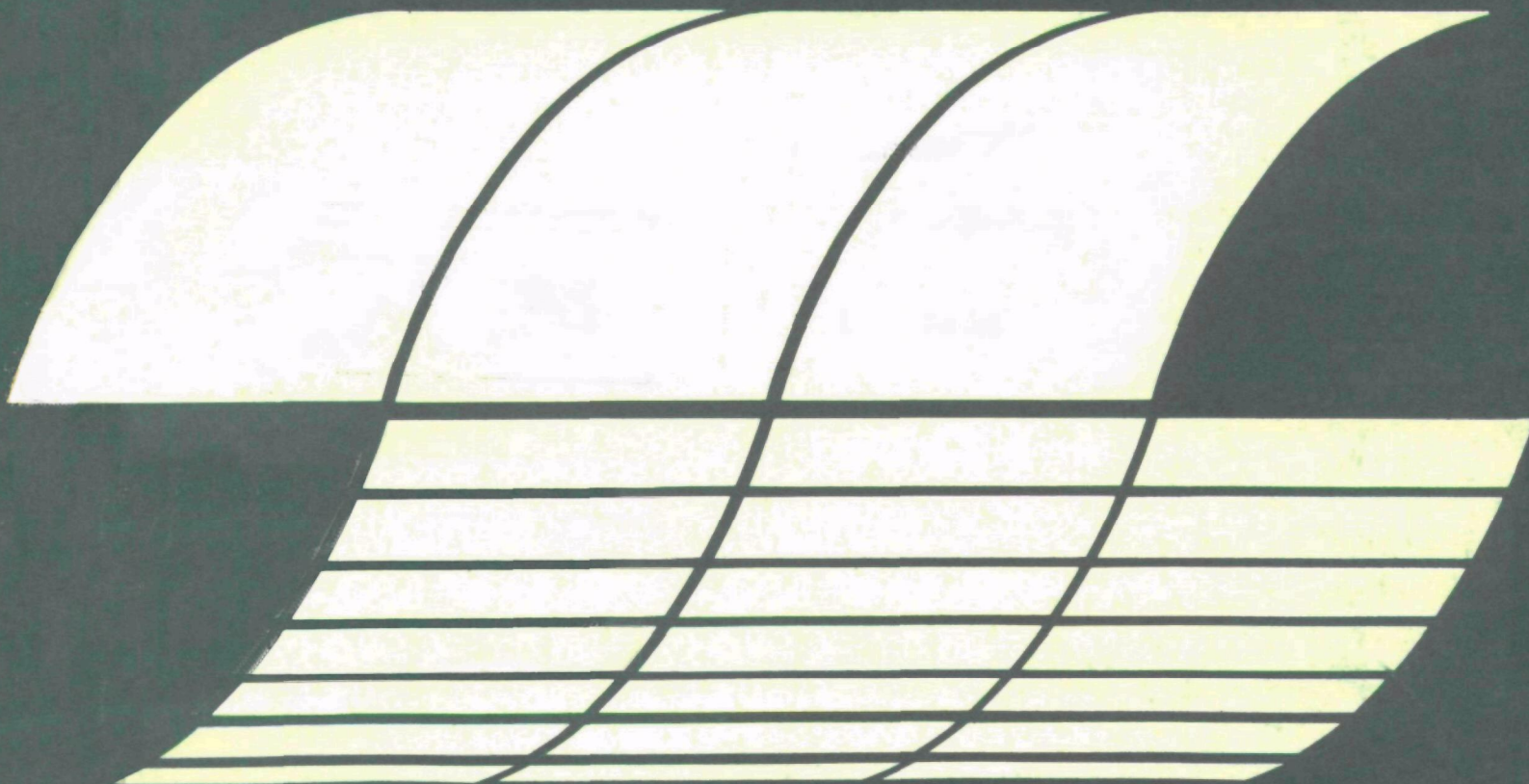
Research Triangle Park, North Carolina 27711

EPA-600/7-77-094a

August 1977

BURNER DESIGN CRITERIA FOR NO_x CONTROL FROM LOW-BTU GAS COMBUSTION; VOLUME I. AMBIENT FUEL TEMPERATURE

Interagency
Energy-Environment
Research and Development
Program Report



RESEARCH REPORTING SERIES

Research reports of the Office of Research and Development, U.S. Environmental Protection Agency, have been grouped into seven series. These seven broad categories were established to facilitate further development and application of environmental technology. Elimination of traditional grouping was consciously planned to foster technology transfer and a maximum interface in related fields. The seven series are:

1. Environmental Health Effects Research
2. Environmental Protection Technology
3. Ecological Research
4. Environmental Monitoring
5. Socioeconomic Environmental Studies
6. Scientific and Technical Assessment Reports (STAR)
7. Interagency Energy-Environment Research and Development

This report has been assigned to the INTERAGENCY ENERGY-ENVIRONMENT RESEARCH AND DEVELOPMENT series. Reports in this series result from the effort funded under the 17-agency Federal Energy/Environment Research and Development Program. These studies relate to EPA's mission to protect the public health and welfare from adverse effects of pollutants associated with energy systems. The goal of the Program is to assure the rapid development of domestic energy supplies in an environmentally-compatible manner by providing the necessary environmental data and control technology. Investigations include analyses of the transport of energy-related pollutants and their health and ecological effects; assessments of, and development of, control technologies for energy systems; and integrated assessments of a wide range of energy-related environmental issues.

REVIEW NOTICE

This report has been reviewed by the participating Federal Agencies, and approved for publication. Approval does not signify that the contents necessarily reflect the views and policies of the Government, nor does mention of trade names or commercial products constitute endorsement or recommendation for use.

This document is available to the public through the National Technical Information Service, Springfield, Virginia 22161.

EPA-600/7-77-094a

August 1977

BURNER DESIGN CRITERIA FOR NO_x CONTROL FROM LOW-BTU GAS COMBUSTION; VOLUME I. AMBIENT FUEL TEMPERATURE

by

Donald R. Shoffstall

Applied Combustion Research
Institute of Gas Technology
IIT Center, 3424 South State Street
Chicago, Illinois 60616

Contract No. 68-02-1360
Program Element No. EHE624a

EPA Project Officer: David G. Lachapelle

Industrial Environmental Research Laboratory
Office of Energy, Minerals, and Industry
Research Triangle Park, N.C. 27711

Prepared for

U.S. ENVIRONMENTAL PROTECTION AGENCY
Office of Research and Development
Washington, D.C. 20460

ABSTRACT

This research program was initiated to characterize problems associated with retrofitting existing utility boilers with low- and medium-Btu gases manufactured from commercially available coal conversion processes. All the experimental results were gathered from a pilot-scale furnace fired with a movable-vane boiler burner at a heat input of 0.66 MW (2,250,000 Btu/h). The low- and medium-Btu gases tested ranged in heating value from 3.7 to 11.2 MJ/m³ (100 to 300 Btu/SCF). They were synthetically produced with a natural gas reformer system.

Data were collected to permit a comparison between natural gas and low-Btu gases in the areas of flame stability, flame length, flame emissivity, furnace efficiency, and NO_x emissions.

Flame stability was found to be very sensitive to fuel jet velocity. An injection velocity of 30.5 m/s (100 ft/s) was found to be optimum. Flame length decreased with increasing movable vane angle (swirl of the combustion air), and the low- and medium-Btu gases tested were generally shorter than those of natural gas. Good agreement was obtained between measured and calculated flame emissivities. Some boiler modifications would be necessary to maintain rating when burning gases of less than 7.5 MJ/m³ (200 Btu/SCF) heating value. NO emissions were ordered by adiabatic flame temperature. The NO emission data yielded an activation energy of 153 k-cal/mole compared to kinetic model predictions of 135 k-cal/mole. The use of adiabatic flame temperature provided a good empirical method of predicting NO emissions for the fuels tested.

TABLE OF CONTENTS

	<u>Page</u>
INTRODUCTION	1
SUMMARY	2
PROCESS GASES SELECTED FOR STUDY	5
DESCRIPTION OF FURNACE TEST FACILITY	9
NO and NO ₂ Instrumentation	18
CO, CH ₄ , and CO ₂ Measurements	18
Oxygen Measurements	19
Chromatographic Measurements	19
EXPERIMENTAL PLAN	25
RESULTS	29
Flame Lengths	29
Gas Temperature Measurements	29
Flame Emissivity Determination	57
Nitric Oxide Emissions	77
DATA CORRELATION	88
NO _x Emissions	88
Correlating Furnace Performance	88
Mathematical Model of Furnace Performance	98
In-the-Flame Analysis	104

FIGURES

<u>No.</u>		<u>Page</u>
1	Schematic Diagram of IGT Gas-Generating System	7
2	Gas-Generating System	8
3	Rectangular Test Furnace	10
4	Removable Sidewall Furnace Panels for Interior Flame Probing	11
5	Overall System Schematic Diagram of Rectangular Test Furnace System	12
6	Radiant Tube Preheater for Main Furnace Combustion Air	13
7	Flue-Gas Cooler	15
8	Control Room Facility and Analytical Instrumentation	17
9	Gas-Sampling Probe Head for Nonparticulate Flue Gases	20
10	Modified IFRF Temperature Probe	21
11	General Probe Holder	22
12	Pyroelectric Radiometer (Used for Emissivity Measurements)	24
13	Guide-Vane Boiler Burner	26
14	Method of Measuring Movable-Vane Angle for Boiler Burner	26
15	Natural Gas Flame Using a 0.5-Inch Axial Nozzle	30
16	Lurgi Oxygen Gas Flame Using a 2-Inch Axial Nozzle	30
17	Winkler Oxygen Gas Flame Using a 2-Inch Axial Nozzle	31
18	Koppers-Totzek Oxygen Gas Flame Using a 2-Inch Axial Nozzle	31
19	Wellman-Galusha Air Gas Flame Using a 3-Inch Axial Nozzle	32
20	Winkler Air Gas Flame Using a 3-Inch Axial Nozzle	32

FIGURES, Cont.

<u>No.</u>		<u>Page</u>
21	Average Gas Temperature Profile for Natural Gas With a 15-Degree Vane Rotation	35
22	Average Gas Temperature Profile for Natural Gas With a 30-Degree Vane Rotation	36
23	Average Gas Temperature Profile for Natural Gas With a 45-Degree Vane Rotation	37
24	Average Gas Temperature Profile for Natural Gas With a 60-Degree Vane Rotation	38
25	Average Gas Temperature Profile for Lurgi Oxygen Gas With a 15-Degree Vane Rotation	41
26	Average Gas Temperature Profile for Lurgi Oxygen Gas With a 30-Degree Vane Rotation	42
27	Average Gas Temperature Profile for Lurgi Oxygen Gas With a 45-Degree Vane Rotation	43
28	Average Gas Temperature Profile for Lurgi Oxygen Gas With a 60-Degree Vane Rotation	44
29	Average Gas Temperature Profile for Winkler Oxygen Gas With a 15-Degree Vane Rotation	45
30	Average Gas Temperature Profile for Winkler Oxygen Gas With a 30-Degree Vane Rotation	46
31	Average Gas Temperature Profile for Winkler Oxygen Gas With a 45-Degree Vane Rotation	47
32	Average Gas Temperature Profile for Winkler Oxygen Gas With a 60-Degree Vane Rotation	48
33	Average Gas Temperature Profile for Koppers-Totzek Oxygen Gas With a 15-Degree Vane Rotation	49
34	Average Gas Temperature Profile for Koppers-Totzek Oxygen Gas With a 30-Degree Vane Rotation	50
35	Average Gas Temperature Profile for Koppers-Totzek Oxygen Gas With a 45-Degree Vane Rotation	51
36	Average Gas Temperature Profile for Koppers-Totzek Oxygen Gas With a 60-Degree Vane Rotation	52

FIGURES, Cont.

<u>No.</u>		<u>Page</u>
37	Average Gas Temperature Profile for Wellman-Galusha Air Gas With a 15-Degree Vane Rotation	53
38	Average Gas Temperature Profile for Wellman-Galusha Air Gas With a 30-Degree Vane Rotation	54
39	Average Gas Temperature Profile for Wellman-Galusha Air Gas With a 45-Degree Vane Rotation	55
40	Average Gas Temperature Profile for Wellman- Galusha Air Gas With a 60-Degree Vane Rotation	56
41	Average Gas Temperature Profile for Winkler Air Gas With a 15-Degree Vane Rotation	58
42	Average Gas Temperature Profile for Winkler Air Gas With a 30-Degree Vane Rotation	59
43	Average Gas Temperature Profile for Winkler Air Gas With a 45-Degree Vane Rotation	60
44	Average Gas Temperature Profile for Winkler Air Gas With a 60-Degree Vane Rotation	61
45	Refractory Emissivity Versus Refractory Temperature	65
46	Gas Emissivity Versus Axial Position for Natural Gas	66
47	Gas Emissivity Along Furnace Length for Lurgi Oxygen Gas	67
48	Gas Emissivity Along Furnace Length for Koppers-Totzek Oxygen Gas	68
49	Gas Emissivity Along Furnace Length for Winkler Oxygen Gas	69
50	Gas Emissivity Along Furnace Length for Wellman-Galusha Air	70
51	Gas Emissivity Along Furnace Length for Winkler Air	71
52	Flame Flow Pattern Tested	73
53	Emissivity Profile for Coke-Oven Gas	77

FIGURES, Cont.

<u>No.</u>		<u>Page</u>
54	NO Versus Secondary Air Preheat With Natural Gas	78
55	NO Versus Secondary Air Preheat With Lurgi Oxygen Gas	80
56	NO Versus Secondary Air Preheat With Koppers-Totzek Oxygen Gas	81
57	NO Versus Secondary Air Preheat With Winkler Oxygen Gas	82
58	NO Versus Secondary Air Preheat With Wellman-Galusha Air Gas	84
59	NO Versus Secondary Air Preheat With Winkler Air Gas	85
60	Arrhenius Plot of Experimental NO Emissions	87
61	NO Flue Concentration Versus Firing Density	89
62	Emissivity Versus Square Root of Path Length for Natural Gas	95
63	Emissivity Versus Square Root of Path Length for Winkler Air	96
64	Emissivity Versus Square Root of Path Length for Winkler Oxygen	97
65	Comparison of IGT Experimental and B&W Calculated Furnace Efficiencies	101
66	Comparison of Experimental and Well Stirred Speckled-Wall Model Calculated Efficiencies	103
67	Variation of Well Stirred Approximation With Adiabatic Radiance	105
68	Comparison of Experimental and Non-Well Stirred Speckled-Wall Model Calculated Efficiencies	106

TABLES

<u>No.</u>		<u>Page</u>
1	Synopsis of Furnace Operating Conditions and Test Results for a 45-Degree Vane Angle	3
2	Species Concentrations, Adiabatic Flame Temperatures, and Gross Heating Value (Wet) for Medium- and Low-Btu Gases Tested	6
3	Flame Length as a Function of Fuel Type and Vane Rotation	33
4	Summary of Average Gas Temperature Data	39
5	Calculated and Measured Emissivities	75
6	Projected NO _x Emission Levels for a Utility Boiler	90
7	Test Furnace Efficiencies and Combustion Product Properties at the Flue	90
8	B&W Calculated Boiler Efficiencies Using IGT Data	92
9	Calculated and Measured Efficiencies and Gas Emissivities	93
10	Comparison of Measured and Calculated Furnace Efficiencies	107
11	Comparison of Calculated Emissivities	107

INTRODUCTION

The electric power industry is caught between the Federal Government's concern for cleaning up the environment and for decreasing (or eliminating) our dependence on foreign sources for oil. The environmental concerns make the use of coal prohibitively expensive, if not impossible, because of the necessity of decreasing sulfur emissions. Low-sulfur oil could replace coal, but this oil must be imported, which is against long-range government policy. Coal appears to be the only fossil fuel available in sufficient quantities to eliminate the necessity of importing oil; however, an environmentally acceptable and practical way must be found for its use.

One concept that could provide a practical method for using coal is to convert it to low-sulfur, ashless, low-Btu gas for use in boilers. This would alleviate both the utility industry's fuel supply problem and the air pollution problem. Of particular concern, however, are the prospects of operating problems and loss of boiler output (downrating), which can occur when retrofitting a unit originally designed to use another fuel. What are needed are accurate combustion data to define the potential magnitude of these problems and to indicate whether practical solutions are possible.

This report presents results from an experimental program designed to characterize the problems associated with retrofitting existing boilers for low- and medium-Btu gases made from commercially available coal conversion processes. Data were collected to permit a comparison of natural gas and low- and medium-Btu gases in the areas of :

- Flame stability
- Flame length
- Flame emissivity
- Flue-gas pollutant emissions
- Detailed temperature profiles, and
- Calculated changes in heat transfer in the radiant and convective sections of a boiler.

SUMMARY

All of the experimental results presented in this report were taken from a pilot-scale furnace fired with a movable-vane boiler burner (MVBB) at a heat input of 2.25 million Btu/hr.* In addition to natural gas, five medium- and low-Btu gases were tested: Lurgi oxygen, Koppers-Totzek oxygen, Winkler oxygen, Wellman-Galusha air, and Winkler air. A synopsis of the test results for a 45-degree vane angle is presented in Table 1. This table includes furnace operating conditions, burner operating conditions, fuel combustion properties, and experimental data for the MVBB with a 45-degree vane angle. The information includes gross heating value of the fuel; adiabatic flame temperature with 3% excess oxygen and combustion air preheat of 325°F; input velocity of fuel and combustion air at 60°F; hydrogen-to-carbon monoxide ratio of fuel; gross input enthalpy, including combustion air preheat; chemical species analysis of flue gases; volume of flue gases at 60°F; measured flue-gas temperature; measured furnace rear-wall temperature; calculated and measured emissivity; and concentration of NO measured in the flue at 3% excess oxygen.

Based on a detailed analysis of the experimental data, the following conclusions were made:

1. Flame stability was established for each test fuel under the most severe operating conditions, that is, with the furnace walls, burner block, and combustion air at ambient temperature. The flame stability was very sensitive to fuel jet velocity leaving the fuel nozzle. An injection velocity of 100 ft/s was found to give the best operation.
2. For all fuel gases tested, the flame length decreased with increasing movable-vane angle (swirl of the combustion air). Medium- and low-Btu fuel gas flames were shorter than those for natural gas with the exception of Winkler air at a 45-degree vane angle, which produced a flame 10% longer than the natural gas flame.
3. Babcock and Wilcox used the pilot-scale test furnace data as input to their utility boiler design calculation to evaluate overall unit output when retrofit with medium- and low-Btu gases. The calculation technique used divided the boiler into a radiant (furnace) section and a convective section. The IGT experimental data were used as input conditions to the convective section. The

* It is EPA policy to use metric units; however, in this report English units are occasionally used for convenience. See attached conversion table.

**Table 1. SYNOPSIS OF FURNACE OPERATING CONDITIONS AND TEST RESULTS
FOR A 45-DEGREE VANE ANGLE
(Part 1)**

Fuel	Gross heating value, Btu/SCF	Adiabatic flame temp, °F	H ₂ /CO ratio	Fuel input vel, ft/s	Combustion air inlet vel, ft/s
Natural gas	1035.0	3337	--	100.6	53.3
Lurgi oxygen	285.4	3164	2.2	100.0	51.2
Winkler oxygen	270.2	3329	1.3	105.6	52.3
Koppers-Totzek oxygen	285.0	3578	0.7	97.6	50.4
Wellman-Galusha air	159.4	2948	0.5	136.4	54.6
Winkler air	116.3	2579	0.6	109.6	74.7

**Table 1. SYNOPSIS OF FURNACE OPERATING CONDITIONS AND TEST RESULTS
FOR A 45-DEGREE VANE ANGLE
(Part 2)**

Fuel	Gross heat input, Btu/hr	Flue products				Vol of flue products, CFH at 60°F	SCF air	SCF flue products
		N ₂	CO ₂	H ₂ O	O ₂			
		%					SCF fuel	SCF fuel
Natural gas	2,371,265	72.5	8.3	16.7	2.5	27,357	11.23	12.26
Lurgi oxygen	2,356,066	62.9	16.8	17.8	2.5	27,565	2.71	3.41
Winkler oxygen	2,350,940	63.1	18.3	16.1	2.5	26,169	2.43	3.06
Koppers-Totzek oxygen	2,348,367	65.0	20.2	12.2	2.6	24,356	2.51	3.07
Wellman-Galusha air	2,358,036	72.3	15.8	9.2	2.7	32,772	1.54	2.33
Winkler air	2,358,940	74.5	14.6	8.2	2.8	38,339	1.13	1.96

**Table 1. SYNOPSIS OF FURNACE OPERATING CONDITIONS AND TEST RESULTS
FOR A 45-DEGREE VANE ANGLE
(Part 3)**

Fuel	Flue-gas temp, °F	Rear-wall temp, °F	Emissivity		Flue NO, ppm
			Calc	Meas	
Natural gas	2553	2309	0.159	0.177	65
Lurgi oxygen	2442	2300	0.194	0.185	32
Winkler oxygen	2523	2309	0.189	0.218	73
Koppers-Totzek oxygen	2554	2327	0.174	0.190	104
Wellman-Galusha air	2434	2066	0.154	0.190	15
Winkler air	2335	2012	0.150	0.170	4

design of the computer program did not allow information from the IGT tests to be inputs for the radiant section, although a comparison between the IGT experiment results and Babcock and Wilcox's predictions was made. The IGT data were used as input conditions to the convective section. It was found that all fuel gases tested were capable of maintaining boiler output; however, those with a heating value below 200 Btu/SCF may require retubing in the convective sections.

4. A second evaluation of furnace efficiency – defined for the purposes of this report as the fraction of the total enthalpy input to the furnace that is transferred to the furnace load – was made by Babcock and Wilcox using their standard design calculation technique. The inputs required for this calculation were: 1) fuel composition and 2) desired temperature of combustion products leaving the air heater. The values calculated for the combustion products of the fuel gases tested leaving the radiant section of the boiler agreed remarkably well with experimental values.
5. An iterative calculation technique using a non-well stirred reactor model produced efficiencies for each test fuel in good agreement with the experimental results.
6. The furnace efficiency (fraction of heat transferred within the furnace) calculated with the well stirred model was found to be rather insensitive to emissivity, with a 10% change in emissivity producing only a 3% change in efficiency.
7. NO concentration levels from the medium- and low-Btu gases were ordered by adiabatic flame temperature. Only test fuels with heating values below 200 Btu/SCF had emission levels that conformed to the New Source Performance Standard.
8. The NO emission data yielded an activation energy of 153 kcal/mol compared to kinetic models which predict 135 kcal/mol. This good agreement suggests that peak temperatures approaching the adiabatic flame temperature are controlling the rate of NO formation. Also, the use of the adiabatic flame temperature provides a good empirical method of predicting NO emissions.

PROCESS GASES SELECTED FOR STUDY

To ensure the immediate relevance of the program's results, only gas compositions from commercially available coal conversion processes (Lurgi, Koppers-Totzek, Winkler, and Wellman-Galusha) were considered. The gas properties of interest were heating value and hydrogen-to-carbon monoxide ratio (H_2/CO). To permit the study of a complete range of heating values and hydrogen-to-carbon monoxide ratios five gases were selected for testing. These five gases are listed below, and a detailed gas composition analysis for each is given in Table 2.

<u>Test gas</u>	<u>Heating value, Btu/SCF (wet)</u>	<u>H_2/CO</u>
Lurgi oxygen	285	2.2
Winkler oxygen	269	1.3
Koppers-Totzek oxygen	284	0.6
Wellman-Galusha air	160	0.5
Winkler air	117	0.6

These representative medium- and low-Btu gases are produced using the gas-generating and fuel-preparation facility shown schematically in Figure 1. The critical item in the gas supply system is the reformer, shown in Figure 2. This is a special gas generator that produces varying ratios of H_2/CO . Natural gas and carbon dioxide are fed to the reformer through a specially designed mixing tee. Additionally, steam may also be mixed, depending on the desired H_2/CO ratio. The resulting mixture is supplied to four reaction retorts contained in a vertical cylindrical furnace. The catalyst-filled retorts are heated by the furnace, and the input gases undergo endothermic chemical reactions at a temperature of $2100^{\circ}F$ as they pass through the retort tubes. Globally, the reaction scheme is the water-gas shift. The gas generated within the reaction tubes passes through water-jacketed coolers, where it is quenched to prevent deterioration of the H_2/CO ratio.

The reformed gas is compressed to 30 psig and pushed through an MEA (methyl-ethyl-amine)- CO_2 (carbon dioxide) absorbing tower. This tower is used to remove

CO₂ from the reformed gas if its concentration is above what is needed to synthesize the desired low-Btu gas. The reformed gas then enters a mixing chamber where it is blended with nitrogen, carbon dioxide, steam, and natural gas to reach the desired mixture of gas to be modeled. The product gas is analyzed by a gas chromatograph to ensure that the correct composition is attained. The synthesized gas is then fed to the pilot-scale furnace for combustion testing.

Table 2. SPECIES CONCENTRATIONS, ADIABATIC FLAME TEMPERATURES, AND GROSS HEATING VALUE (Wet) FOR MEDIUM- AND LOW-Btu GASES TESTED

Fuel	CO	H ₂	CO ₂	CH ₄	N ₂	H ₂ O	Adiabatic flame temp, °F	Heating value, Btu/SCF
Lurgi oxygen	18.5	40.2	29.4	9.4	0.6	1.9	3156	285
Winkler oxygen	32.9	41.2	20.0	3.0	1.0	1.9	3327	269
Koppers-Totzek oxygen	52.1	34.5	9.2	0.5	1.0	1.9	3578	284
Wellman-Galusha air	26.3	14.3	7.4	2.6	46.9	1.9	2948	160
Winkler air	21.1	13.0	6.9	0.6	56.5	1.9	2579	116

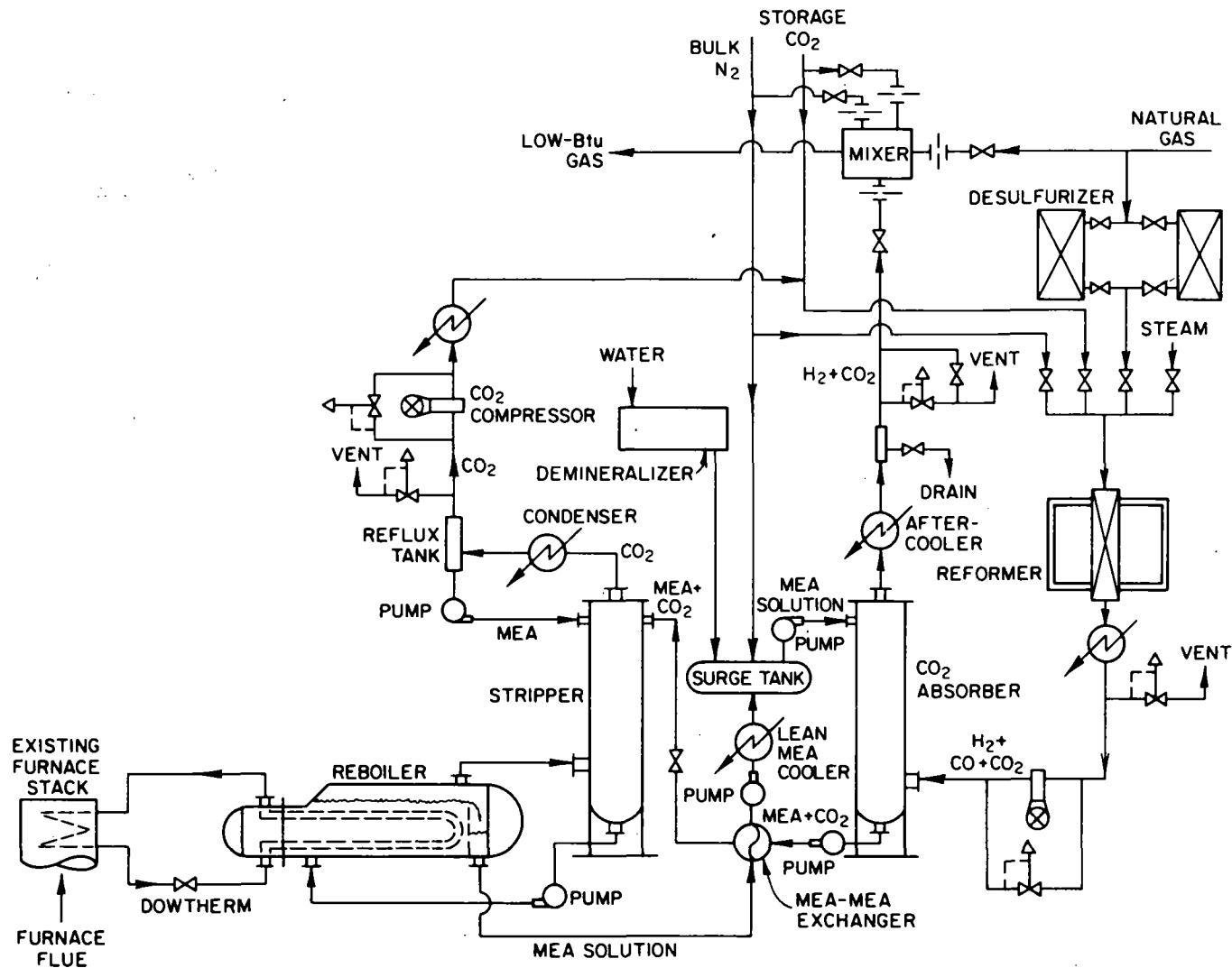
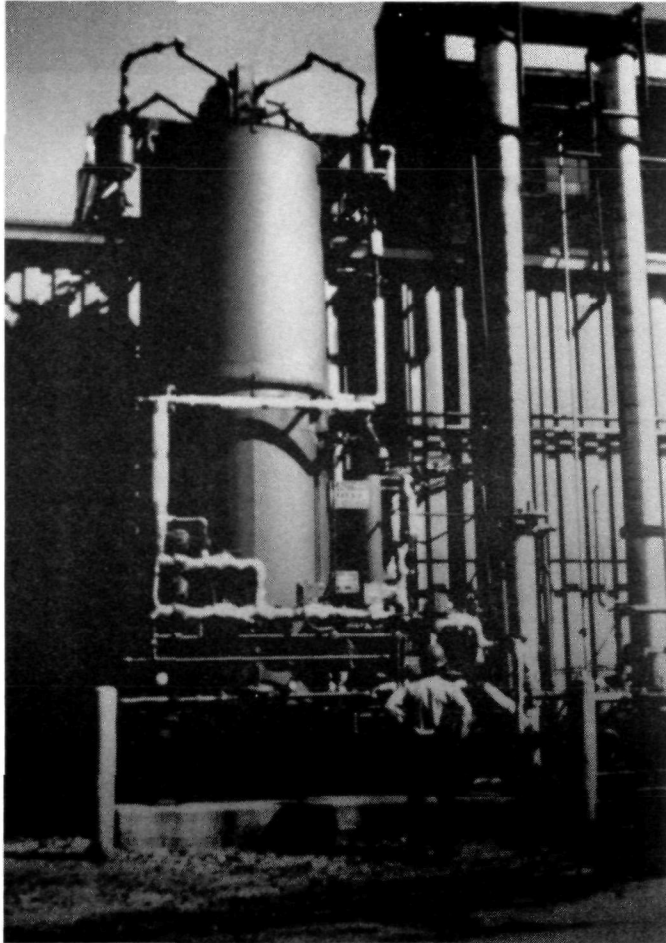


Figure 1. Schematic diagram of IGT gas-generating system



2a. Natural gas reforming system



2b. Reformer controls and
synthetic gas mixing panel

Figure 2. Gas-generating system

DESCRIPTION OF FURNACE TEST FACILITY

The experimental work was conducted on a rectangular furnace with a 25-sq ft cross-sectional area and a 13-foot length. This furnace can be end- or sidewall-fired at a rate of 4 million Btu/hr. The furnace is equipped for in-the-flame sampling, preheated air, and flue-gas recirculation. (See Figure 3.) This furnace is capable of operating at temperatures up to 3000°F or as low as 1600°F at a constant (maximum) gas input of 4 million Btu/hr and up to 40% excess air. Cooling is achieved with cooling coils embedded in the refractory walls. The furnace is constructed completely of 9-inch thick cast refractories, with removable panels in one sidewall to permit insertion of sampling probes (Figure 4). The overall furnace system is shown schematically in Figure 5. The system is flexible enough that the following operating parameters can be independently varied:

- Heat input, up to 4 million Btu/hr (8.0 million for certain burners)
- Air input, up to 40% excess
- Heat losses to the furnace walls by changing flow in water-cooling tubes cast into the refractories
- Combustion air temperature, up to 1000°F
- Flue-gas recirculation capability, up to 35% of combustion air
- Furnace pressure, up to +0.05 inch of water.

The combustion air for the main furnace can be preheated up to a temperature of 1000°F with a separately fired radiant tube air preheater. The radiant tube furnace (Figure 6) consists of an insulated airtight steel chamber 4 feet high, 4 feet wide, and 16 feet long. As the combustion air to be preheated passes through this chamber, it is heated by convection from three 6-inch diameter "hairpin" gas-fired radiant tubes.

The radiant tubes and refractory flow passages inside the preheater are arranged to provide an S-shaped flow pattern, which maximizes residence time for heating at the maximum allowable pressure drop (20 ounces) for which the flow pattern will provide the necessary air flow of 75,000 SCF/hr.



Figure 3. Rectangular test furnace

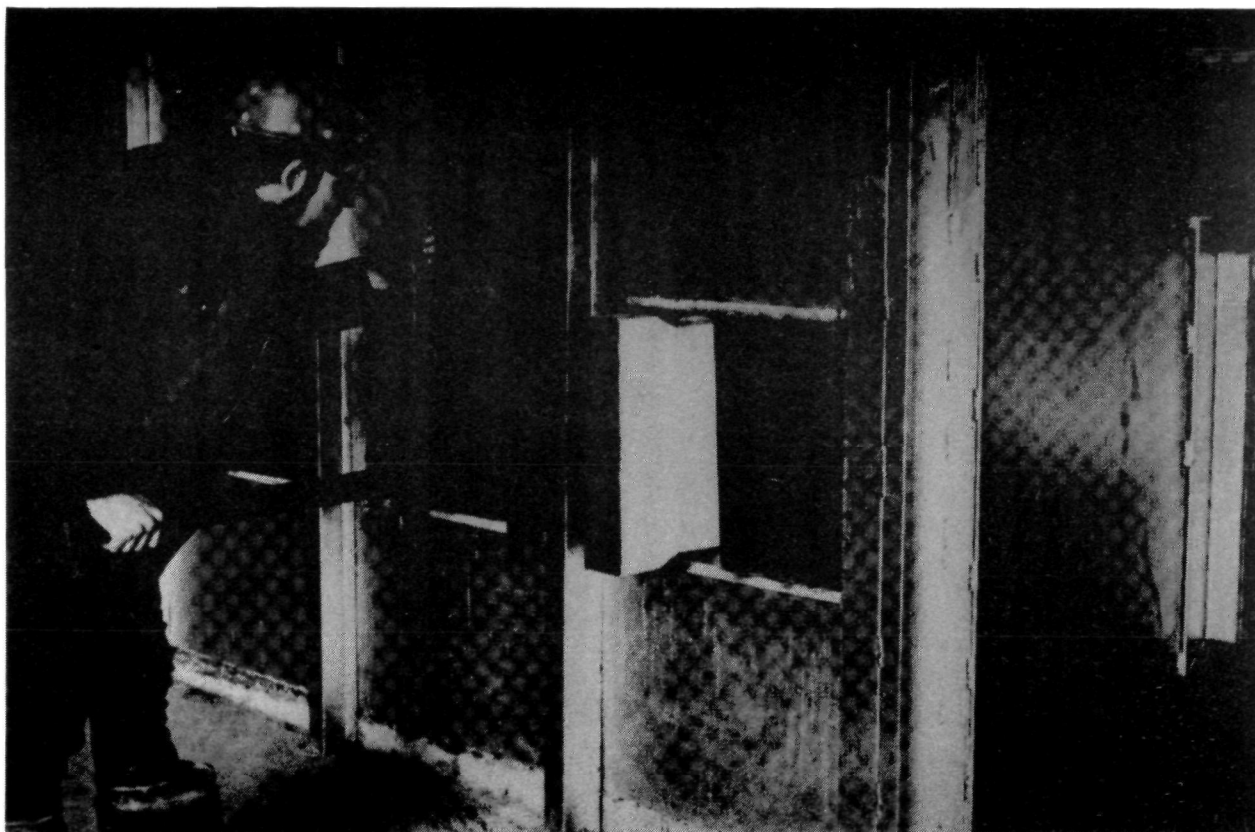


Figure 4. Removable sidewall furnace panels
for interior flame probing

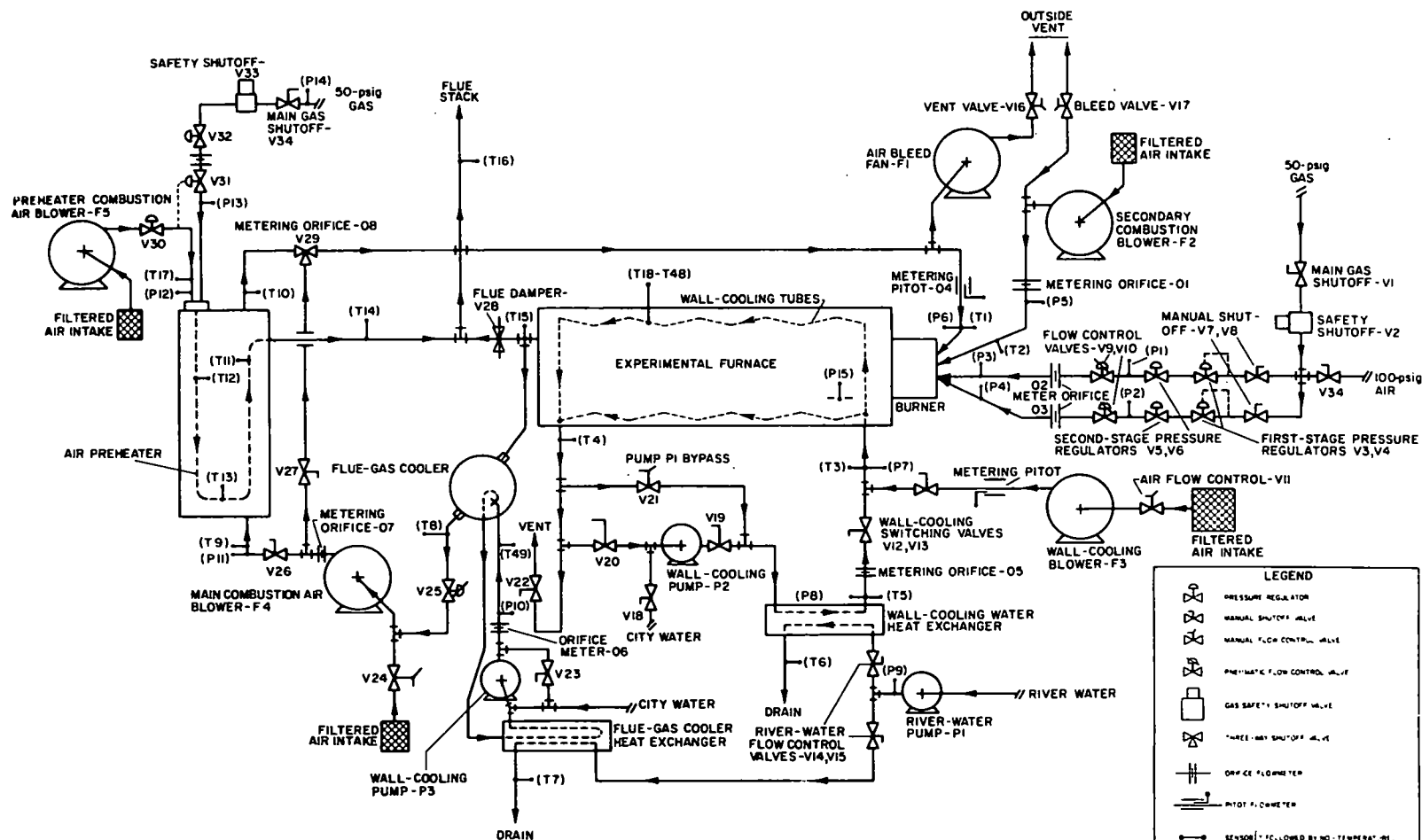


Figure 5. Overall system schematic diagram of rectangular test furnace

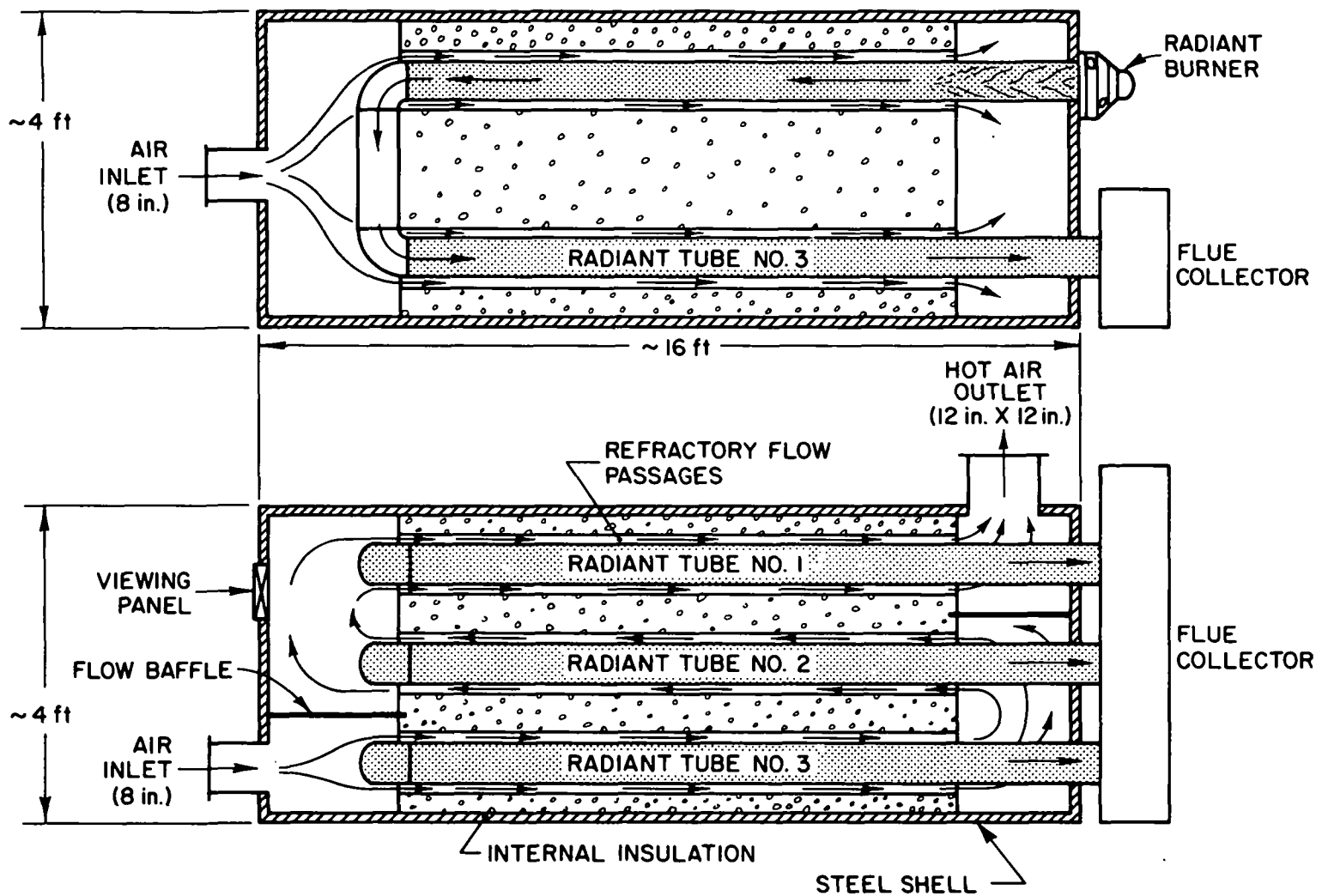


Figure 6. Radiant tube preheater for main furnace combustion air

The temperature of the air can be regulated by changing the heat input to the radiant tubes. Ambient temperature air can be supplied by completely shutting down the preheater or by directing the air through the preheater bypass pipe. The bypass pipe was installed to allow working on the preheater without shutting down the air supply to the main furnace. Air bypass is achieved by selective switching of valves.

Flue products for recirculation back to the burner and main furnace are obtained from the furnace itself. Flue products can be withdrawn from the furnace flue passage just prior to the main furnace flue damper. Up to 14,000 SCF/hr of flue products can be withdrawn from the flue, which provides a 30% recirculation factor when the furnace is fired at 3.5 million Btu/hr with 20% excess air.

The main furnace flue products are actually pulled from the flue (Figure 5) by the suction in the inlet side of the main furnace combustion air fan (F4). The flue products enter the recirculation withdrawal and treatment system at about 2800°F through a short length of internally insulated steel duct. These hot gases are cooled to about 125°F in a packed-bed water cooler (Figure 7). Cooled city water (about 70°F) is sprayed down on a bed of refractory packings as the hot gases pass up through the packed bed. This cooling system lowers the water content of the flue gas from about 0.008 to about 0.007 lb/CF, which is the dew point of the gases at about 125°F. (The lost water content can be added again later in the system if experimental conditions require this treatment.) The cooled gases then pass through a flow-control shutoff valve (V25 in Figure 5). This valve controls the flue-gas flow rate, which regulates the percentage of recirculated products. This valve is interlocked to an outlet temperature sensor on the gas cooler. If the outlet temperature of the gases exceeds 150°F, which would damage the combustion air fan, the control valve (V25) shuts down. This stops the flow of flue gases. Beyond the flue-gas control valve, the flue gases are mixed with the required amount of air for combustion. A control valve (V24) regulates the amount of air pulled in by the fan. The total amount of air for combustion and flue products is metered with an orifice plate (O7) at the outlet of the fan. The flue products and air then pass into the air preheater or preheater bypass pipe.

The water used in the flue-gas cooler is clean city water, which is continuously recycled. A water flow of 60 gpm is supplied at 150 psig by a turbine pump to a

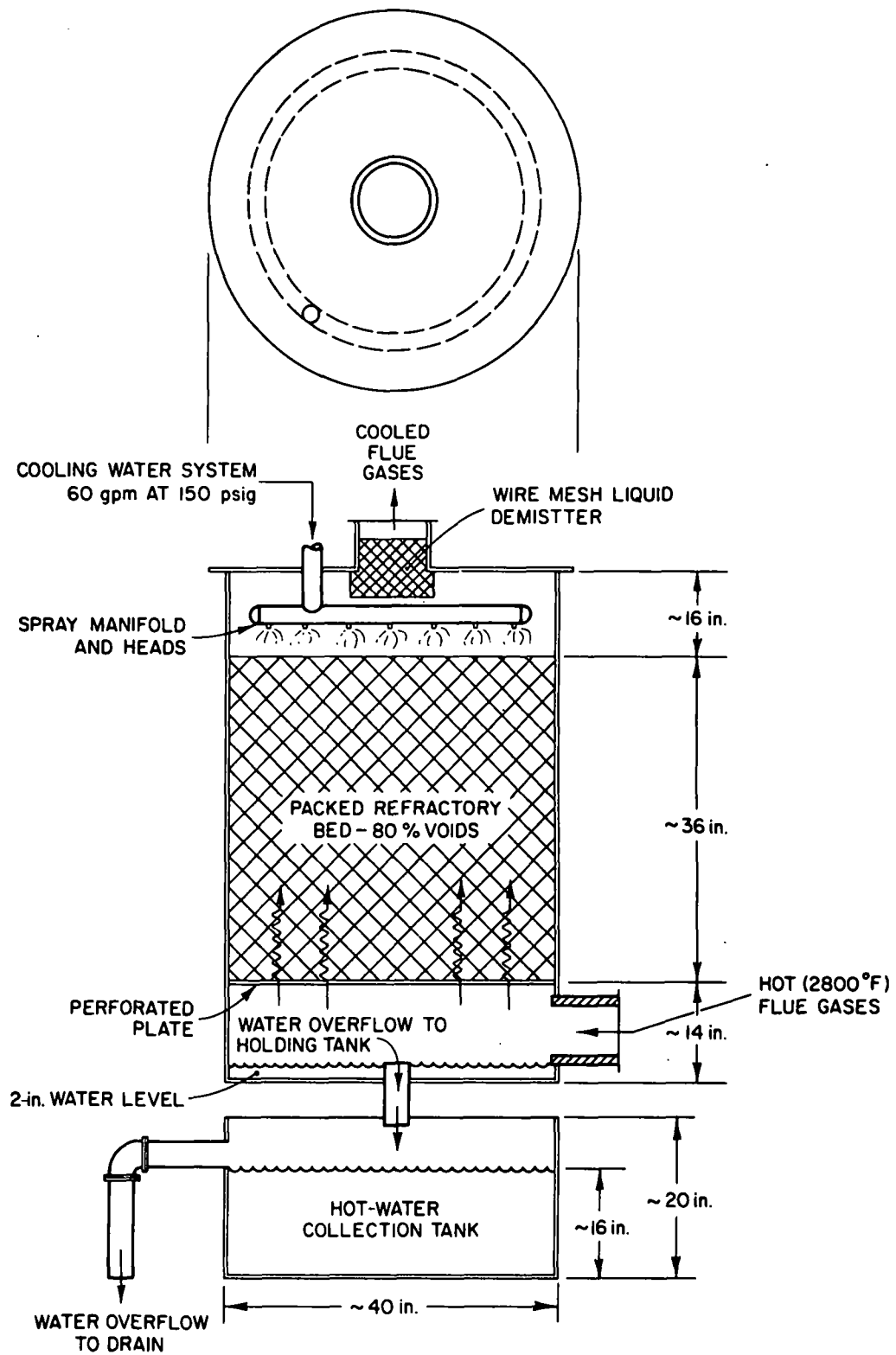


Figure 7. Flue-gas cooler

series of spray heads in the gas cooler. The hot (200°F) spent water flows out of the cooler into an atmospheric holding tank. This tank is equipped with a constant-level overflow to the building drain. In this way, any condensed water from the combustion is removed and disposed of in the sewer. The water in the holding tank is periodically treated with sodium hydroxide to prevent acid buildup in the water due to condensing flue-gas components. One such component removed by the flue-gas cooler is NO₂. The hot water from the water holding tank is cycled through an American Standard heat exchanger capable of removing 1.5 million Btu/hr of heat from the water. Cooling in the heat exchanger is provided by a flow of river water at a rate of about 150 gpm at 80 psig. The river water is supplied by a river adjacent to the test facility through a service pump (P1) maintained by IGT.

Figure 8 is an overall view of furnace controls and the analytical instrumentation package. The equipment used for concentration measurements of chemical species during this program is listed below; these analyzers included the following items:

1. Beckman 742 Polarographic Oxygen (O₂)
2. Beckman Paramagnetic Oxygen (O₂)
3. Beckman NDIR Methane (CH₄)
4. Beckman NDIR Carbon Monoxide (CO)
5. Beckman NDIR Carbon Dioxide (CO₂)
6. Varian 1200 Flame Ionization Chromatograph (Total HC and C₂ to C₉)
7. Beckman NDIR Nitric Oxide (NO)
8. Beckman UV-NO₂
9. Hewlett-Packard Thermoconductivity Chromatography, Hydrogen (H), Nitrogen (N₂), Argon (A₂), CO, CO₂, C₁ to C₅, Oxygen (O₂)
10. Beckman Chemiluminescent NO-NO₂
11. Data Integration System.

This instrumentation package allowed concentration measurements of the following major components: 1) measurement of hydrocarbon compounds C₁ to C₉;

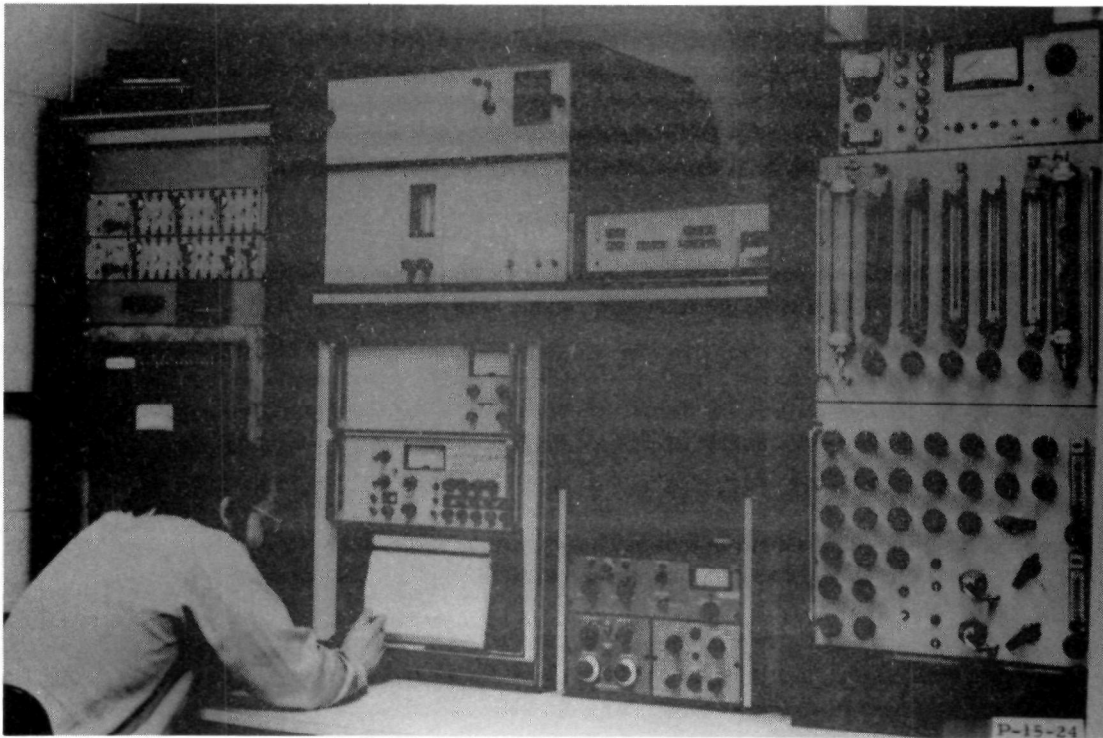


Figure 8. Control room facility and analytical instrumentation

2) independent check of NO-NO₂ chemiluminescent with NDIR-NO and NDUV-NO₂; 3) independent check of paramagnetic O₂, polarographic O₂, NDIR-CH₄, NDIR-CO, and NDIR-CO₂ with the respective chromatographic species concentration; and 4) measurement of hydrogen (H₂), argon (A₂), and nitrogen (N₂).

The following sections give a general description of the measurement system used for this program.

NO AND NO₂ INSTRUMENTATION

The chemiluminescent NO_x and NDUV-NO₂ system was mounted in a roll-around cabinet that could be placed out at the furnace. This was important in minimizing sampling distances, which can affect accuracy. The chemiluminescent unit was equipped with a carbon converter. Test work by IGT and others has demonstrated that in a reducing environment the carbon converter maintains a better conversion efficiency than converters made of stainless steel, quartz, or molybdenum.

The instrumentation was calibrated by using both a permeation tube with a controlled known release of NO_x and certified prepared cylinders of NO and NO₂ gases.

The sample gas was drawn from the furnace through a special alumina probe by a Dia-Pump Model 08-800-73 all stainless-steel and Teflon[®] pump delivering approximately 0.4 CF/min. (This sample delivery rate was dictated by the requirements of the measuring instruments.) The sample is immediately passed through a stainless-steel large-particle filter. Both the pump and filter were kept above 100°C to prevent condensation of the water vapor inherent to combustion products.

CO, CH₄, AND CO₂ MEASUREMENTS

Nondispersive infrared analyzers were used for carbon monoxide, methane, and carbon dioxide measurements. These analyzers do not affect the sample gas and can be operated in series. They were calibrated by using certified gases with known concentrations of the species being determined. The infrared analyzers require a completely dry sample. Therefore, the sample was first passed through a water trap and a 3 Å molecular drying sieve. A small in-line filter was placed immediately after the drying tube to trap particles of sieve that may be carried over by the gas stream.

OXYGEN MEASUREMENTS

A portion of the "conditioned" sample gas is diverted from the NDIR units to a Beckman Model 600 paramagnetic analyzer. A second oxygen analyzer, a Beckman Model 742 polarographic, was used as a cross-check on the oxygen concentration. The Model 742 analyzer has an advantage over the paramagnetic in time response.

CHROMATOGRAPHIC MEASUREMENTS

As a detailed gas analysis was required, the sample was fed to a Hewlett-Packard 7620-A thermal conductivity chromatograph, which permitted concentration evaluations of hydrogen, nitrogen, argon, oxygen, carbon monoxide, carbon dioxide, and hydrocarbons C_1 to C_5 . To achieve separation of these species, a helium carrier gas was used in conjunction with a Porapak Q column. Three temperature program rates were also required, ranging from -100° to 300°C . A sample loop volume of 100 ml was used to ensure linearity in the hydrogen response for concentrations up to 60%.

For total hydrocarbon analysis, a Beckman hydrocarbon analyzer was used. A detailed hydrocarbon analysis could be made using a Varian 1200 flame-ionization chromatograph. All chromatographic readings were electronically integrated and printed out as a function of resolution time.

In addition to flue-gas analysis, a major task of this program was to map profiles of temperature, chemical species, and flame emissivity. Modified designs of the International Flame Research Foundation (IFRF) were used to construct probes, which enabled this type of data collection.

Figure 9 shows the assembly drawing of the gas-sampling probe used in both the flame and the flue. To minimize NO_2 reduction in the probe, an alumina tube was inserted for the first 18 inches and was joined to Teflon tubing to carry the gas sample to the analyzers.

Temperature data were collected using a suction pyrometer; the design is illustrated in Figure 10. A Pt-Pt Rh 10% thermocouple was used. The efficiency of the pyrometer was measured at 96% with a 25-second response time.

The gas-sampling probe, suction pyrometer, and radiation cooling target were all designed to be installed in the general probe holder shown in Figure 11.

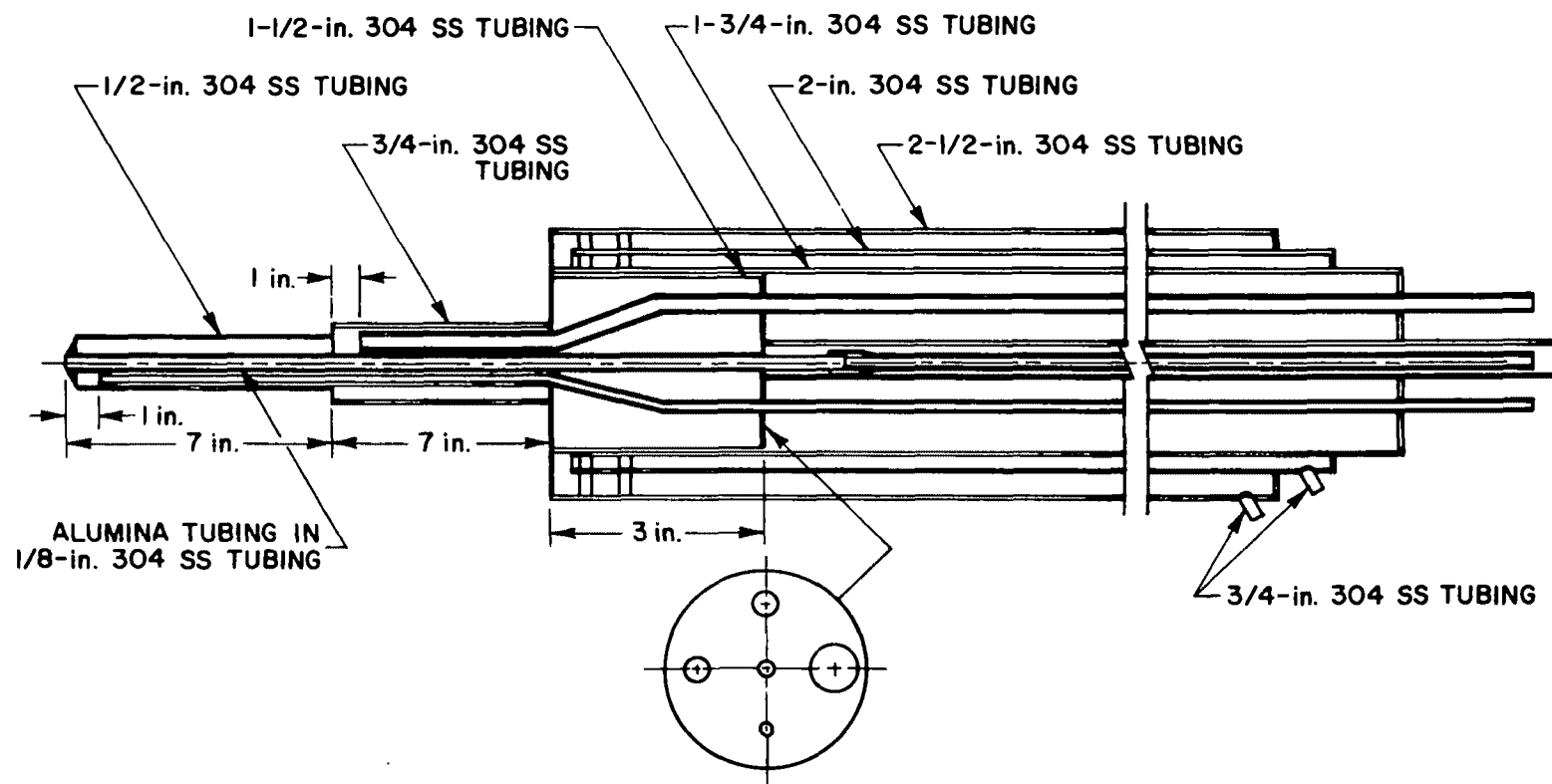


Figure 9. Gas-sampling probe head for nonparticulate flue gases

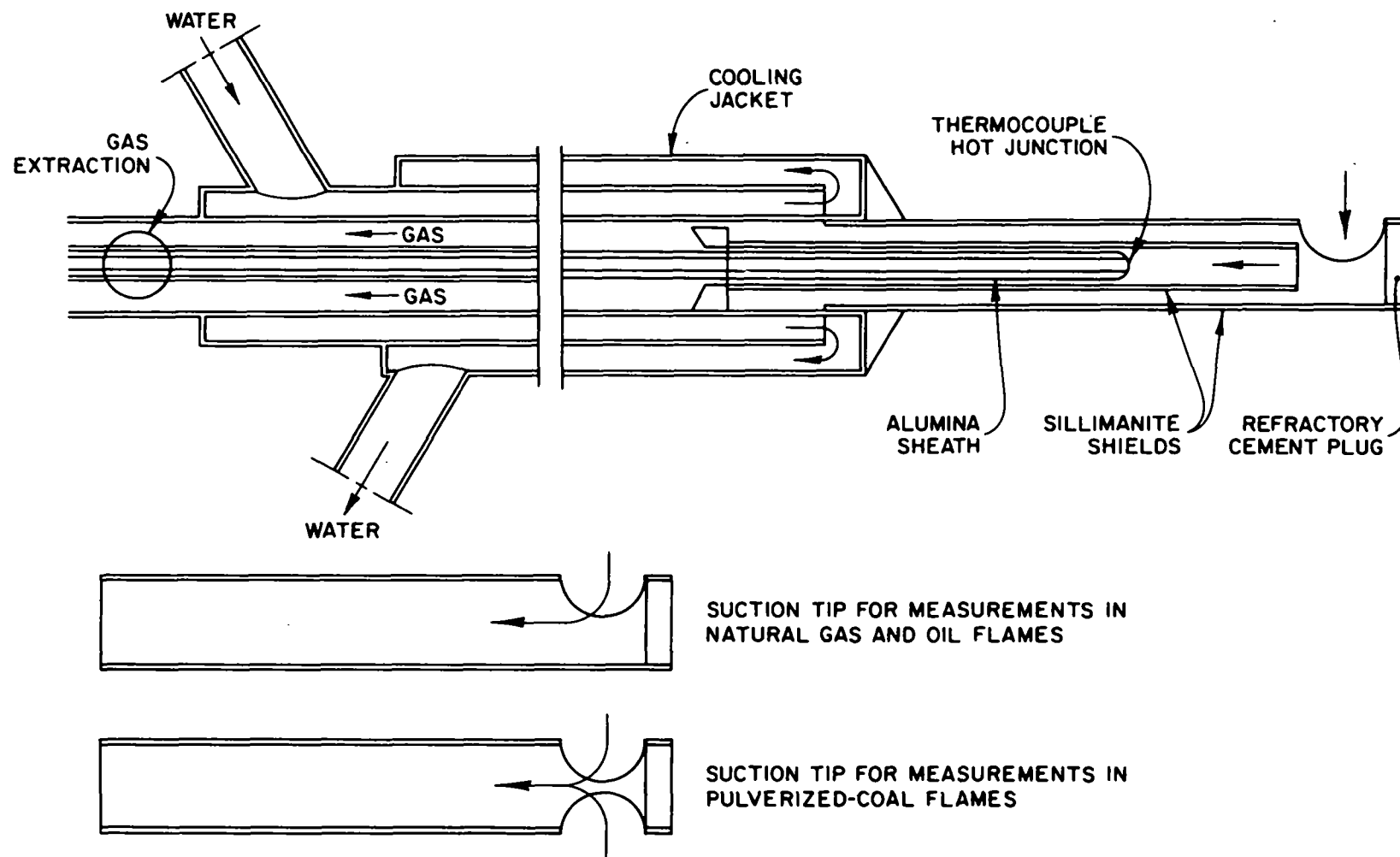


Figure 10. Modified IFRF temperature probe

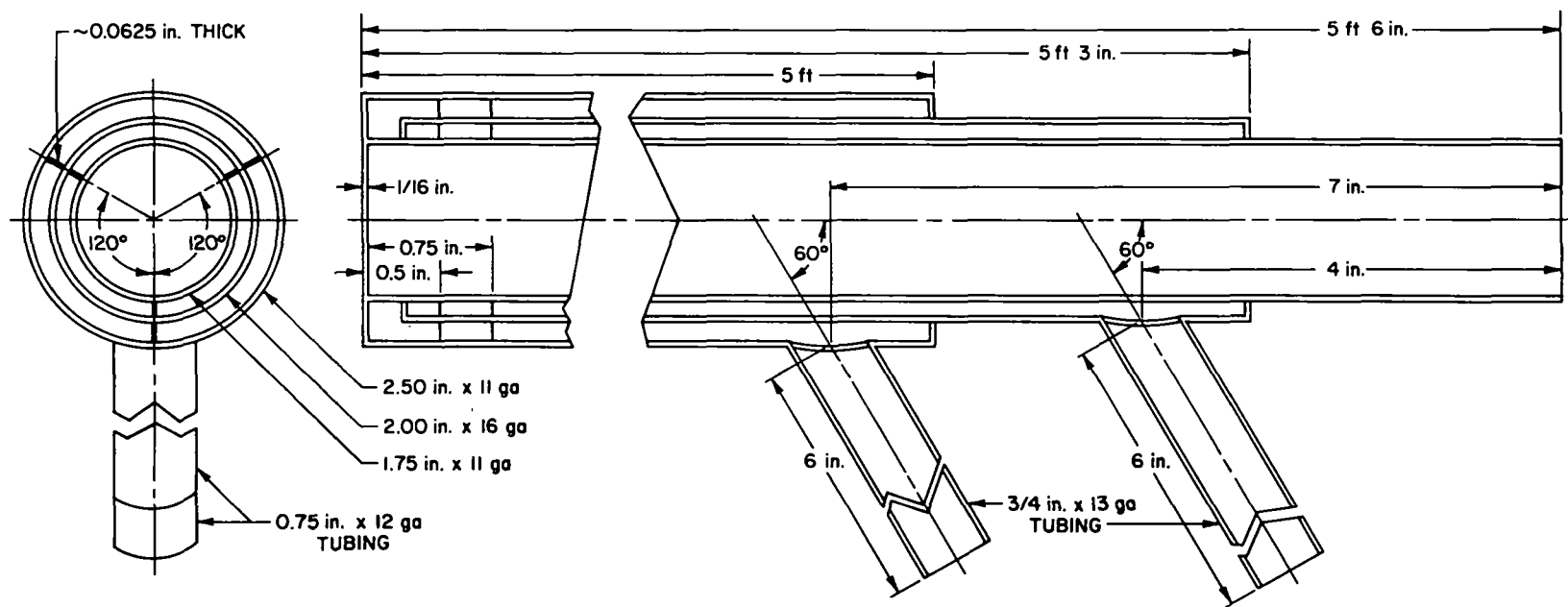


Figure 11. General probe holder

To evaluate radiation intensity, which is needed for a determination of flame emissivity, a PR 200 Pyroelectric Radiometer, manufactured by Molelectron Corp. in Sunnyvale, California, was used. Figure 12 shows the pyroelectric radiometer plus radiation shield. This radiometer uses a permanently poled lithium tantalate detector that is capable of resolving radiant power into the nanowatt range while maintaining a continuous spectral response from the vacuum UV to 500 μm . A built-in optical calibration system in the form of a highly stable LED (light-emitting diode) that is calibrated against an NBS traceable standard of total irradiance permits a direct correlation of experimental data from different trials.

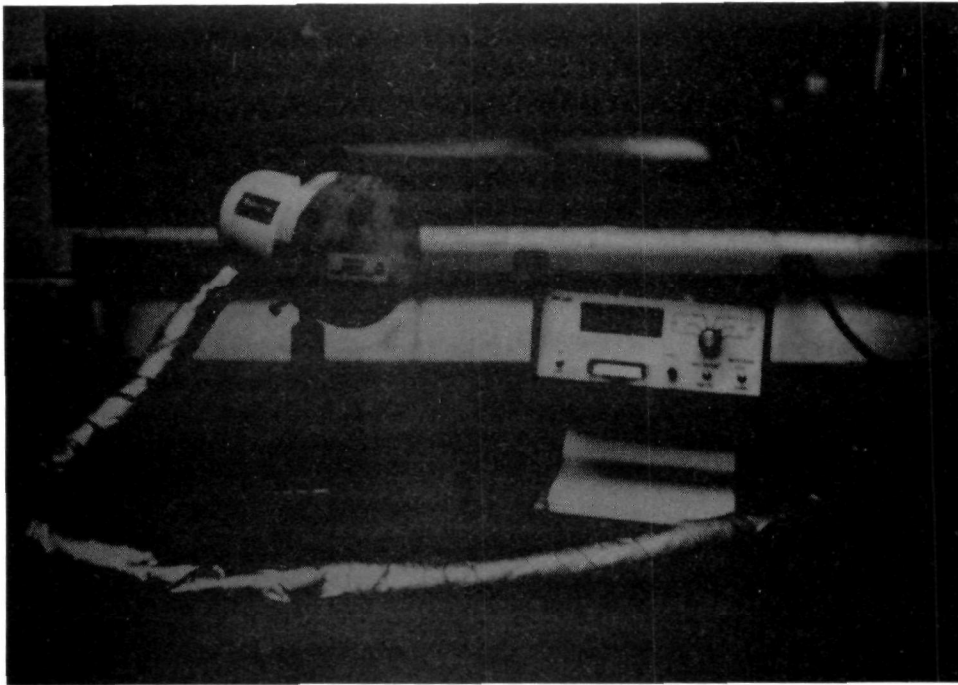


Figure 12. Pyroelectric radiometer
(used for emissivity measurements)

EXPERIMENTAL PLAN

All test data were collected using a single-register movable-vane boiler burner with an axial fuel injector. An assembly drawing of the MVBB tested is shown in Figure 13. The combustion air enters perpendicular to the axes of the burner and passes through a register of guide vanes that impart a degree of spin to the air, dependent on the vane orientation. Figure 14 illustrates how the angle of the movable vane is measured. The ratio of the average tangential and radial velocity components at the exit of the movable-vane register depends only on the geometric dimensions of the vanes in the axis perpendicular cross section (assuming a negligible Reynolds number influence).

A straight pipe was used as the fuel injector, guaranteeing that the fuel had only an axial velocity. This type of injector was used for two reasons. First, this type of nozzle would be the most stringent test for flame stability in the cold-wall stability tests; and, second, medium- and low-Btu gases would normally be available at relatively low pressures, dictating the use of a low-pressure injector. The diameter of the fuel injector was varied for fuel type to maintain an injection velocity of 100 ft/s.

The burner block used during this program had a 30-degree divergent angle with a 15.2-cm (diameter) entrance and a 48.2-cm (diameter) exit to the furnace. To maximize flame stability the throat nozzle position was used throughout this program. The throat nozzle position is located 2.5 cm from the burner block entrance within the 15.2-cm (diameter) refractory duct connecting the burner with the block.

Burner operating conditions used throughout the program had the level of flue oxygen fixed at 3% with the combustion air preheated to 325°F (unless specified differently). These conditions are considered typical for utility boiler burners.

Based on the overall program objective of evaluating boiler performance changes when retrofitting from natural gas to medium- and/or low-Btu gas, it was necessary to select an operating variable to model the pilot-scale test furnace against a field service boiler. Several parameters were considered, including operating wall temperature, heat absorption profile, and firing density. It was decided to match the temperature of the combustion products from natural gas at the pilot-scale

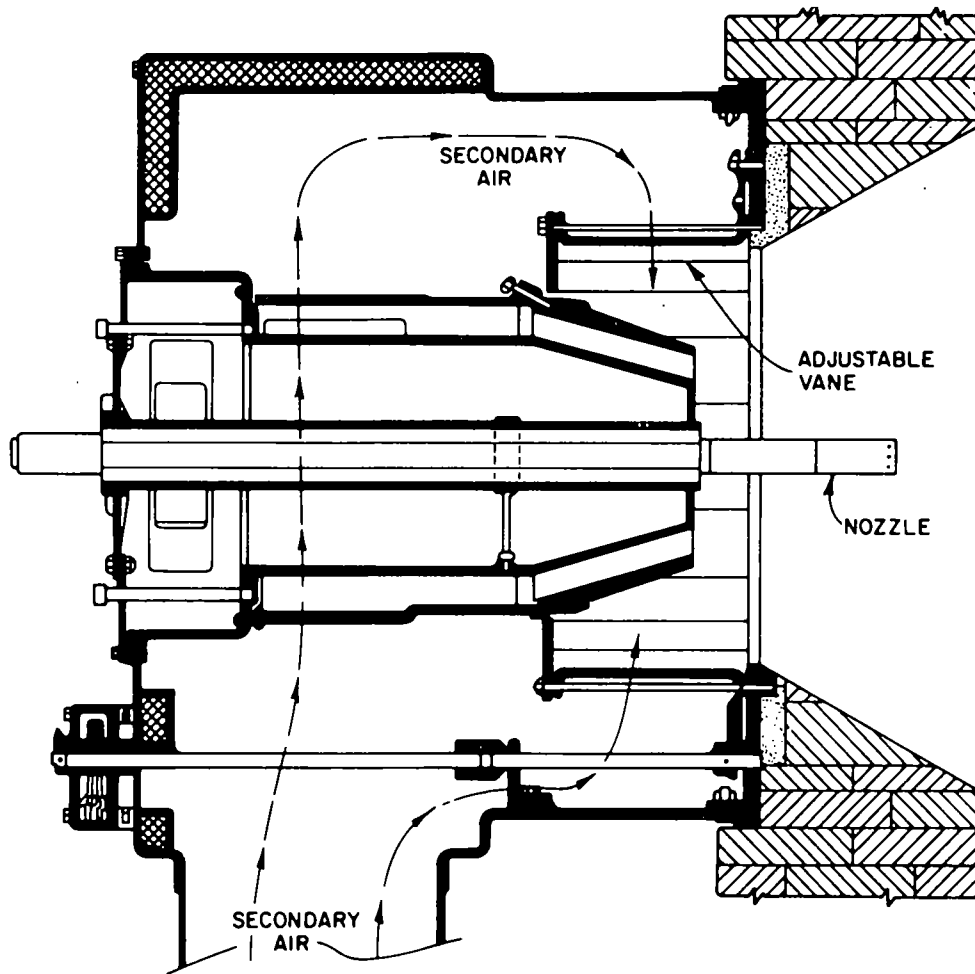


Figure 13. Diagram of movable-vane boiler burner

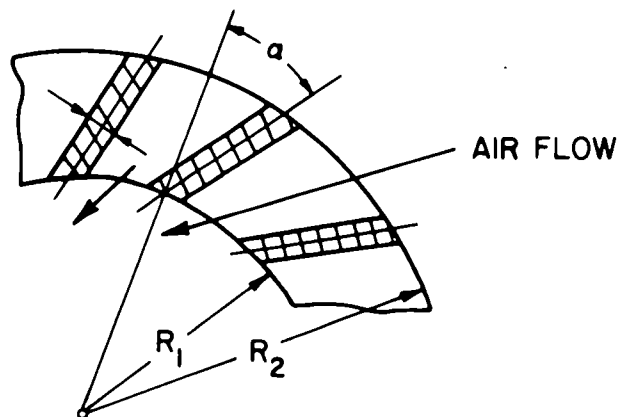


Figure 14. Method of measuring movable-vane angle for boiler burner

furnace exit to the temperature measured between the boiler and the secondary superheater section of a utility boiler. This decision was based on the complexities of multiburner interactions within a utility boiler versus the single-burner test furnace, where several flames would not view the boiler water walls. The data of most interest in evaluating performance changes were gas volume, temperature, and gas emissivity entering the secondary superheater. Thus, baseline data were collected for natural gas after the furnace load had been adjusted to give an exit-gas temperature of 2550°F.

The first task to be conducted after the baseline furnace operating conditions had been fixed was to determine flame stability. The stability trials were to be conducted under the most stringent operating conditions, that is, with the furnace walls, burner block, and combustion air at ambient temperature.

The second problem addressed was the relative flame length of the medium- and low-Btu gases compared with natural gas. It was anticipated that flame length changes could affect the rate of heat transfer from the flame to the boiler tubes through a change in flame emissivity. If the flame length change resulted in a lower heat removal within the boiler, the combustion products entering the secondary superheater would be at a higher than normal temperature. This condition could result in tube damage or a loss in efficiency, because the convective section would be undersized. Using the burner and furnace operating conditions outlined for the baseline tests, flame length measurements were made as a function of vane angle for each test gas. In each case, measurements were taken only after the exit-gas and furnace-wall temperatures had stabilized. As stated above, a straight nozzle was used with a diameter giving a fuel velocity of 100 ft/s. The criterion for evaluating the end of the flame was when 1% of the total gas-sample volume was combustibles.

The third problem to be answered by this program was what the changes in efficiency – that is, the fraction of total enthalpy input transferred to the load – would be when retrofitting a unit designed for natural gas with a medium- or low-Btu gas. Detailed temperature and emissivity data were collected for each test gas. These measurements provide not only the information needed to evaluate changes in efficiency within the boiler but also the data that can be used by manufacturers to calculate any redesign that may be needed in the convective

passes. These data are presented and discussed, and calculation methods are presented in the "RESULTS" section of this report.

The final question addressed by the program was the level of NO emissions from each test fuel gas and how it compares with emissions from natural gas combustion. These data are presented in detail and analyzed in the "RESULTS" section.

RESULTS

During the flame stability trials, fuel-gas velocities from 25 ft/s up to 500 ft/s were investigated. The optimum fuel-gas injection velocity range was 75 to 200 ft/s. Above 200 ft/s the flame began to lift (detach) from the injector, and below 75 ft/s the flame became lazy and buoyed badly (moved toward the furnace roof). A velocity of 100 ft/s was selected for use throughout the program because the velocity could be maintained for the spectrum of fuel gases being studied using standard pipe sizes.

Figures 15 through 20 show photographs of the flame for each test gas.

FLAME LENGTHS

Table 3 presents the flame length data determined by radial scans at various points down the furnace axis. The end of the flame was defined as the point where 99% of the fuel was consumed. In general, the flame length decreased with increasing burner vane angle, except for the 60-degree angle natural gas and Wellman-Galusha air, which exhibited longer flames than the corresponding 45-degree burner vane angle. All medium- and low-Btu fuel-gas flames tested were shorter than the natural gas flames except Winkler air at a 45-degree vane angle, which was 21 cm longer than the natural gas flame produced with a 45-degree vane angle.

All gas temperature measurements reported were gathered using a suction pyrometer. The head of the pyrometer consisted of a thermocouple (Pt-Pt Rh 10%) protected by refractory radiation shields. These shields are fitted to the end of a water-cooled probe through which gases are sucked and the thermocouple wires passed. The efficiency of the pyrometer was determined to be 94%, using the technique presented by Land.¹

GAS TEMPERATURE MEASUREMENTS

In order to have a standard of comparison for the medium- and low-Btu gases, baseline data were collected for natural gas at seven axial positions for vane-

1. Land, T., Instrum. Autom. 29, (No. 7): 1956.



Figure 15. Natural gas flame using a 0.5-inch axial nozzle

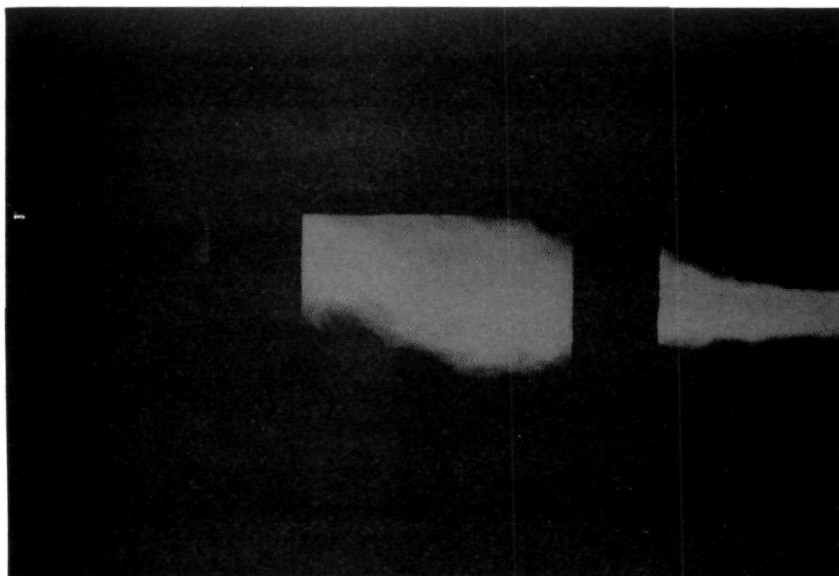


Figure 16. Lurgi oxygen gas flame using a 2-inch axial nozzle

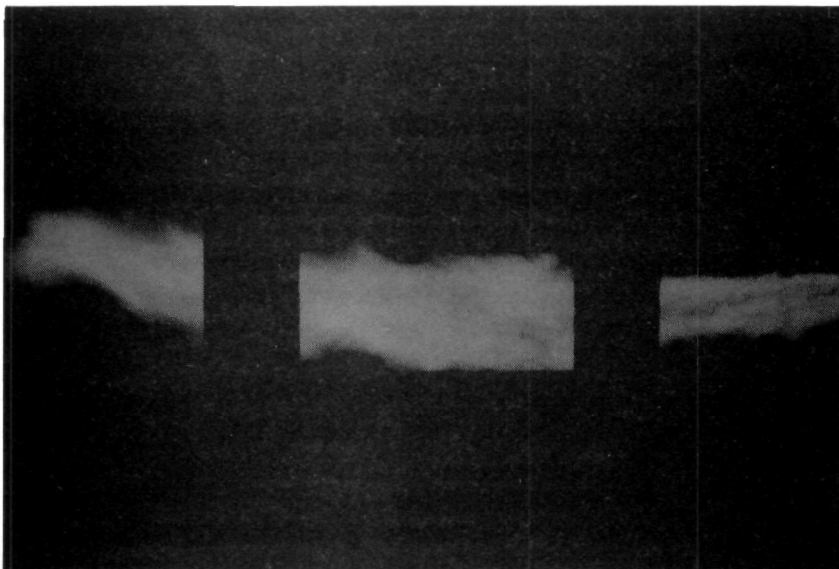


Figure 17. Winkler oxygen gas flame using a 2-inch axial nozzle

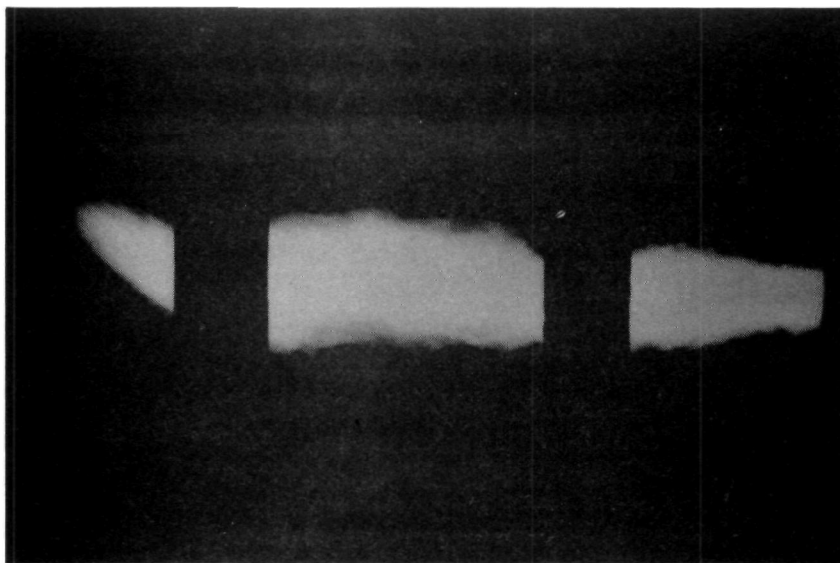


Figure 18. Koppers-Totzek oxygen gas flame
using a 2-inch axial nozzle

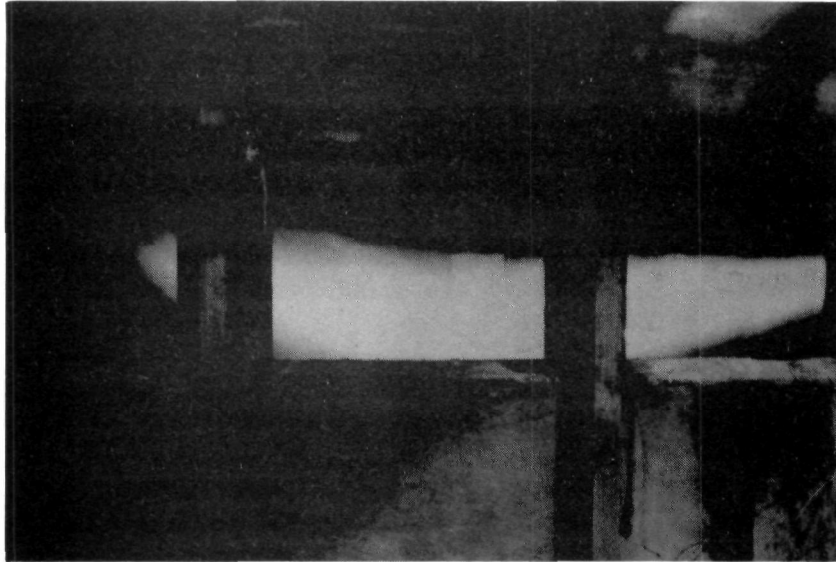


Figure 19. Wellman-Galusha air gas flame
using a 3-inch axial nozzle

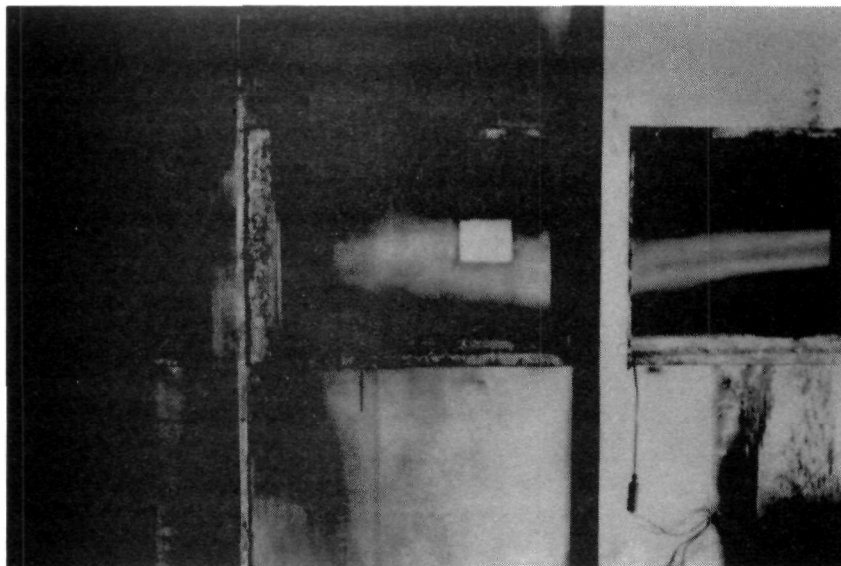


Figure 20. Winkler air gas flame using a 3-inch axial nozzle

Table 3. FLAME LENGTH (cm) AS A FUNCTION OF FUEL TYPE AND VANE ROTATION

Fuel	Vane angle			
	15°	30°	45°	60°
Natural gas	290	250	219	226
Lurgi oxygen	250	227	208	157
Winkler oxygen	250	208	188	146
Koppers-Totzek oxygen	281	208	188	156
Wellman-Galusha air	250	226	188	198
Winkler air	250	250	240	208

angle orientations of 15, 30, 45, and 60 degrees. These data are plotted in Figures 21 through 24. The axis of the flame was located at the 15.2-cm axial position by making several radial scans at different vertical positions. The flame center line was then confirmed by gas analysis. Selected profiles were measured several times to establish their integrity. Table 4 gives a list of rear-wall temperatures measured with an optical pyrometer and average flue-gas temperatures measured with the suction pyrometer at the 395.5-cm axial position as a function of vane-angle rotation for each of the gases studied. Table 4 also presents the maximum flame temperature measured and its axial position.

Lurgi oxygen gas temperature data are presented in Figures 25 through 28. Generally, the maximum average temperature is 112° to 363°F lower than those measured for natural gas. This difference reflects the 173°F lower adiabatic temperature of the Lurgi oxygen flame. Because of the complex wall-gas radiant flux equilibrium, this difference reduces to 21° to 110°F at the flue.

Winkler oxygen temperature profiles are shown in Figures 29 through 32, the adiabatic flame temperature of Winkler oxygen being up to 8°F lower than for natural gas. For the 15, 45, and 60-degree vane-angle rotations, Winkler oxygen has a lower maximum average temperature, between 14° and 113°F. The 30-degree vane rotation produces a maximum temperature 56°F higher than does natural gas. The flue temperatures, however, are higher than those measured for natural gas for the 15, 30, and 60-degree vane angles, with temperature differences in the range of 30° to 56°F.

Koppers-Totzek oxygen has a 241°F higher adiabatic flame temperature than natural gas. For all vane rotations, the Koppers-Totzek oxygen yielded higher maximum average temperatures than natural gas. The differences ranged between 70° and 322°F. These differences have been reduced to 1° to 60°F at the flue because of wall-gas equilibrium. These temperature profiles are shown in Figures 33 through 36.

The Wellman-Galusha air temperature profiles are presented in Figures 37 through 40. The maximum average gas temperature is 123° to 225°F lower than that measured for natural gas. This reflects the 389°F lower adiabatic flame temperature.

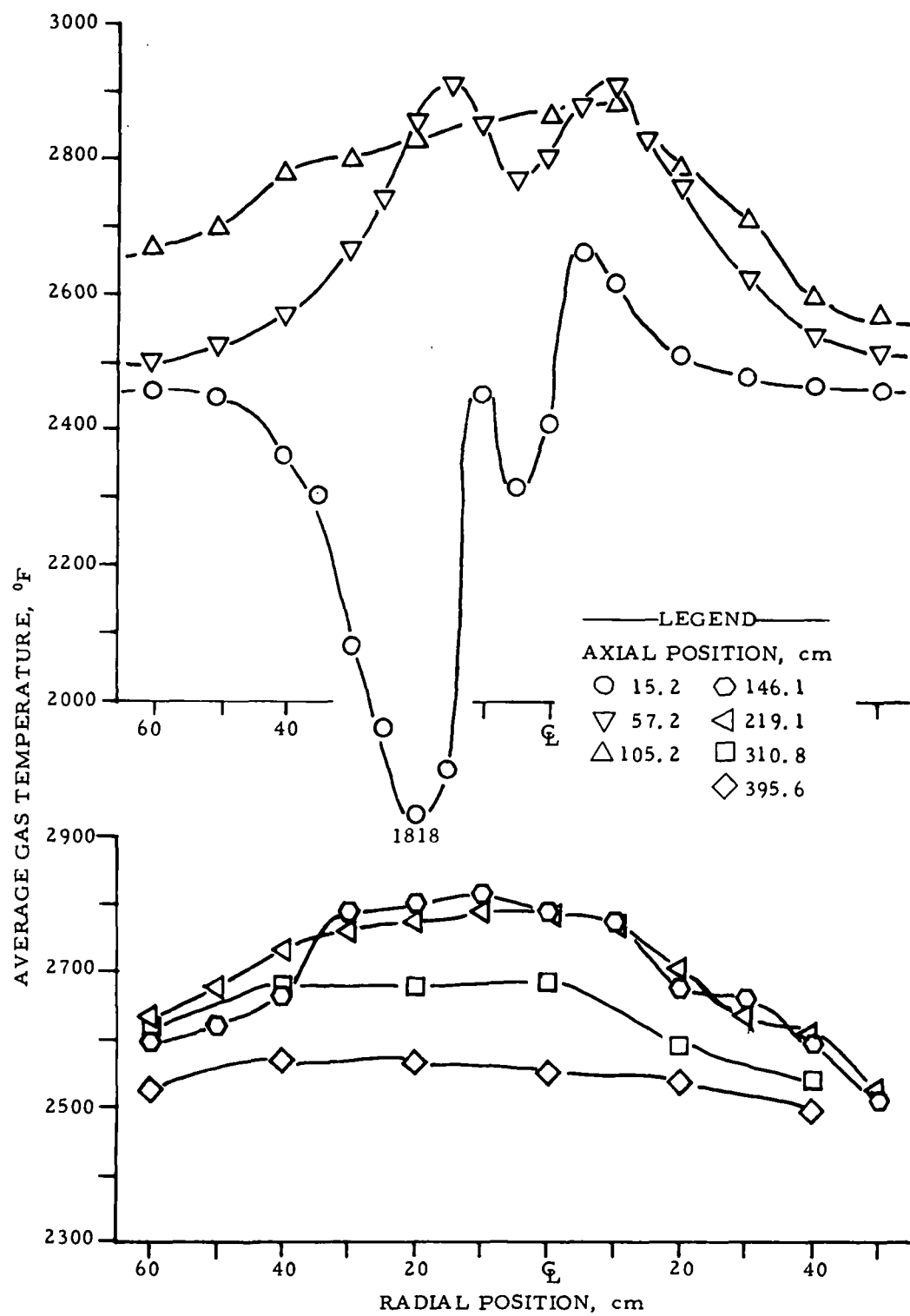


Figure 21. Average gas temperature profile for natural gas with a 15-degree vane rotation

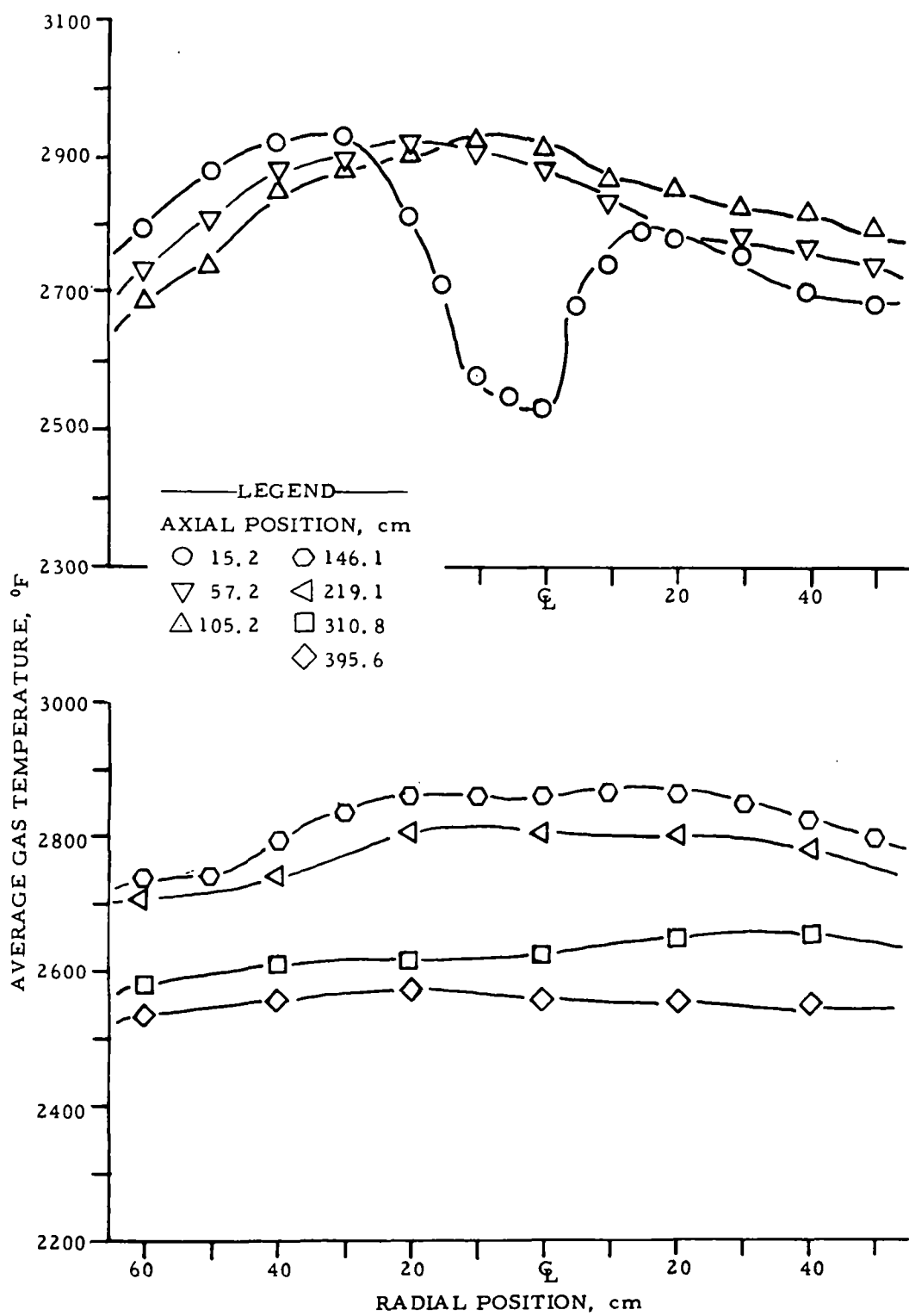


Figure 22. Average gas temperature profile for natural gas with a 30-degree vane rotation

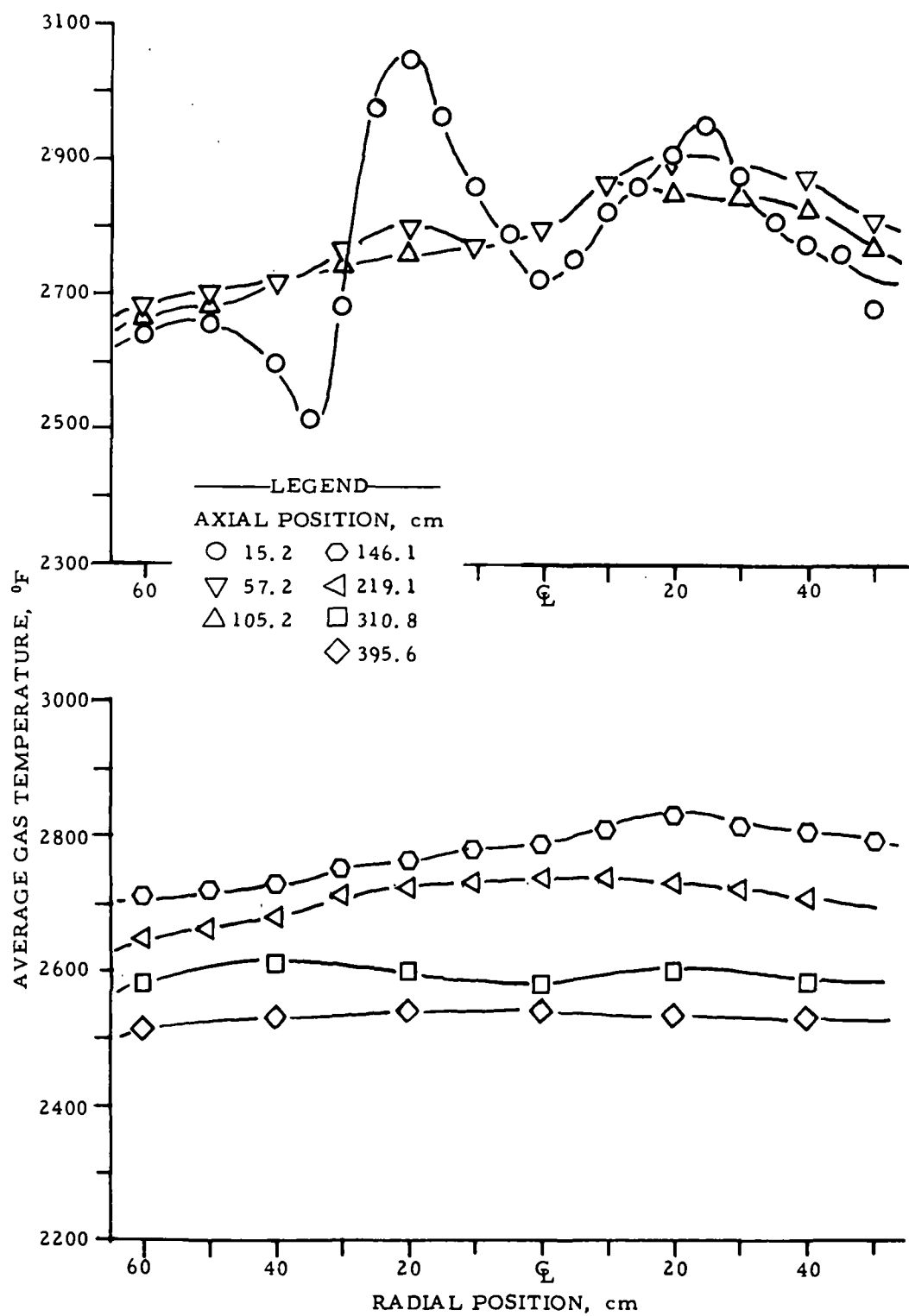


Figure 23. Average gas temperature profile for natural gas with a 45-degree vane rotation

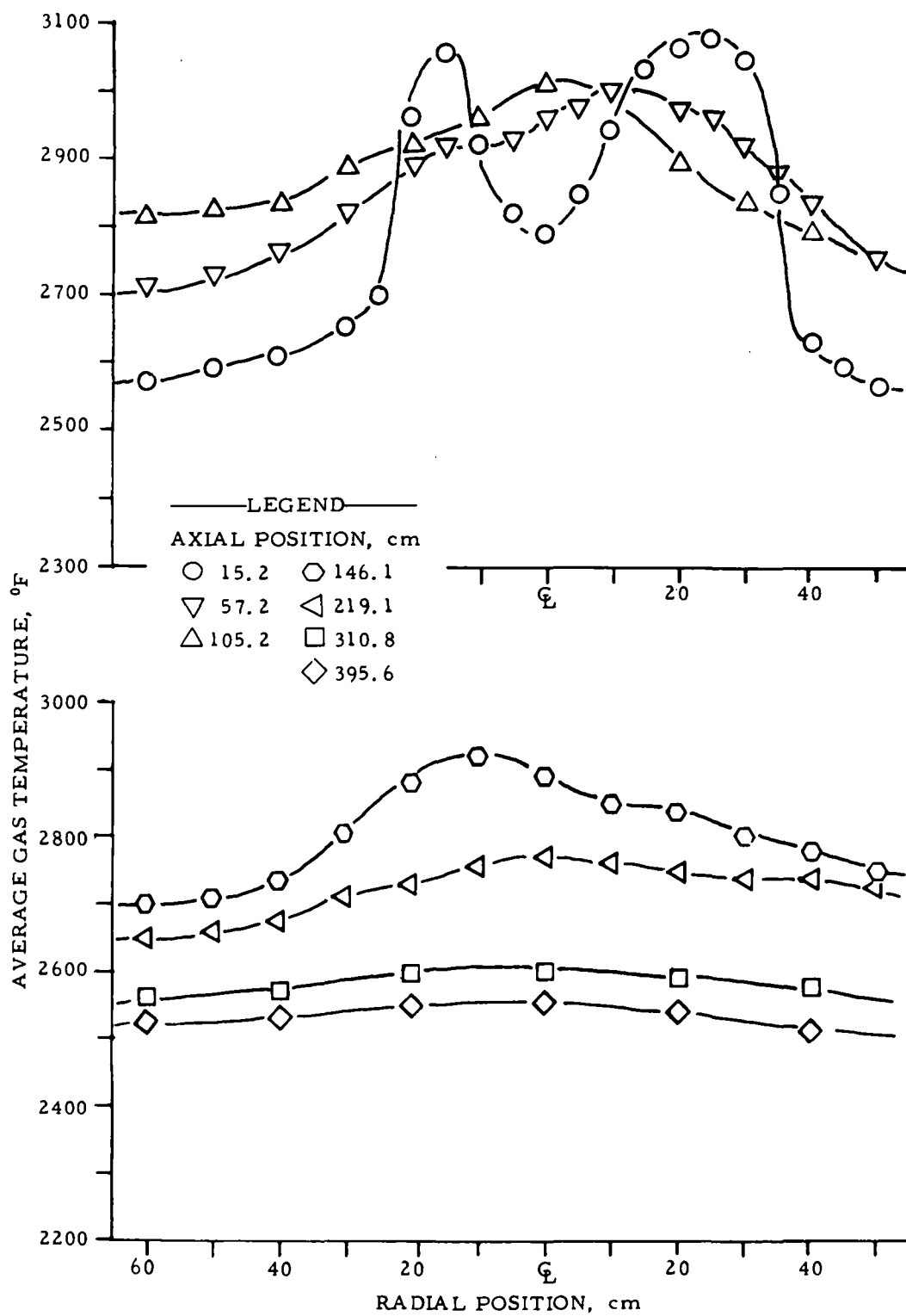


Figure 24. Average gas temperature profile for natural gas with a 60-degree vane rotation

**Table 4. SUMMARY OF AVERAGE GAS TEMPERATURE DATA
(Part 1)**

Fuel	Adiabatic flame temp	15°vane-angle rotation			Axial position, cm
		Wall	Flue	Max	
		°F			
Natural gas	3337	2300	2554	2918	57.2
Lurgi oxygen	3164	2238	2533	2723	146.1
Winkler oxygen	3329	2291	2610	2904	146.1
Koppers-Totzek oxygen	3578	2377	2606	2988	146.1
Wellman-Galusha air	2948	2129	2497	2795	146.1
Winkler air	2579	1886	2245	2515	146.1

**Table 4. SUMMARY OF AVERAGE GAS TEMPERATURE DATA
(Part 2)**

Fuel	30°vane-angle rotation			Axial position, cm
	Wall	Flue	Max	
	°F			
Natural gas	2371	2631	2918	57.2
Lurgi oxygen	2318	2454	2806	146.1
Winkler oxygen	2318	2567	2974	146.1
Koppers-Totzek oxygen	2372	2554	3240	146.1
Wellman-Galusha air	2129	2456	2737	146.1
Winkler air	1994	2345	2556	146.1

**Table 4. SUMMARY OF AVERAGE GAS TEMPERATURE DATA
(Part 3)**

Fuel	45°vane-angle rotation			Axial position, cm
	Wall	Flue	Max	
	°F			
Natural gas	2309	2553	3045	15.2
Lurgi oxygen	2300	2442	2682	57.2
Winkler oxygen	2309	2523	2932	57.2
Koppers-Totzek oxygen	2327	2554	3115	57.2
Wellman-Galusha air	2066	2434	2820	146.1
Winkler air	2012	2335	2556	146.1

**Table 4. SUMMARY OF AVERAGE GAS TEMPERATURE DATA
(Part 4)**

Fuel	60°vane-angle rotation			Axial position, cm
	Wall	Flue	Max	
	°F			
Natural gas	2345	2534	3087	15.2
Lurgi oxygen	2309	2460	2780	105.2
Winkler oxygen	2336	2564	3016	57.2
Koppers-Totzek oxygen	2372	2594	3254	105.2
Wellman-Galusha air	2147	2424	2877	105.2
Winkler air	2012	2306	2515	146.1

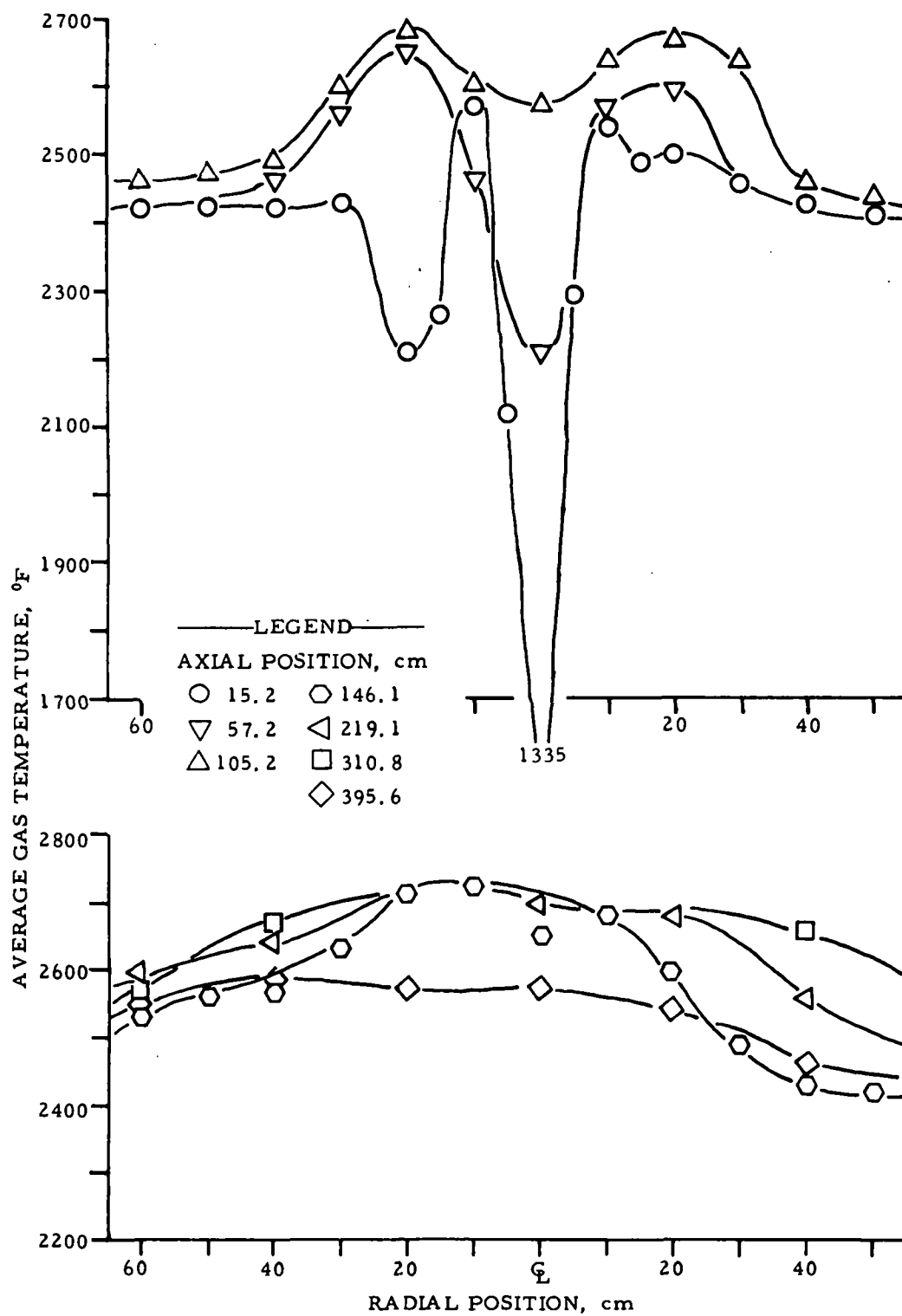


Figure 25. Average gas temperature profile for Lurgi oxygen gas with a 15-degree vane rotation

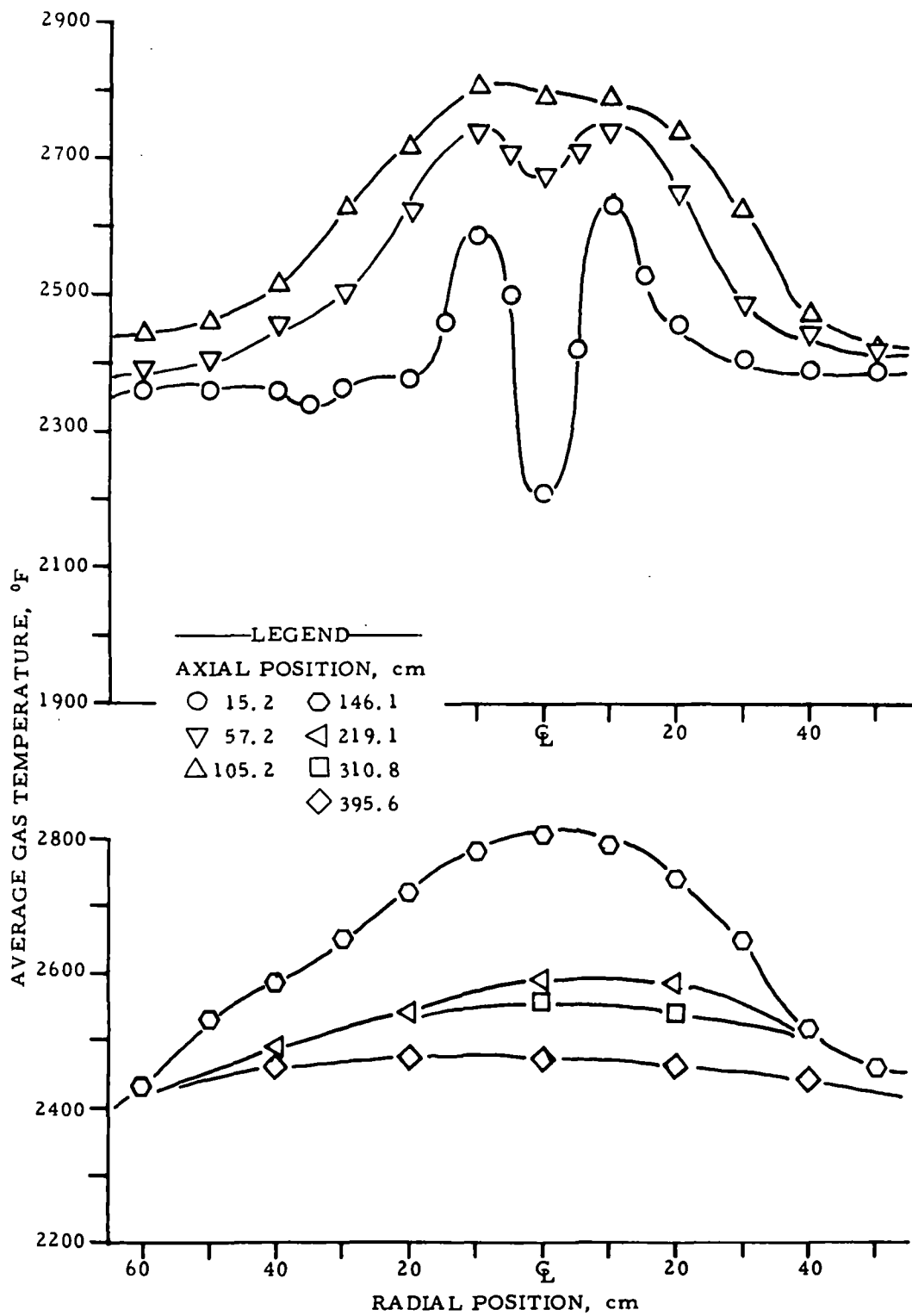


Figure 26. Average gas temperature profile for Lurgi oxygen gas with a 30-degree vane rotation

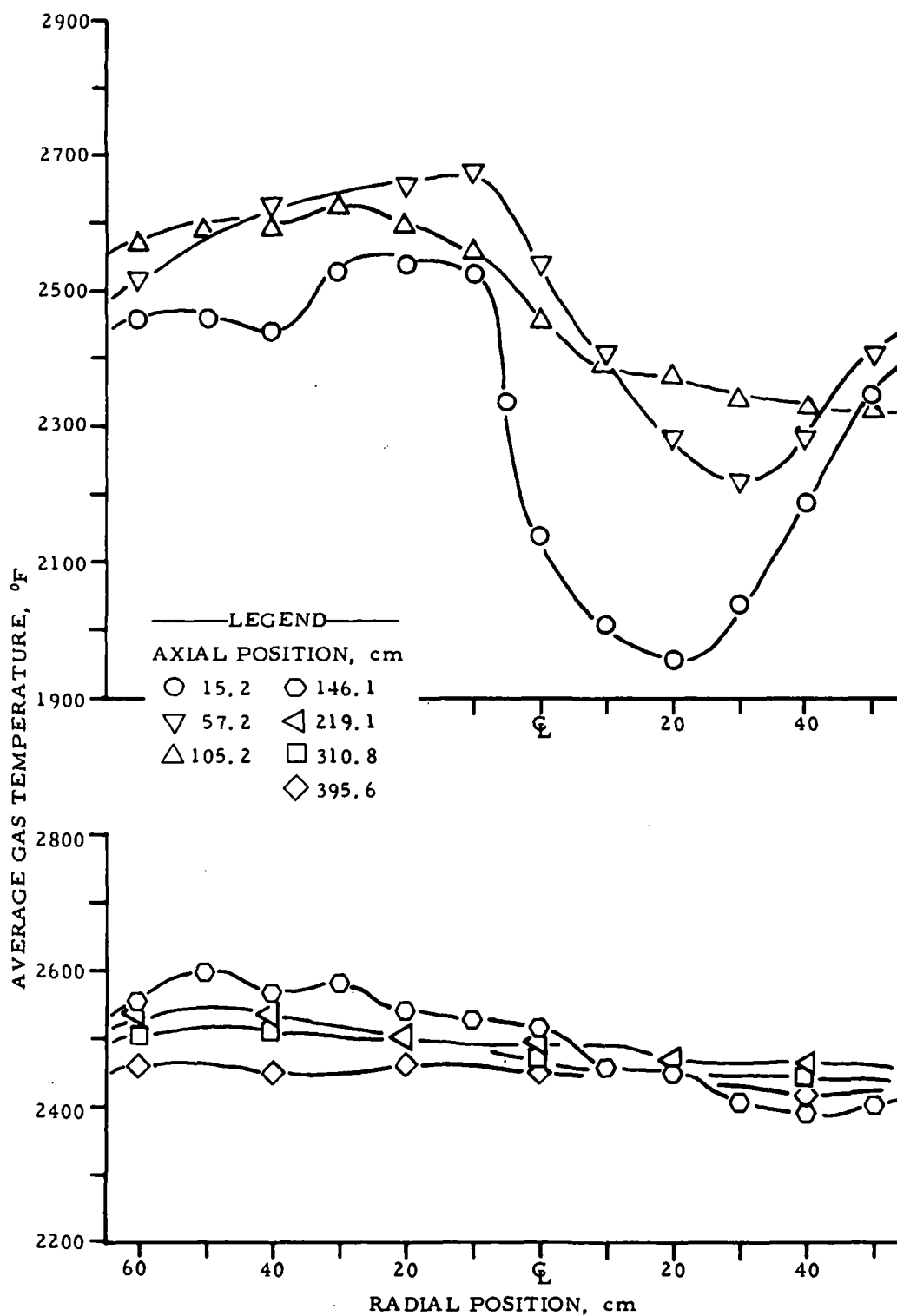


Figure 27. Average gas temperature profile for Lurgi oxygen gas with a 45-degree vane rotation

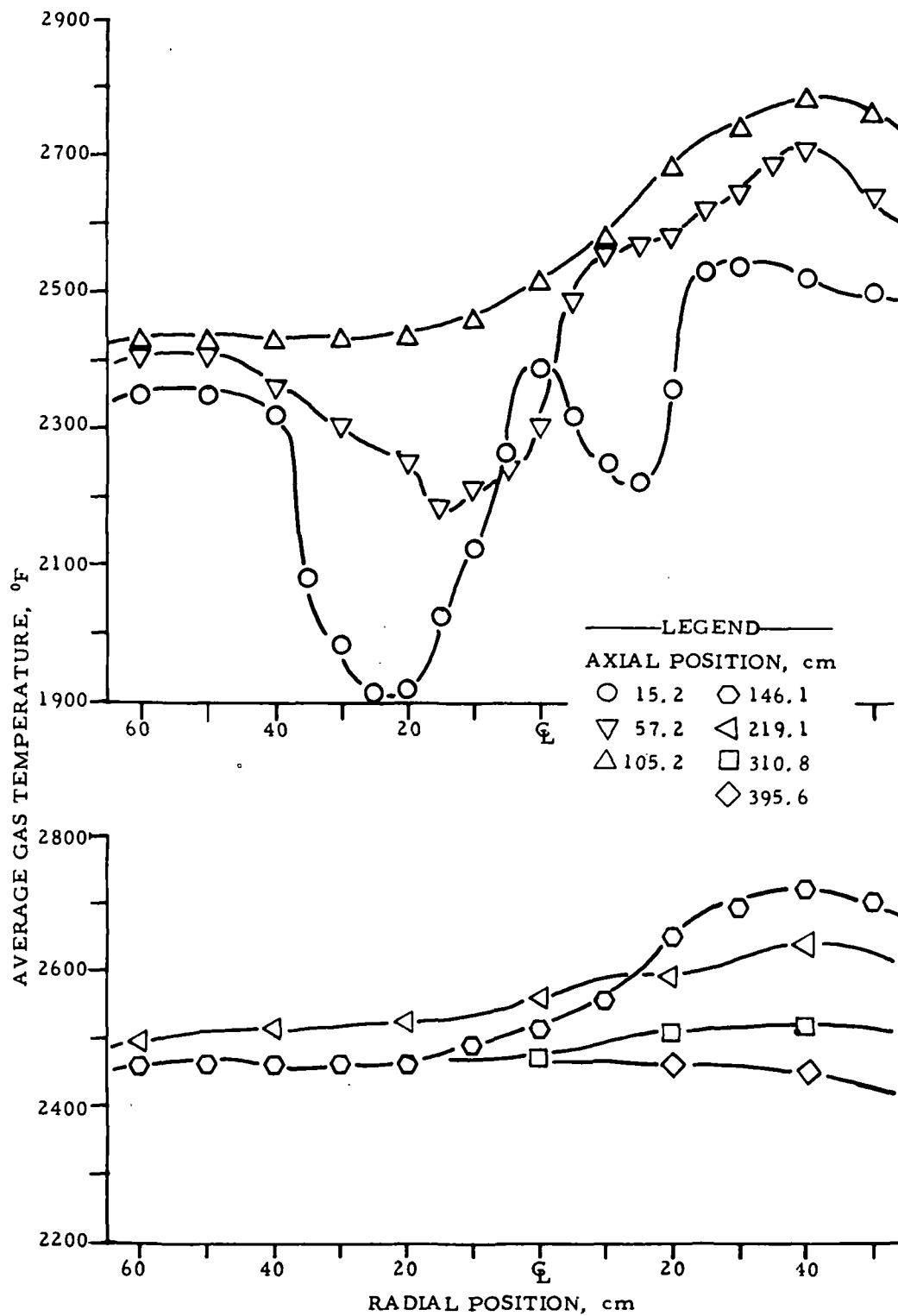


Figure 28. Average gas temperature profile for Lurgi oxygen gas with a 60-degree vane rotation

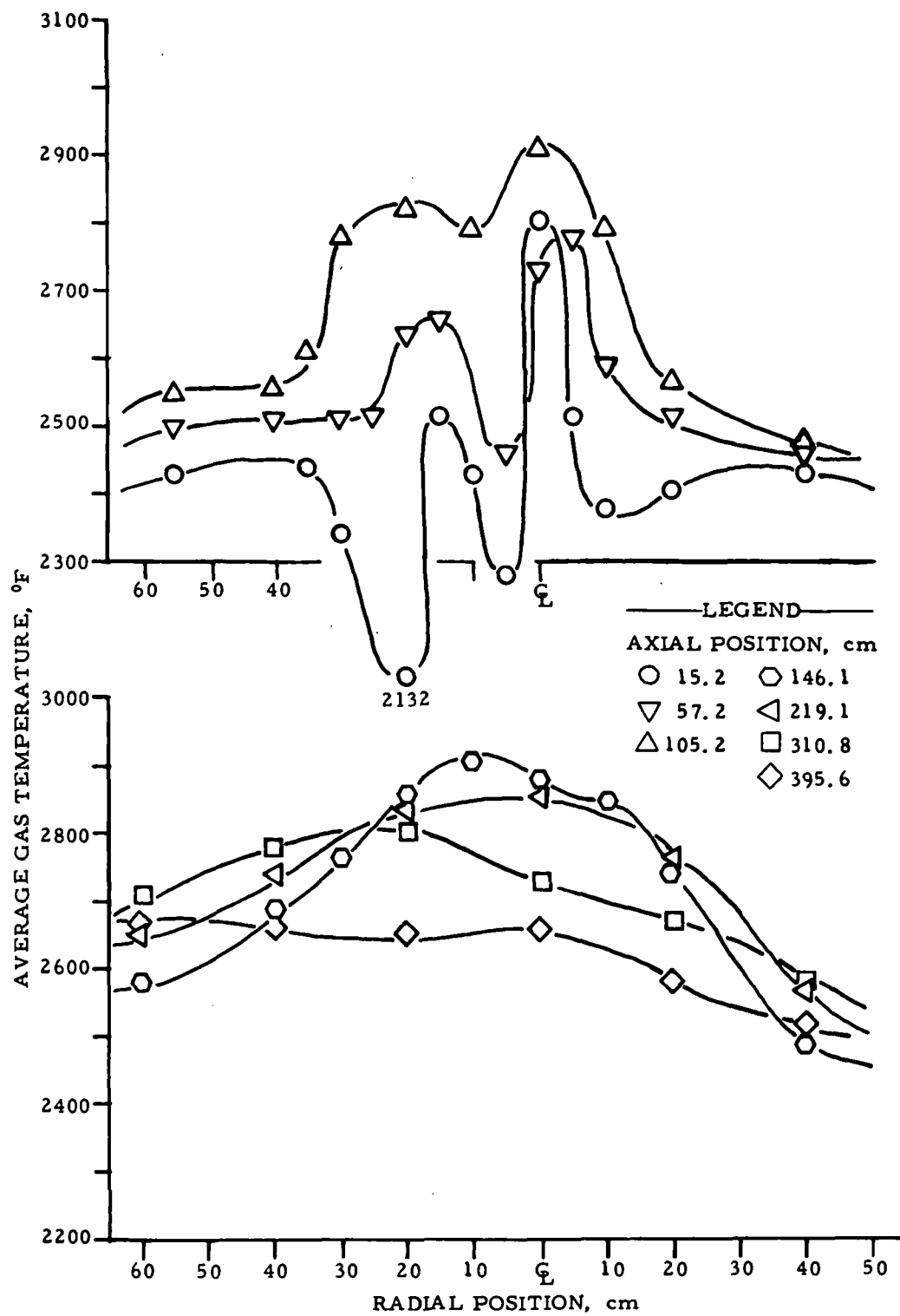


Figure 29. Average gas temperature profile for Winkler oxygen gas with a 15-degree vane rotation

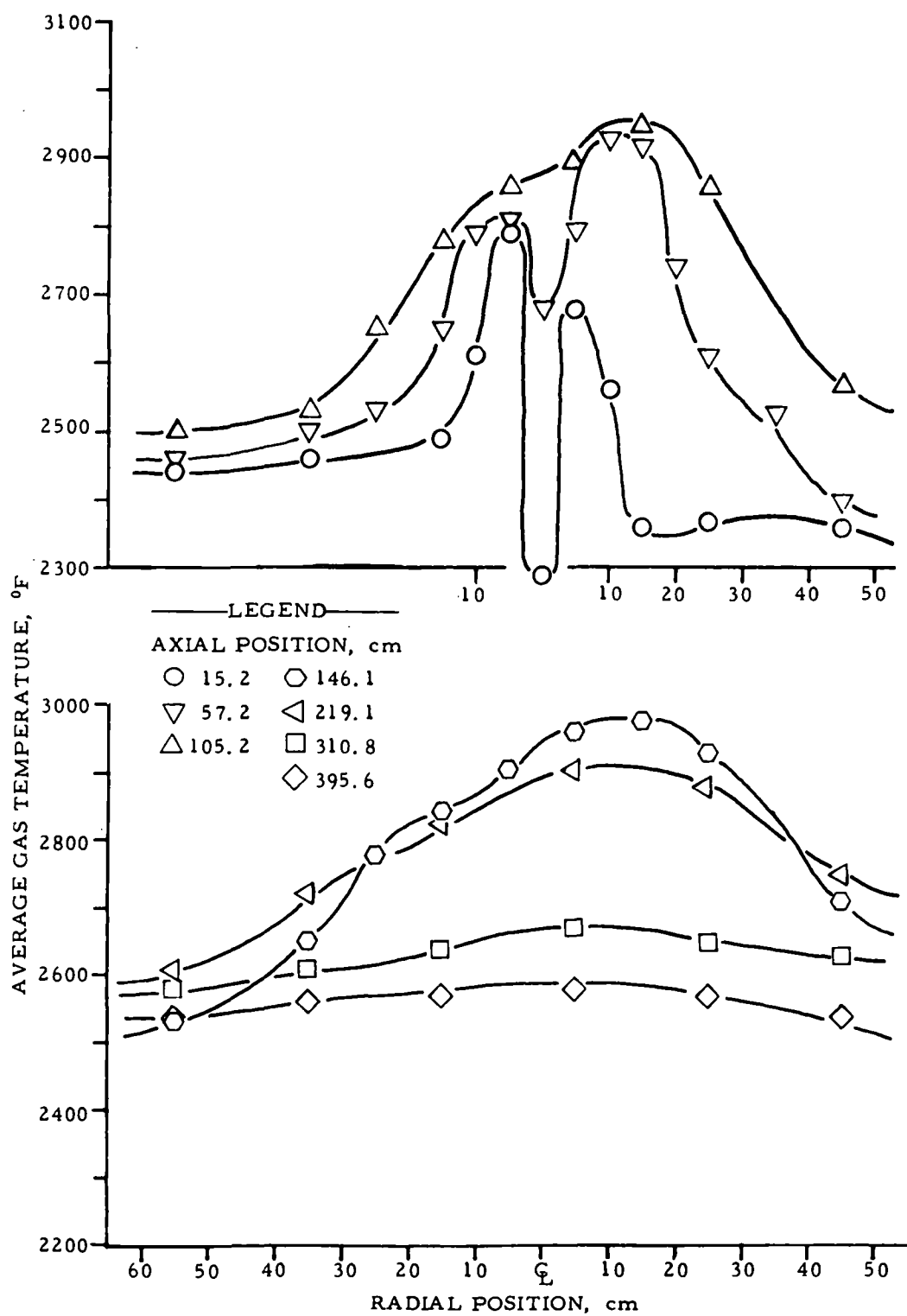


Figure 30. Average gas temperature profile for Winkler oxygen gas with a 30-degree vane rotation

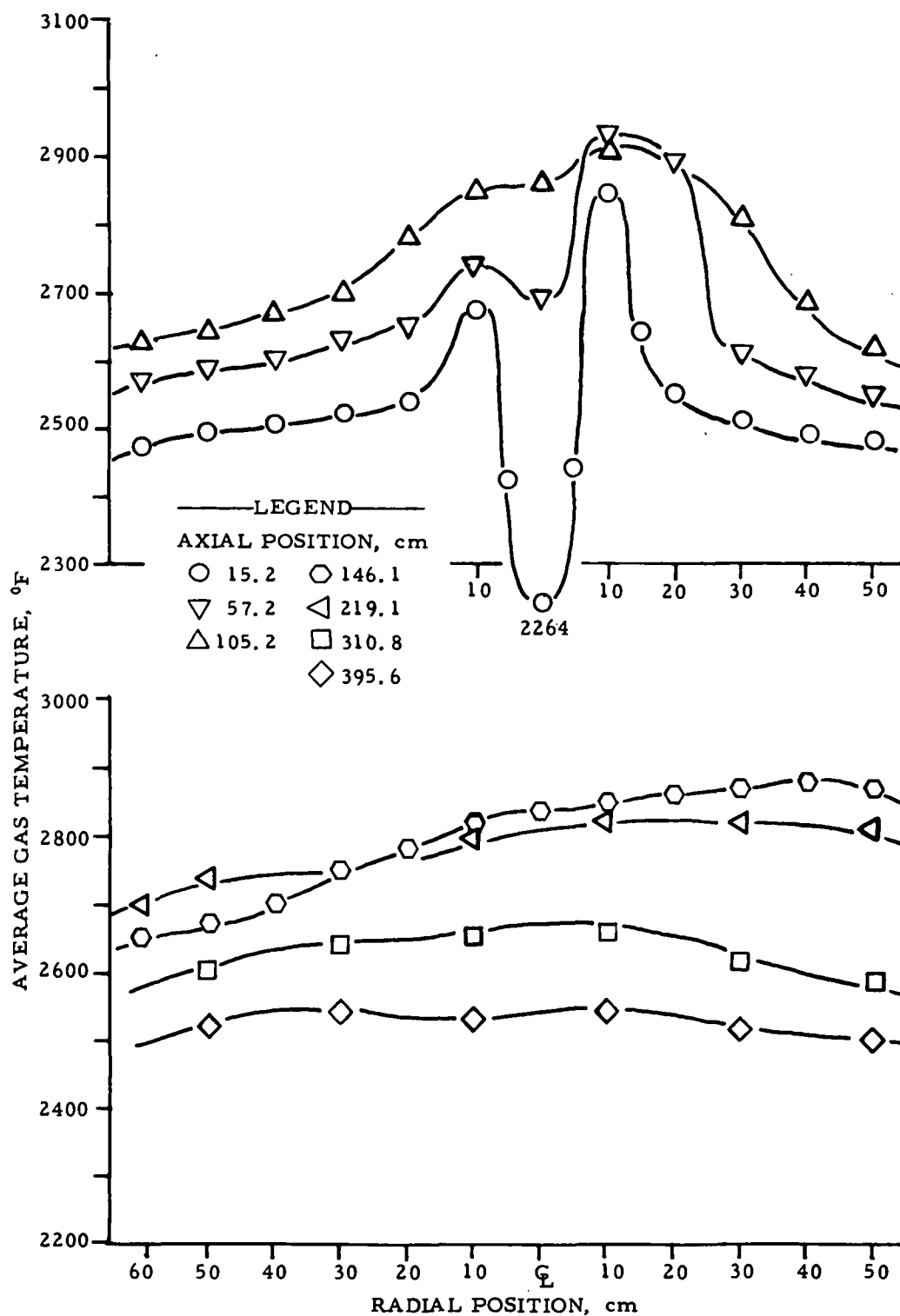


Figure 31. Average gas temperature profile for Winkler oxygen gas with a 45-degree vane rotation

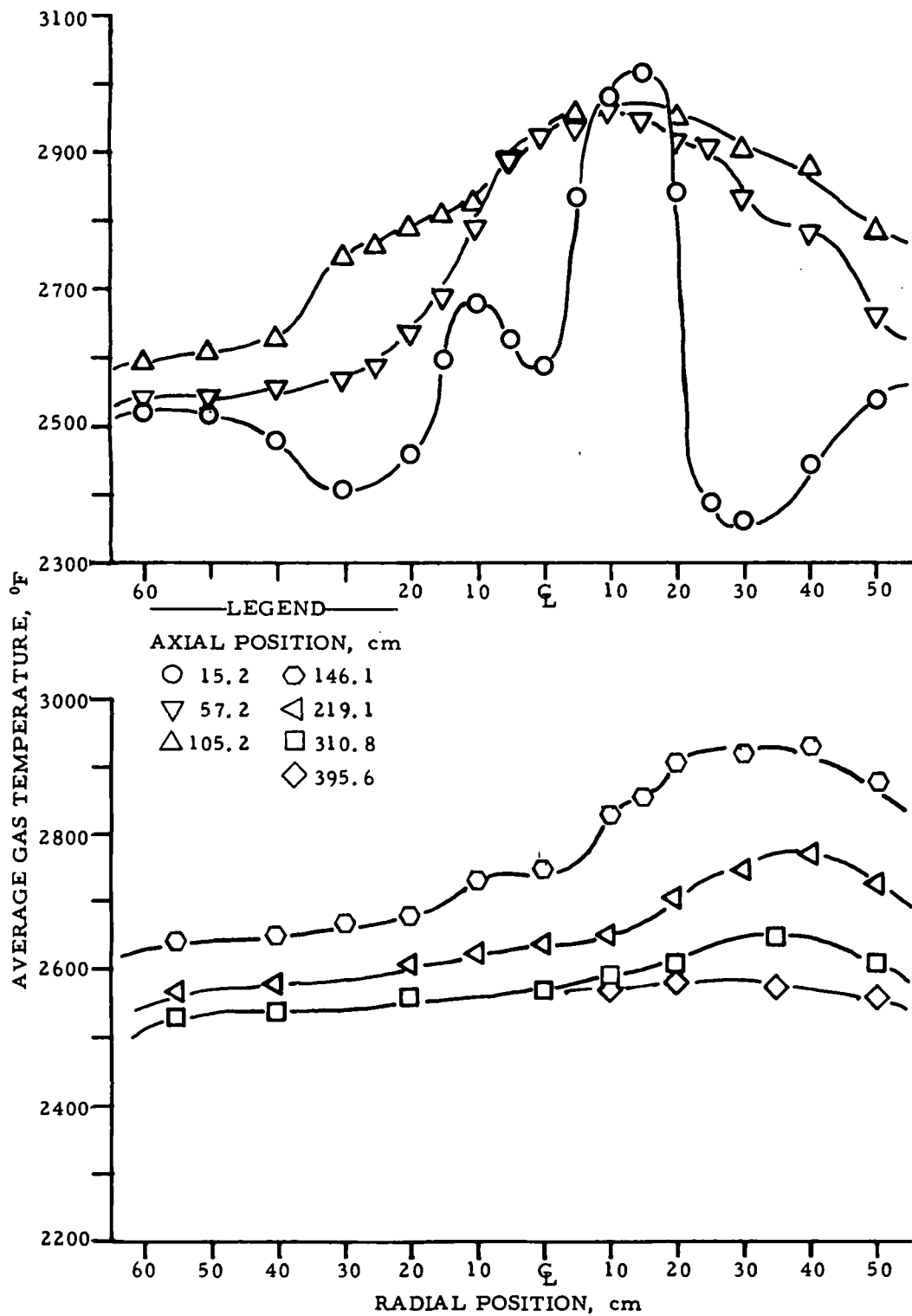


Figure 32. Average gas temperature profile for Winkler oxygen gas with a 60-degree vane rotation

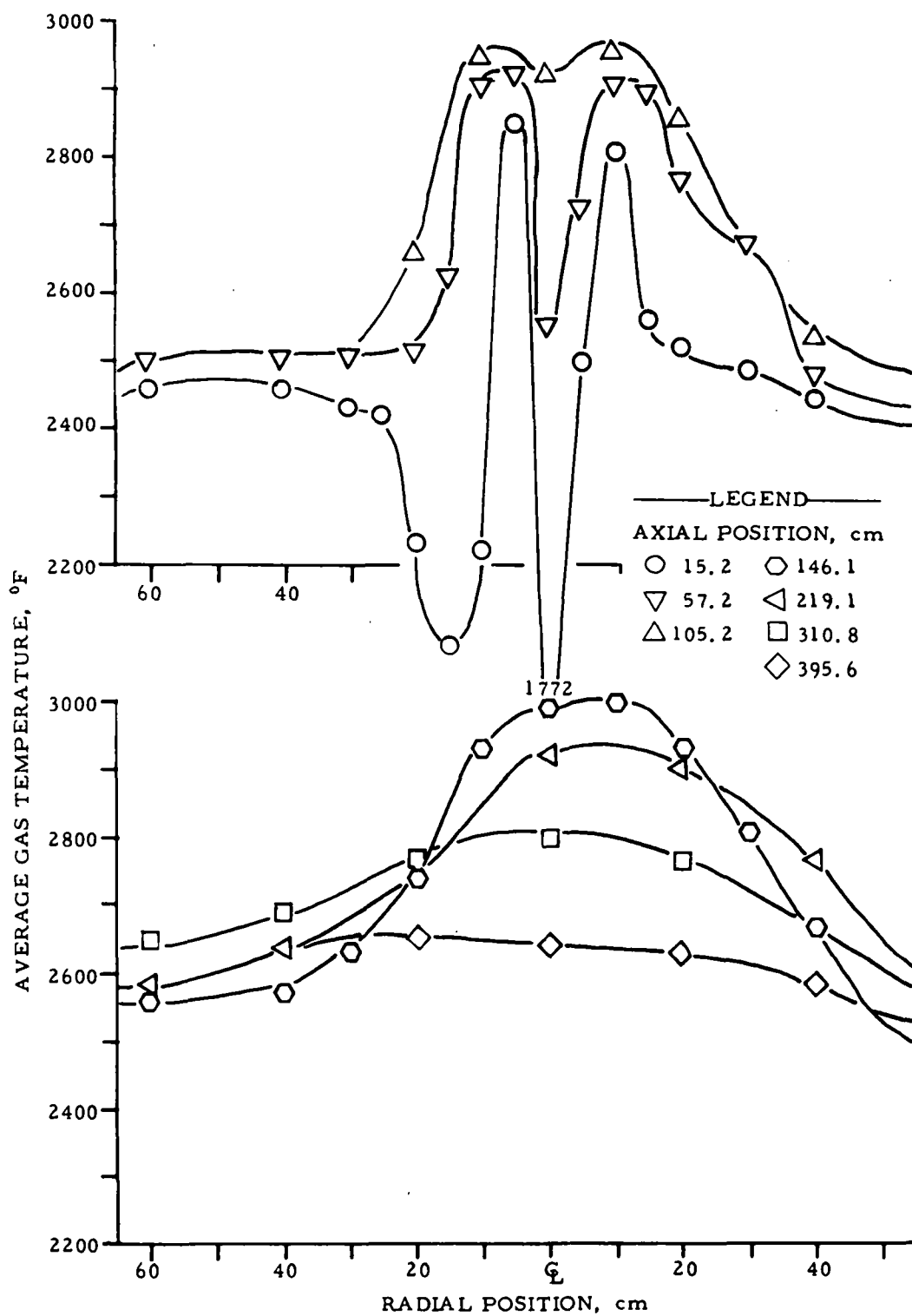


Figure 33. Average gas temperature profile for Koppers-Totzek oxygen gas with a 15-degree vane rotation

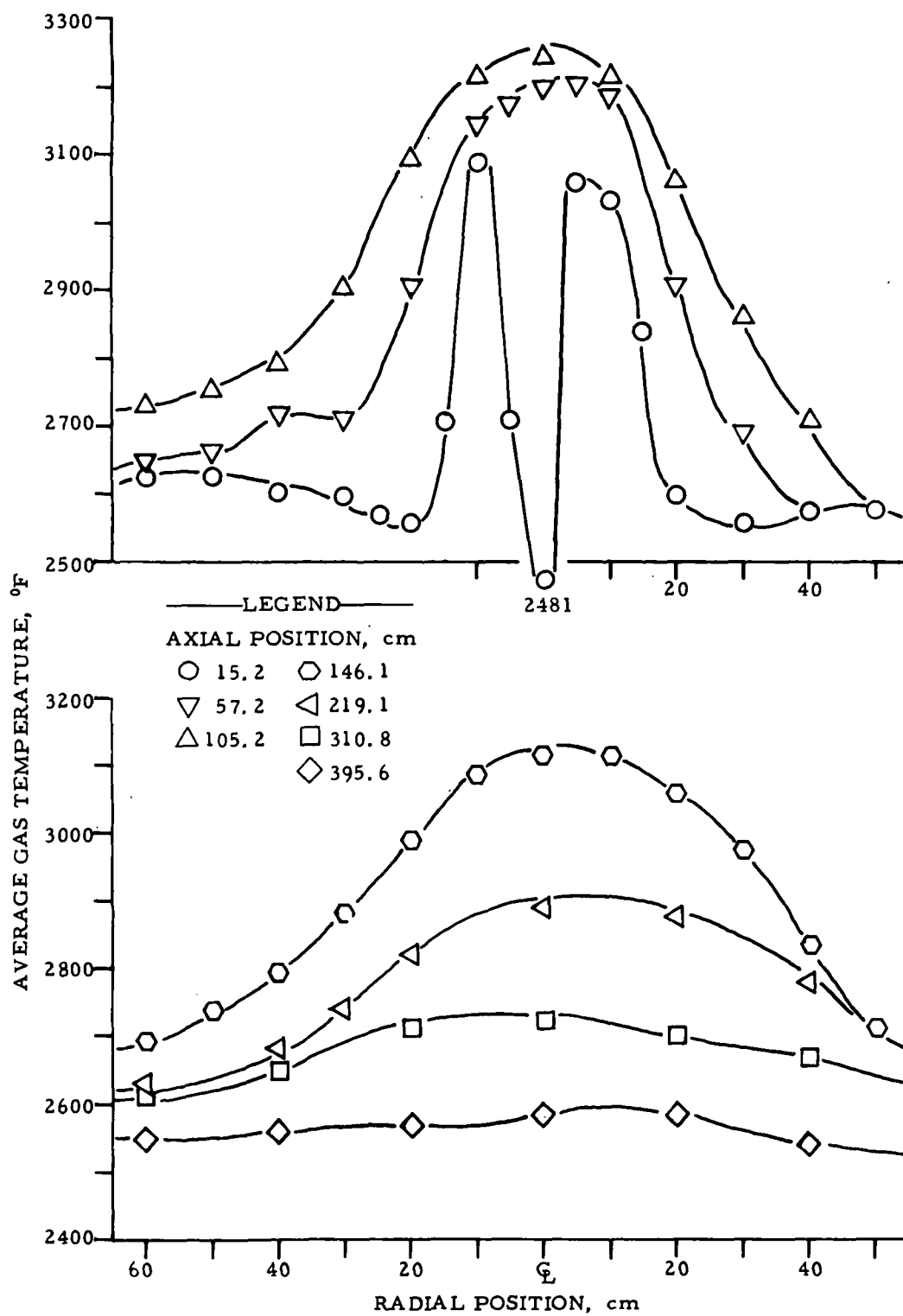


Figure 34. Average gas temperature profile for Koppers-Totzek oxygen gas with a 30-degree vane rotation

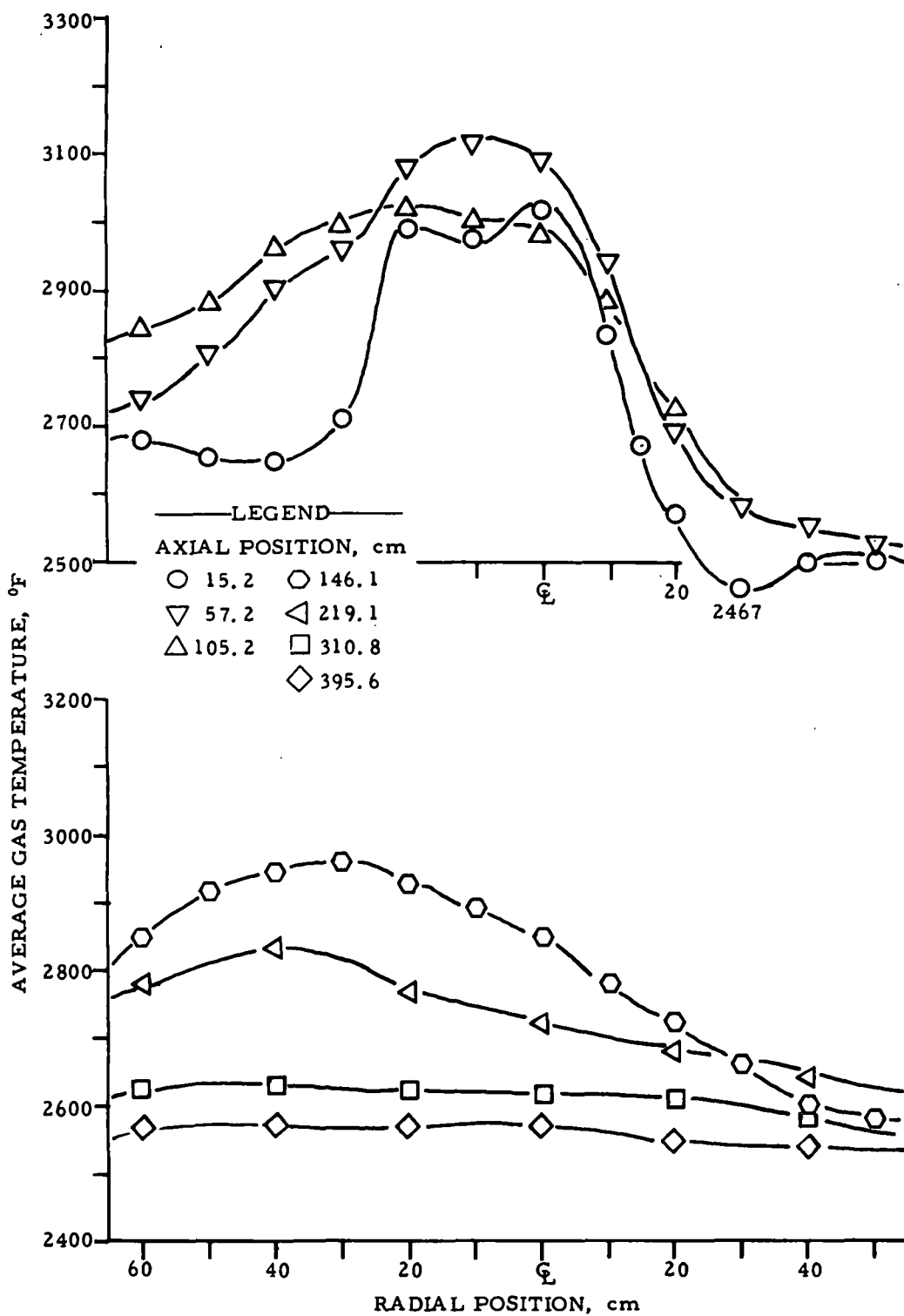


Figure 35. Average gas temperature profile for Koppers-Totzek oxygen gas with a 45-degree vane rotation

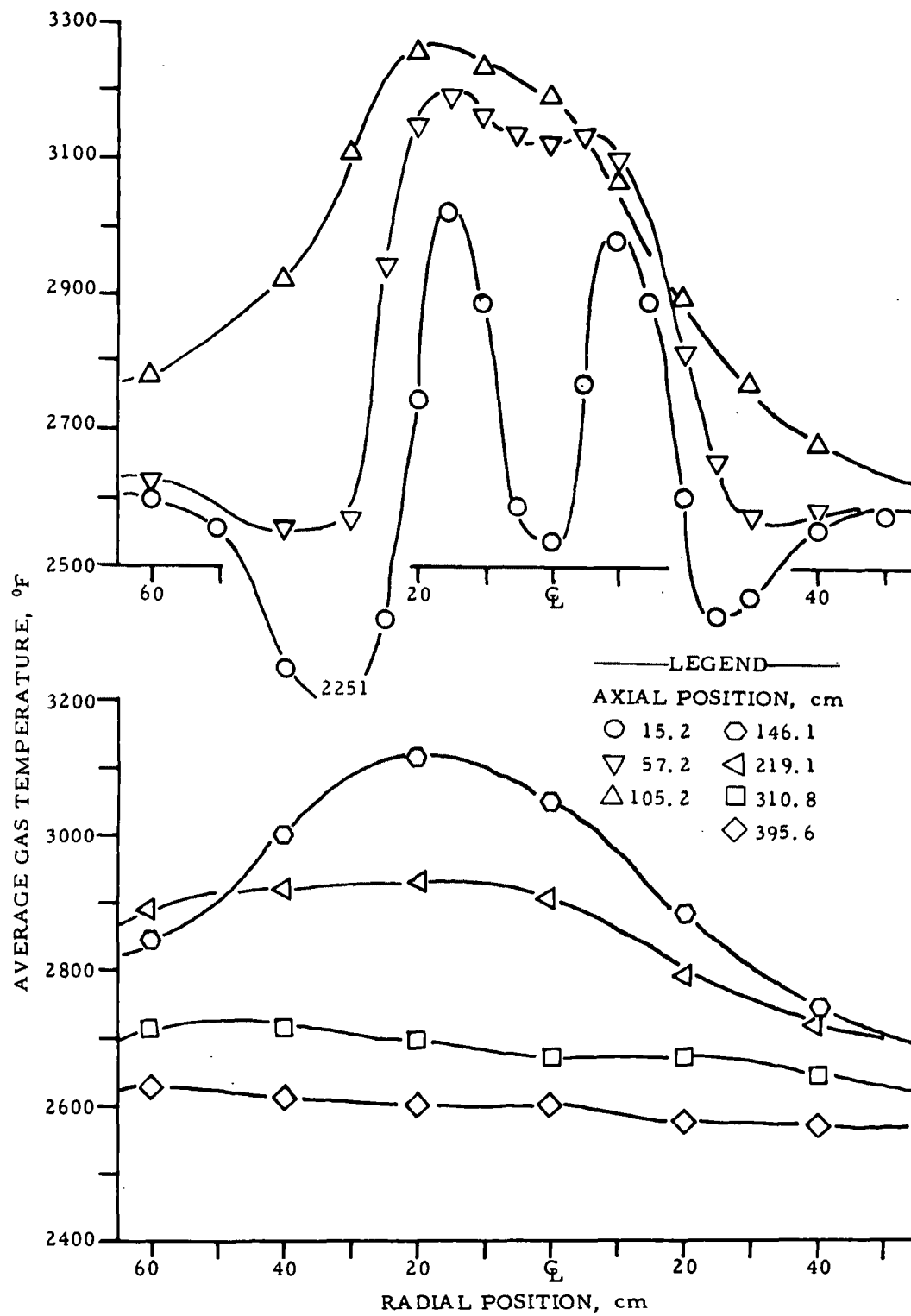


Figure 36. Average gas temperature profile for Koppers-Totzek oxygen gas with a 60-degree vane rotation

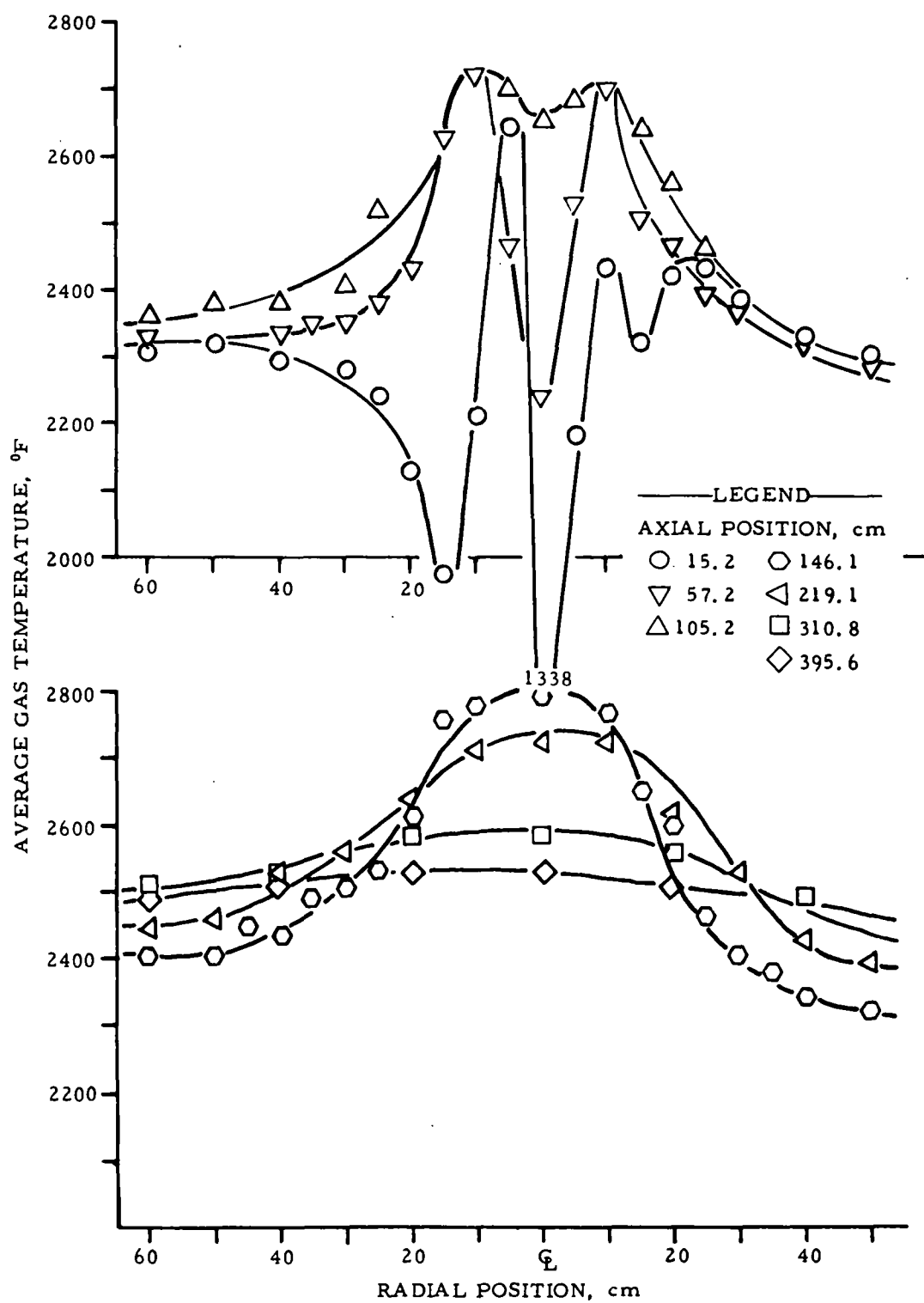


Figure 37. Average gas temperature profile for Wellman-Galusha air gas with a 15-degree vane rotation

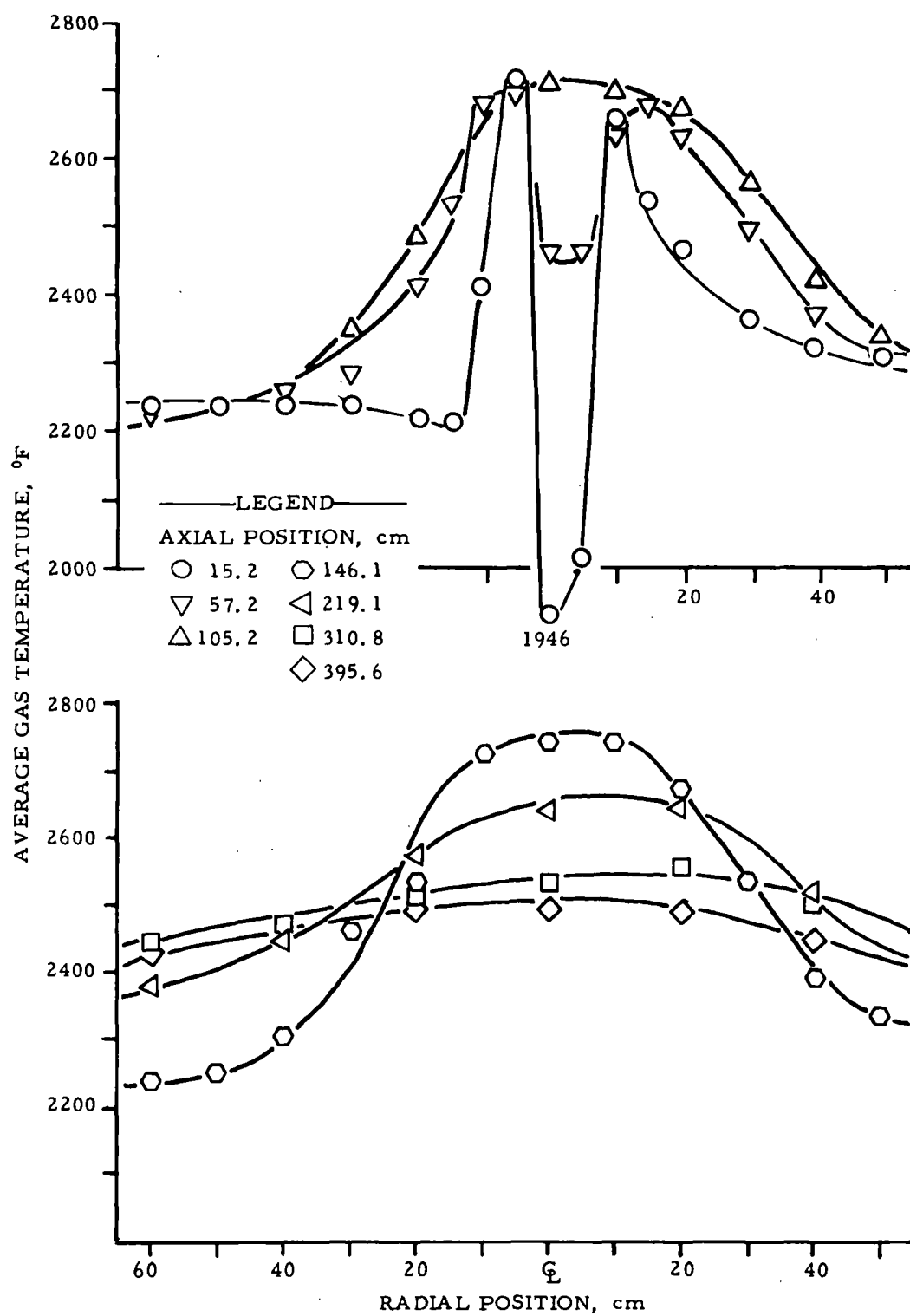


Figure 38. Average gas temperature profile for Wellman-Galusha air gas with a 30-degree vane rotation

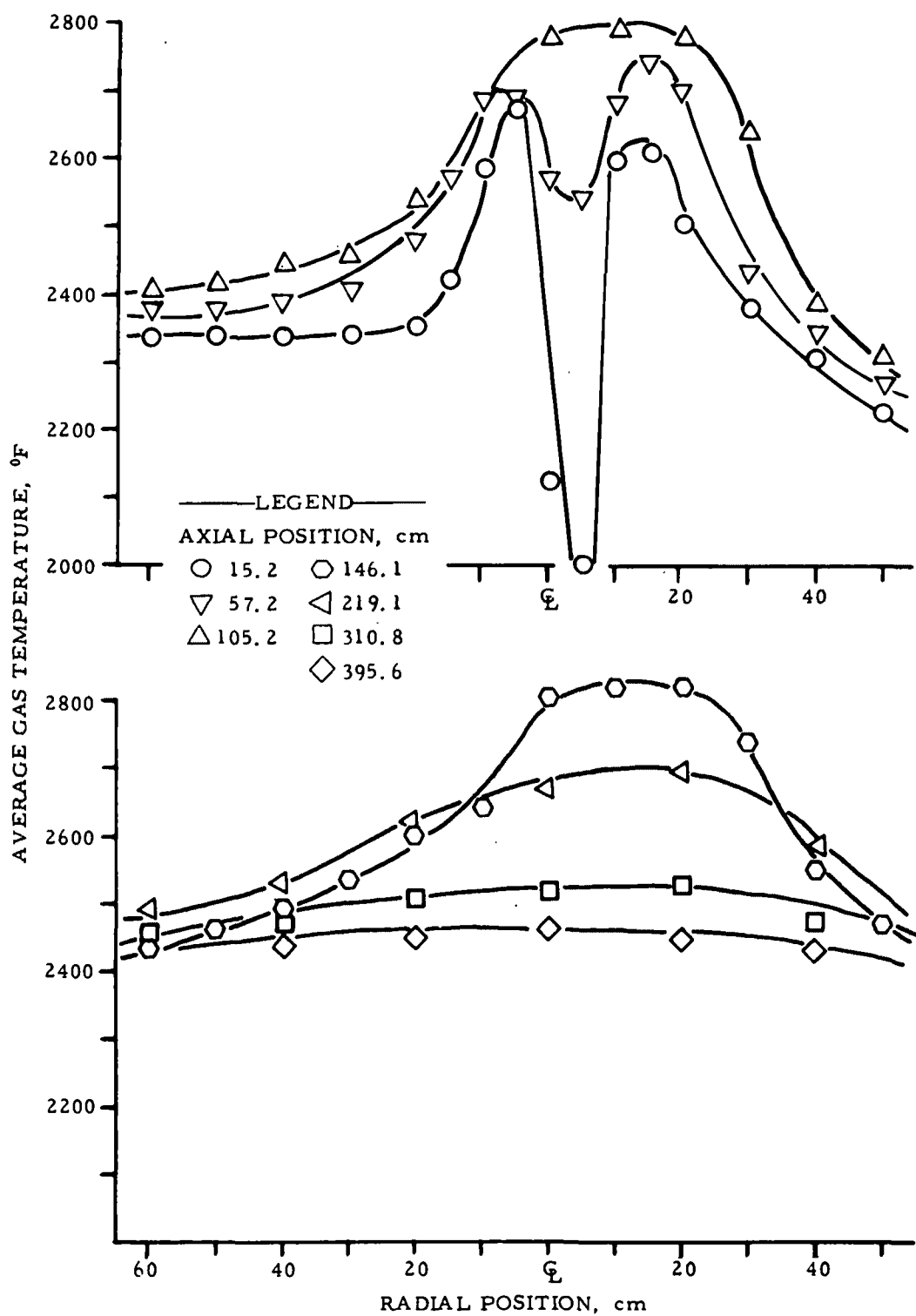


Figure 39. Average gas temperature profile for Wellman-Galusha air gas with a 45-degree vane rotation

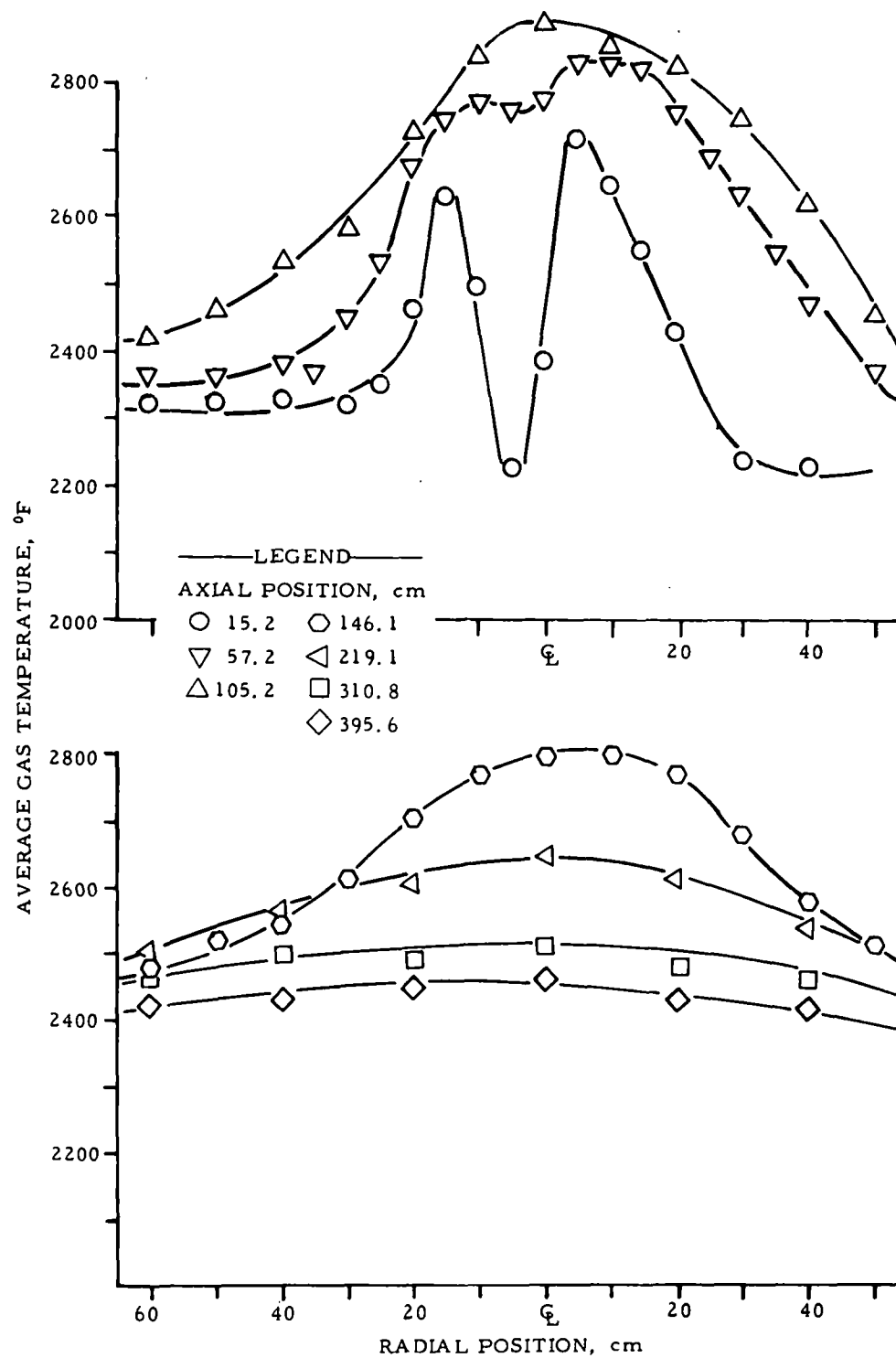


Figure 40. Average gas temperature profile for Wellman-Galusha air gas with a 60-degree vane rotation

The Winkler air temperature profiles are presented in Figures 41 through 44. This 116 Btu/CF gas's maximum average temperature is 362° to 572°F lower than that of natural gas, reflecting its 758°F lower adiabatic flame temperature. Both Wellman-Galusha air and Winkler air appear able to approach their adiabatic flame temperatures in conventional hot-wall combustion systems.

To maintain similar mixing between fuel and air, the inlet velocity gradient between the fuel and air jets was fixed. The fuel inlet velocity was approximately 100 ft/s, while the combustion air inlet velocity was 50 ft/s. This constant velocity ratio was maintained by increasing the diameter of the fuel injector. Increasing the nozzle diameter naturally increased the nozzle circumference and therefore the interaction area between the fuel and air. The interaction surface for natural gas is initially 3.14 inches, compared with 6.24 inches for the medium-Btu gases. The air/fuel ratio for stoichiometric combustion is also lower for the medium- and low-Btu gases than for natural gas. This, coupled with the larger interaction surface and the high flame speeds of the medium-Btu gases, would indicate a higher rate of combustion. However, for the 12 cases studied, although the flame lengths were generally shorter, the maximum average temperature was measured at larger axial positions when compared with natural gas for all medium- and low-Btu test conditions. For the 15, 30, and 45-degree vane angles, the axial position at which the maximum average temperature was measured was independent of medium-Btu fuel-gas type. This axial position was 146.1 cm for the 15 and 30-degree vane-angle rotation and decreased to 57.2 cm for a 45-degree rotation.

The interaction surface for Wellman-Galusha air gas was 6.87 inches, while for Winkler air it was 9.62 inches. These interaction surfaces are factors of 2.69 and 3.06, respectively, greater than that for natural gas. The resulting flame lengths were shorter than those measured for natural gas, except for Winkler air at the 30-degree vane angle, where they were equal, and at the 45-degree vane angle, where the Winkler air flame length was greater. The position of the maximum temperature for these gases was longer than for natural gas.

FLAME EMISSIVITY DETERMINATION

Using the pyroelectric radiometer with a 16-inch diameter cooling target, data were collected for evaluating gas absorptivity. The Schmidt method was

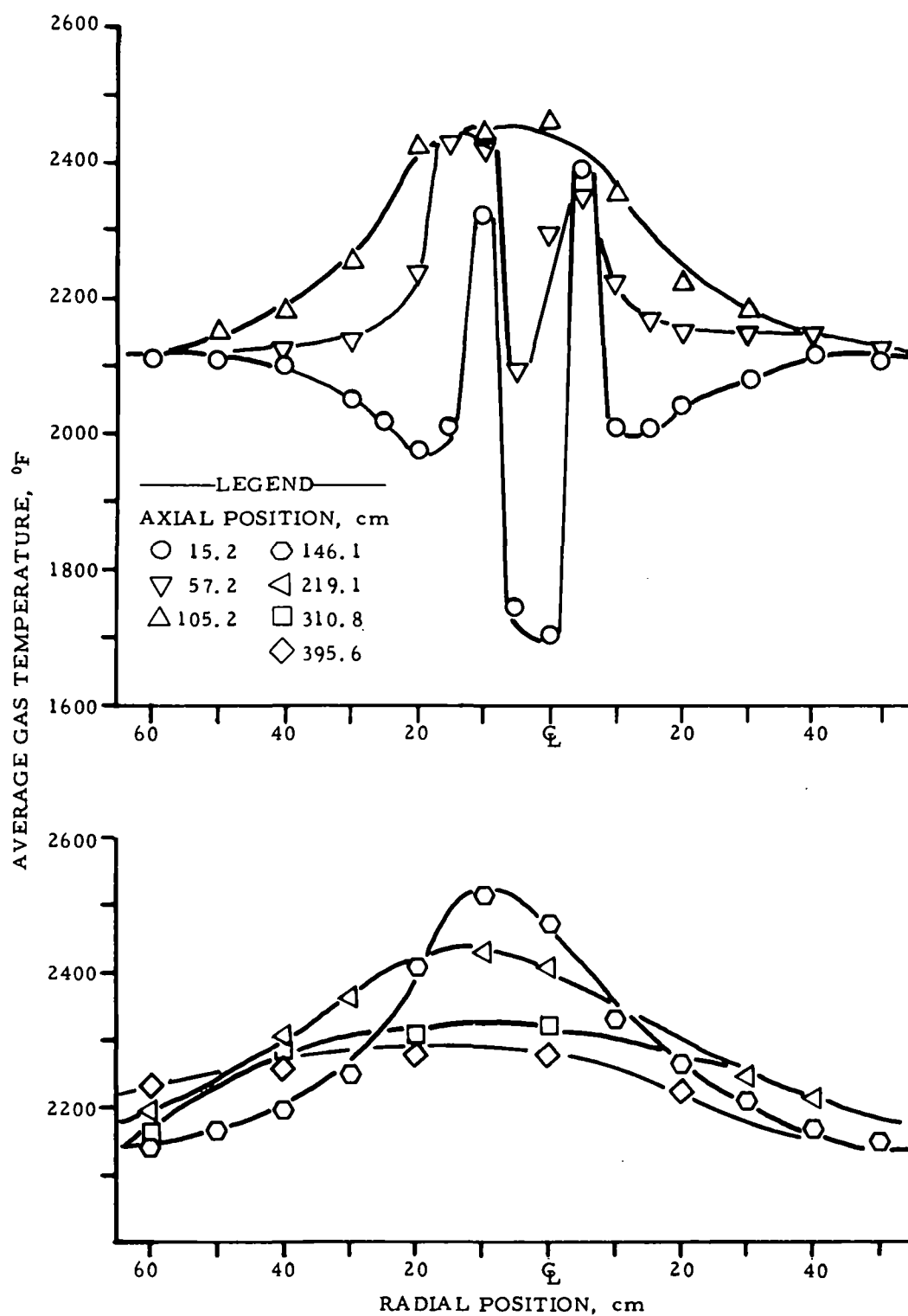


Figure 41. Average gas temperature profile for Winkler air gas with a 15-degree vane rotation

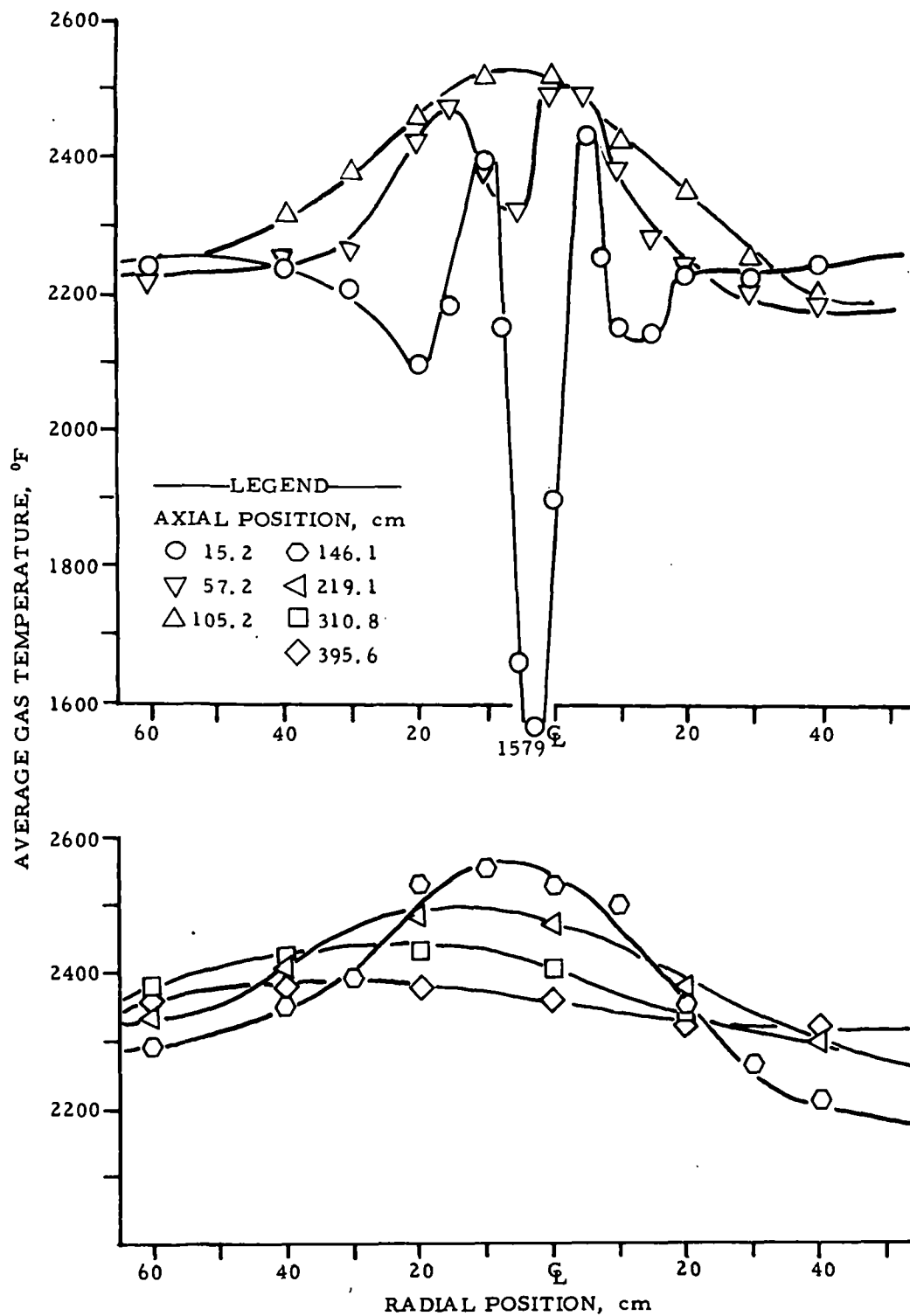


Figure 42. Average gas temperature profile for Winkler air gas with a 30-degree vane rotation

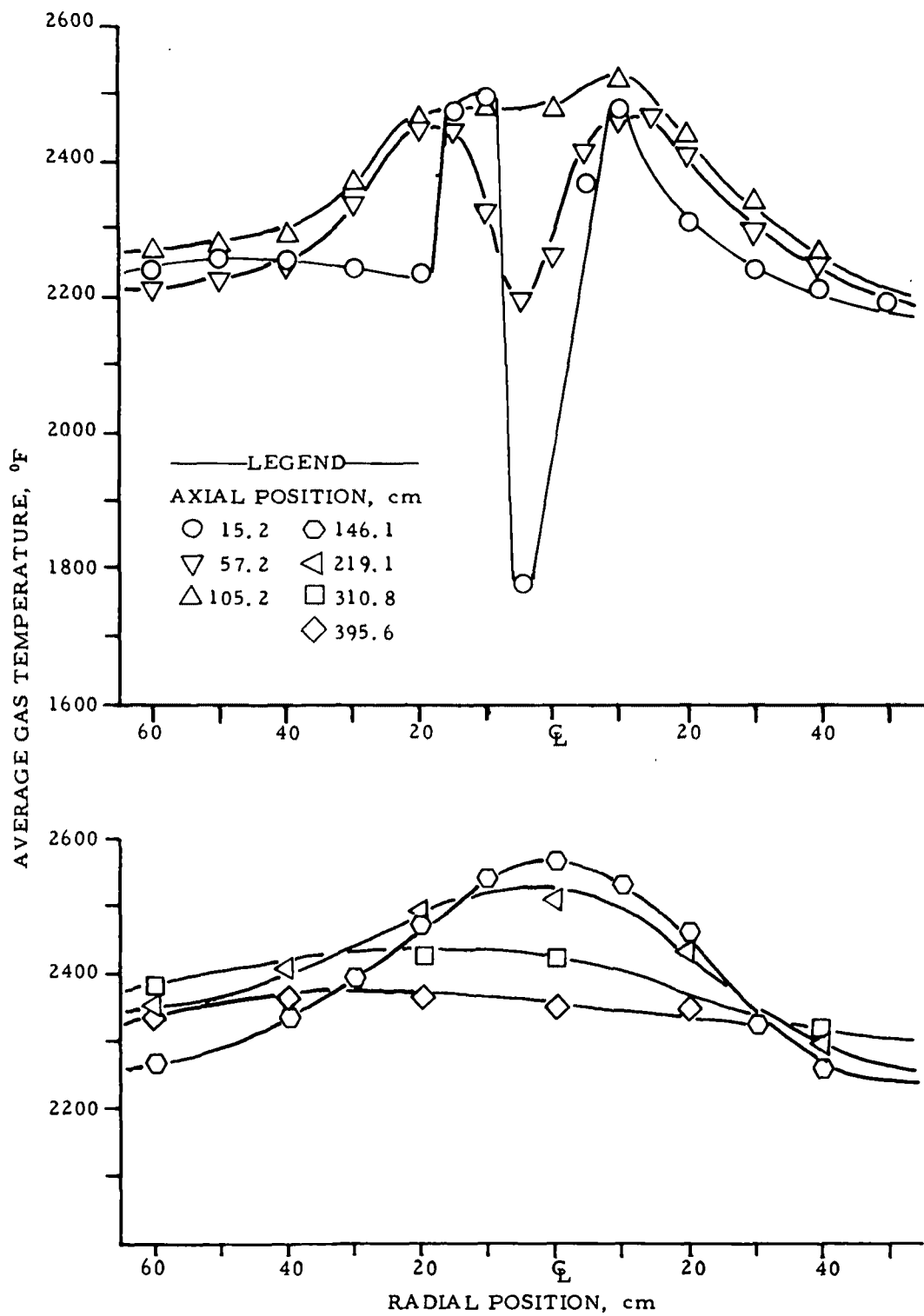


Figure 43. Average gas temperature profile for Winkler air gas with a 45-degree vane rotation

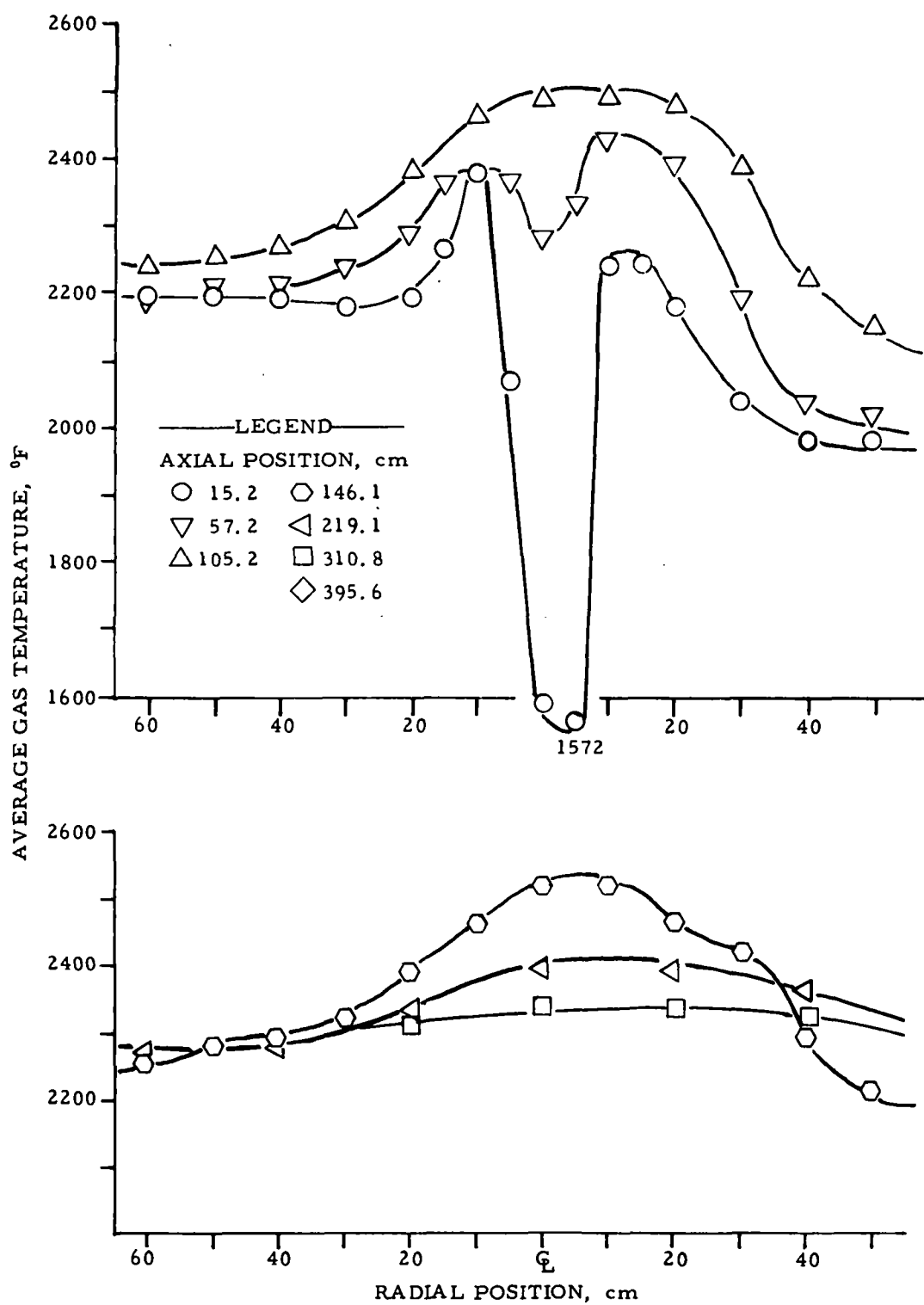


Figure 44. Average gas temperature profile for Winkler air gas with a 60-degree vane rotation

employed to reduce the measured data into absorptivities. The following measurements were made for each data point:

$$\begin{aligned} R_1 &= \text{radiation intensity of flame backed by a cold black target} \\ &= e_f E_f \end{aligned}$$

$$\begin{aligned} R_2 &= \text{radiation intensity of a hot black target} \\ &= E_r \end{aligned}$$

$$\begin{aligned} R_3 &= \text{radiation intensity of a flame backed by a hot black target} \\ &= e_f E_f + (1 - a_f) E_r \end{aligned}$$

where e_f is the flame emissivity, a_f is the flame absorptivity for radiation originating at the hot target, and E_f and E_r are the black body emissive powers (σT^4) at the flame and hot target temperatures. It follows that:

$$a_f = 1 - \frac{R_3 - R_1}{R_2}$$

As the target temperature T_r is usually colder than the flame temperature T_f , and given the properties of nonluminous flame radiation, it is expected that $a_f > e_f$. The relationship between a_f and e_f can be found in Hottel and Sarofim² as:

$$\frac{a_f}{e_f} = \left(\frac{T_r}{T_f} \right)^{a+b-c}$$

Values of $a+b-c$ can be estimated from Hottel and Sarofim's plots of CO_2 and H_2O .

R_2 is measured from a hot refractory surface that is not black; thus the measured radiation intensity contains reflected as well as emitted radiation. When sitting on a refractory of reflectivity ρ_r , one measures a leaving flux density W_r (the apparent emissive power) equal to the sum of the emitted radiation $e_r E_r$, and the reflected radiation $\rho_r H_r$ is the flux density incident on the refractory in question. When there is no flame, the value of H_r is simply the flux density W_r leaving the refractory surfaces viewed from the reference spot. When there is a flame, the

2. Hottel, H. C. and Sarofim, A. F., Radiative Transfer, 300, New York: McGraw-Hill, 1967.

value of H_r is equal to the sum of the flame radiation $\epsilon_f E_f$ and the radiation received from other refractory surfaces after attenuation by the flame $(1 - \epsilon_f) W_r$. The three measurements for the Schmidt are then:

1. Flame with cold black background: $R_1 = \epsilon_f E_f$
2. Hot refractory: $R_2 = W_r = \epsilon_r E_r + \rho_r H_r = \epsilon_r E_r + \rho_r W_r = E_r$
3. Flame backed by hot refractory: $R_3 = \epsilon_f E_f + (1 - \epsilon_f) W_r^*$

$$\begin{aligned}
 &= \epsilon_f E_f + (1 - \epsilon_f) [\epsilon_r E_r + \rho_r H_r] \\
 &= \epsilon_f E_f + (1 - \epsilon_f) \{ \epsilon_r E_r + \rho_r [\epsilon_f E_f + (1 - \epsilon_f) W_r^*] \} \\
 &= \epsilon_f E_f + (1 - \epsilon_f) \{ \epsilon_r E_r + \rho_r [\epsilon_f E_f + (1 - \epsilon_f) (\frac{\epsilon_r E_r + \rho_r \epsilon_f E_f}{1 - \rho_r (1 - \epsilon_f)})] \}
 \end{aligned}$$

Applying the Schmidt method as before:

$$a_f = 1 - \frac{R_3 - R_1}{R_2}$$

the following expression for absorptivity is derived:

$$\alpha_f = 1 - (1 - \epsilon_f) \{ \epsilon_r + \rho_r [\epsilon_f \frac{E_f}{E_r} + (1 - \epsilon_f) (\frac{(\epsilon_r + \rho_r \epsilon_f \frac{E_f}{E_r})}{1 - \rho_r (1 - \epsilon_f)})] \} \quad (1)$$

To quantify the refractory reflectivity, the radiometer was sited on a hot refractory furnace sidewall through the general probe holder (Figure 11) and then with the probe holder removed. All precautions were taken to ensure that the radiometer view angle was identical both with and without the probe holder and that the cold probe holder did not change the refractory temperature during the

measurements. Figure 45 presents data collected during these reflectance trials plotted against the refractory emissivity data provided by Babcock and Wilcox (solid line).

To evaluate the gas composition emissivity using Equation 1, the following experimental data must be collected: 1) R_1 , R_2 , and R_3 are measured using the pyroelectric radiometer and water-cooled black target; 2) a_f is then calculated using the Schmidt technique; and 3) the furnace wall temperature is measured using an optical pyrometer. These measured data are used in conjunction with Figure 45 to evaluate ϵ_r and ρ_r (refractory emissivity and reflectivity). The final item of information needed to use Equation 1 is the flame temperature (T_f). These data were presented in Figures 21 through 43. A review of these temperature profiles points out the large radial temperature gradients that occur near the furnace burner wall. Because the analysis technique is built around a uniform radial temperature, the reliability of the emissivities at the front of the furnace is very small. However, as the gases approach the furnace back wall (flue), these gradients decrease until, at the last axial position where data are collected (395.6 cm from the furnace burner wall), the temperature profile is flat. The flame temperature used in evaluating emissivity is an average of the radial temperature measurements weighted by their annular area. These values (average flame temperature T_f , refractory temperature T_r , refractory emissivity ϵ_r , and refractory reflectivity ρ_r) are plugged into Equation 1, leaving two values to be determined: a_f and ϵ_f . A value for the flame emissivity is assumed, which allows the flame absorptivity to be estimated. This estimated value for a_f is compared with the measured value. If the two values do not correspond, an iterative procedure is started and continued until satisfactory agreement has been reached.

The emissivity profiles evaluated for natural gas, Lurgi oxygen, Koppers-Totzek oxygen, Winkler oxygen, Wellman-Galusha air, and Winkler air are presented in Figures 46 through 51.

The variation of emissivity along the furnace length was observed for all fuel gases tested. Because gas emissivity is a function of composition, temperature, and path length, the variation of emissivity along the furnace axis can best be explained as an aerodynamic effect.

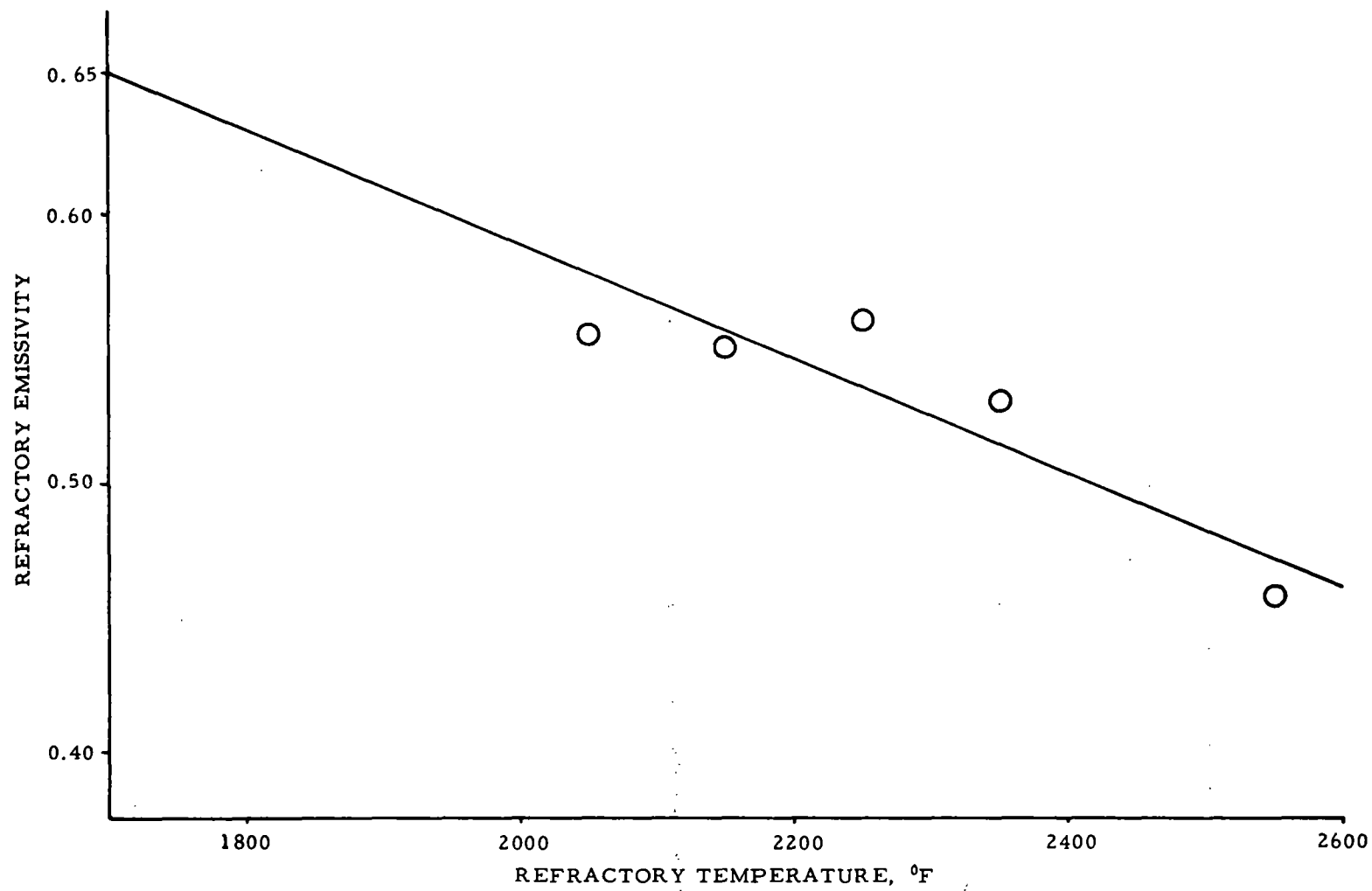


Figure 45. Refractory emissivity versus refractory temperature

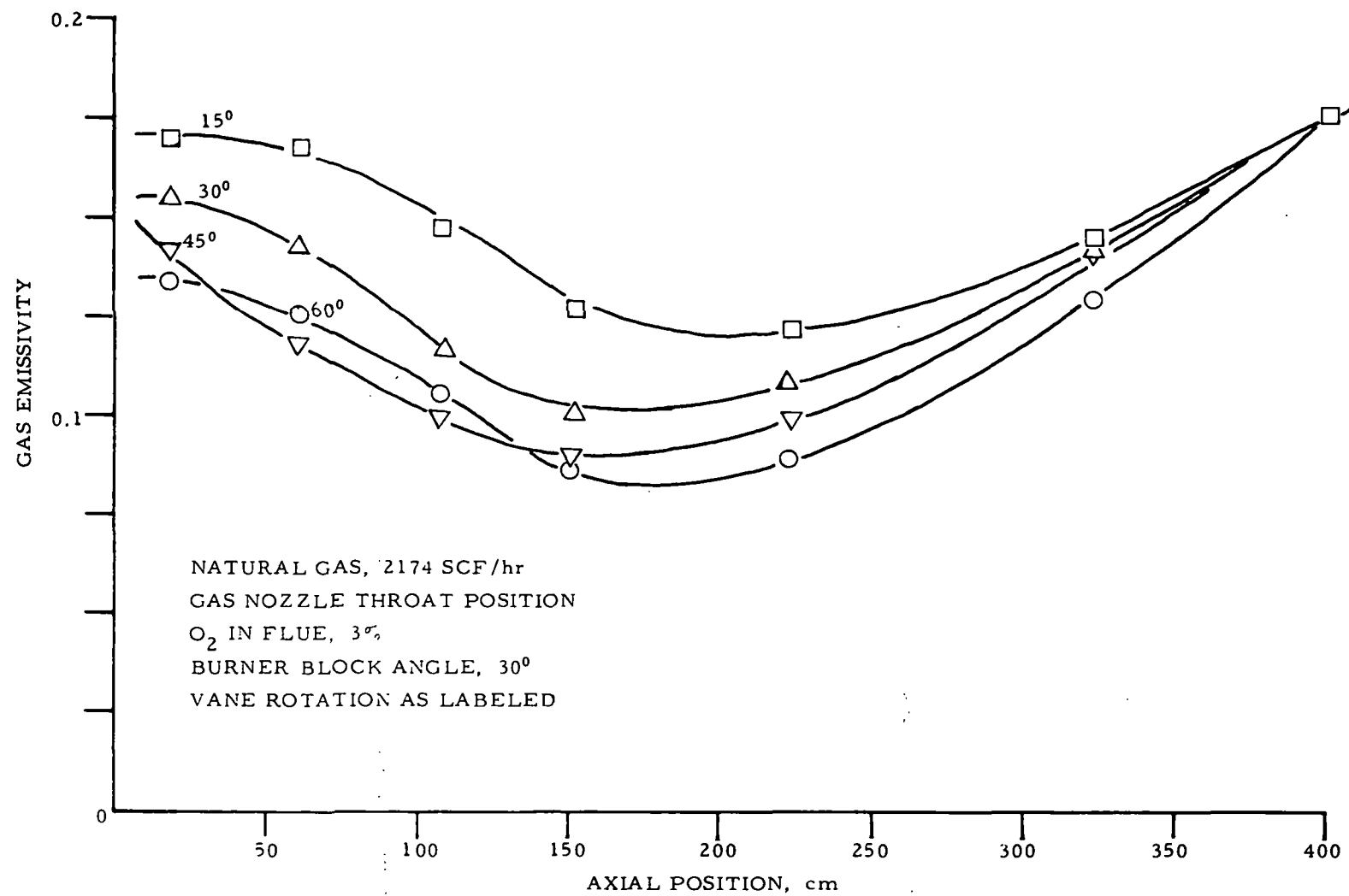


Figure 46. Gas emissivity versus axial position for natural gas

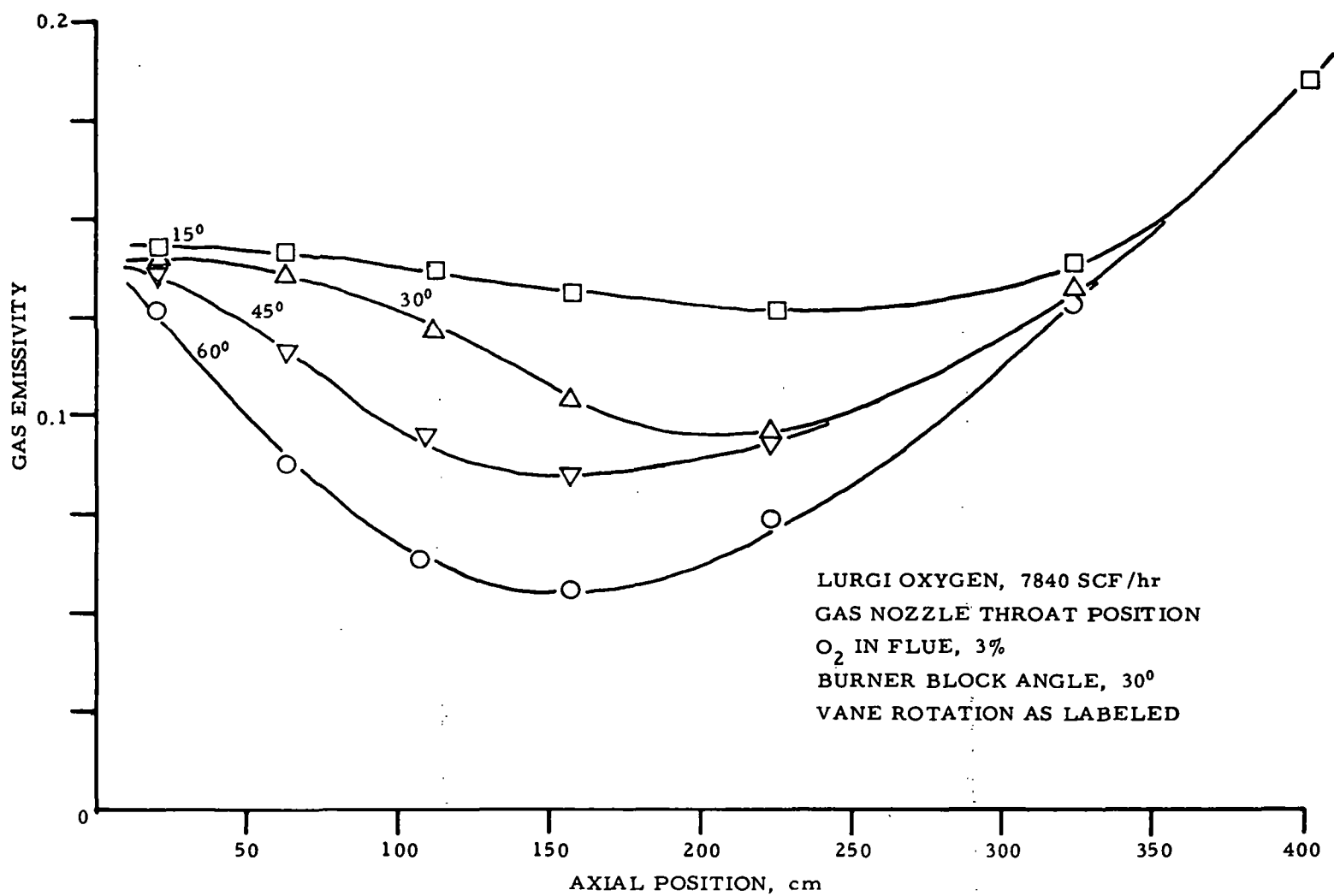


Figure 47. Gas emissivity along furnace length for Lurgi oxygen gas

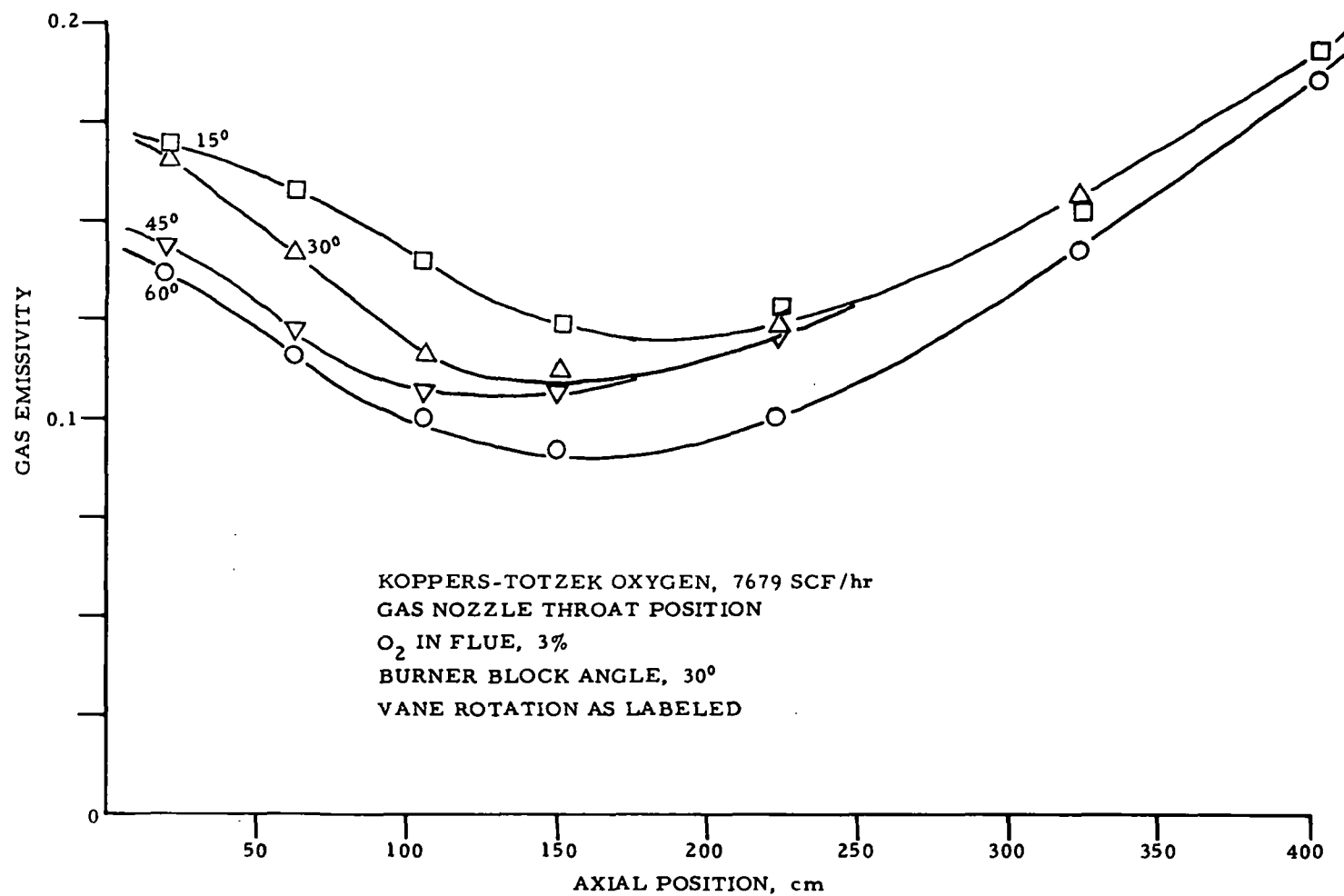


Figure 48. Gas emissivity along furnace length for Koppers-Totzek oxygen gas

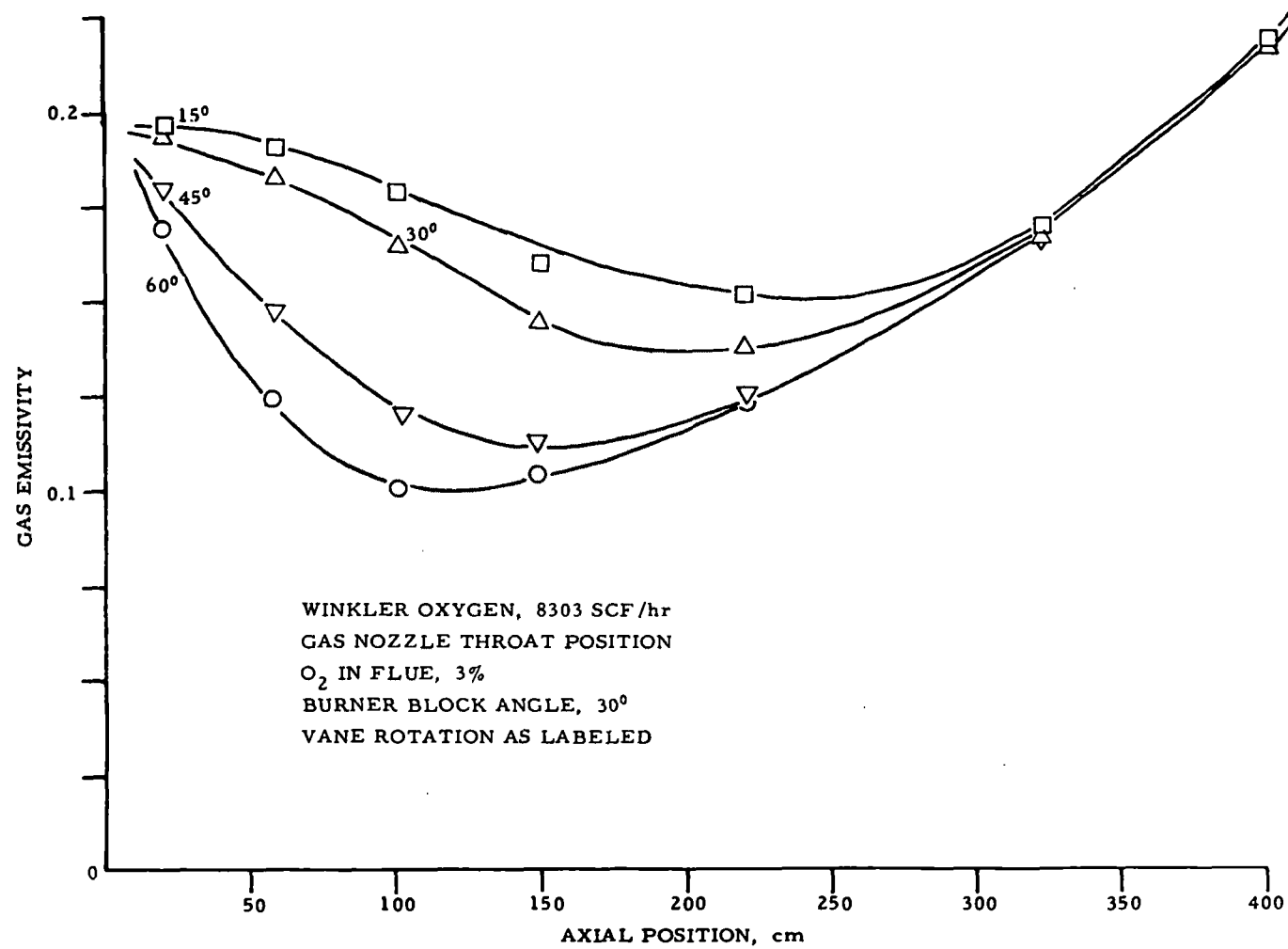


Figure 49. Gas emissivity along furnace length for Winkler oxygen gas

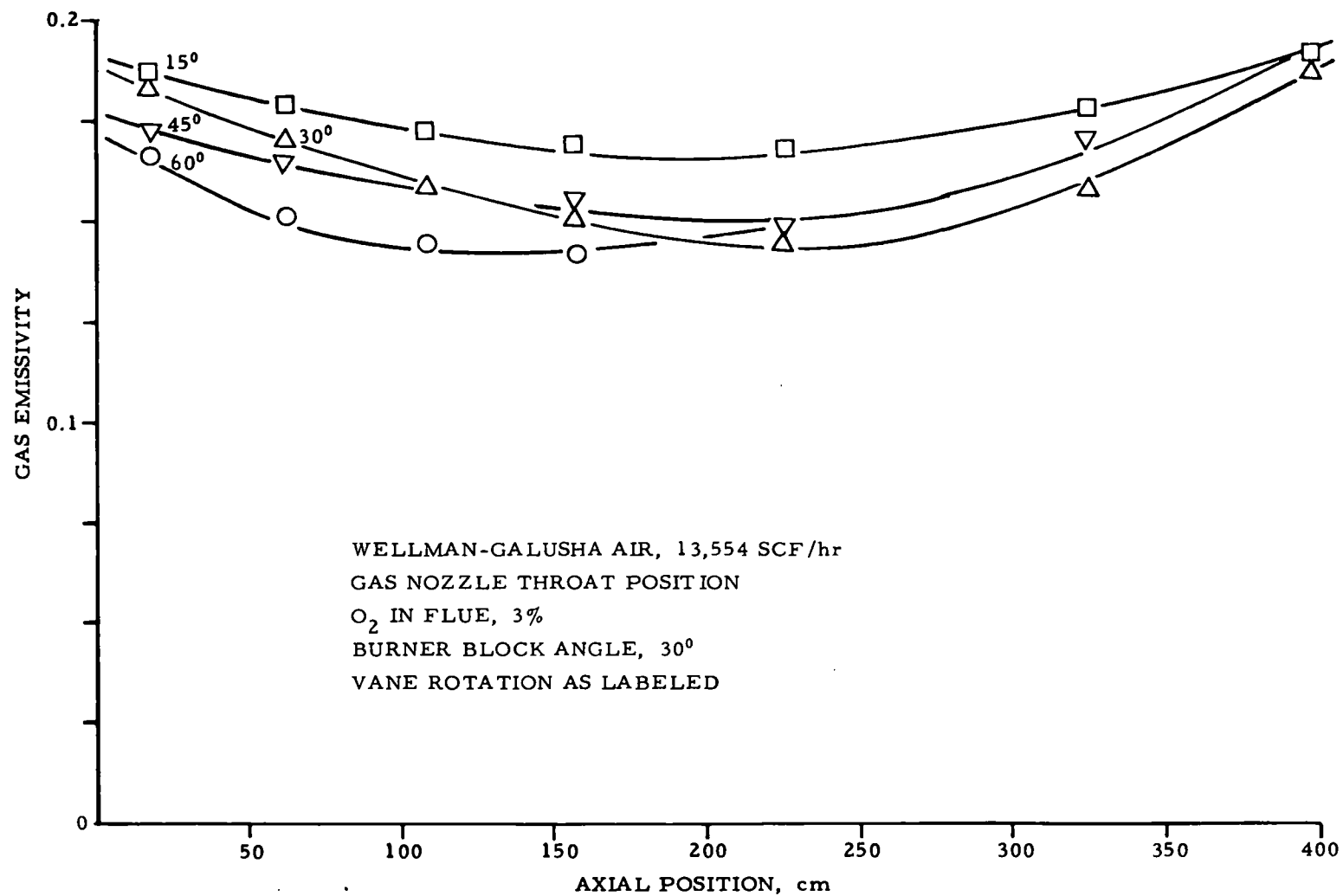


Figure 50. Gas emissivity along furnace length for Wellman-Galusha air

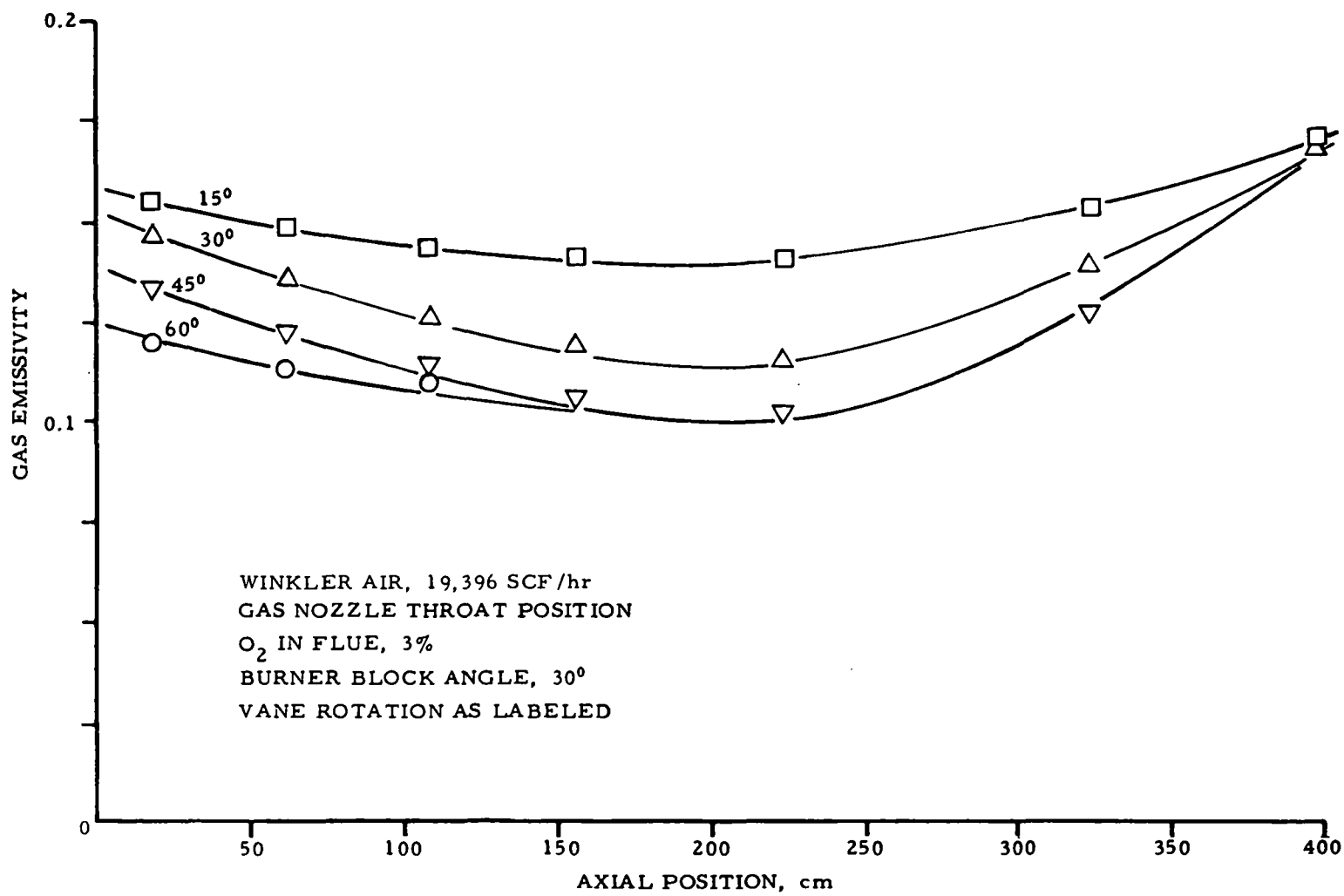


Figure 51. Gas emissivity along furnace length for Winkler air

A general aerodynamic characterization of a flame can be made by determining the different types of flow patterns that exist within a combustion chamber. A detailed flow analysis of a confined flame reveals that the front section of a combustion chamber can be divided into four zones: primary jet, primary recirculation, secondary jet, and secondary recirculation. The primary and secondary jets contain only particles with a forward flow direction (away from the burner), whereas the recirculation zones contain gas particles moving in the reverse flow direction (back toward the burner). The size, shape, and particle density of the recirculation zones are determined by the velocity, the ratio of gas to air, the spin intensity of the secondary jet, the burner-block angle, and, for the secondary recirculation zone, the size and shape of the combustion chamber. Figure 52 shows the type of flow pattern that was observed during this investigation. This flow pattern is conventionally labeled Type II.

A Type II flow pattern is generated when the secondary jet has a tangential velocity component large enough to cause the particles to adhere to and pack tightly against the burner block. This packing creates a low or negative pressure region in the center of the burner block. The pressure differential between the furnace and the central region of the burner block causes gas molecules to be pulled into this region and back toward the burner, thus creating the primary recirculation zone. When the velocity of the primary jet is greater than the velocity of the recirculating gases in the primary recirculation zone, the primary jet penetrates this reverse flow region, and a recirculation lobe occurs on each side of the burner axis.

A gas analysis of the secondary recirculation zone reveals species concentrations similar to those measured at the furnace flue. Thus, an emissivity measured at the furnace front wall would be an addition of the flame plus secondary recirculation zones. The emissivity from the recirculation zone is approximately that measured at the rear of the furnace. As the flame spreads, the optical path of the secondary recirculation zone is decreased, reducing the concentration of radiating sources. As the combustion continues, the concentrations of CO_2 and H_2O along the optical path are increased as products of combustion. At the end of the furnace, the gas temperatures and species concentrations across the width of the furnace are nearly uniform, and the emissivity is as if from a static mixture at a uniform temperature and composition. This is confirmed by the emissivities

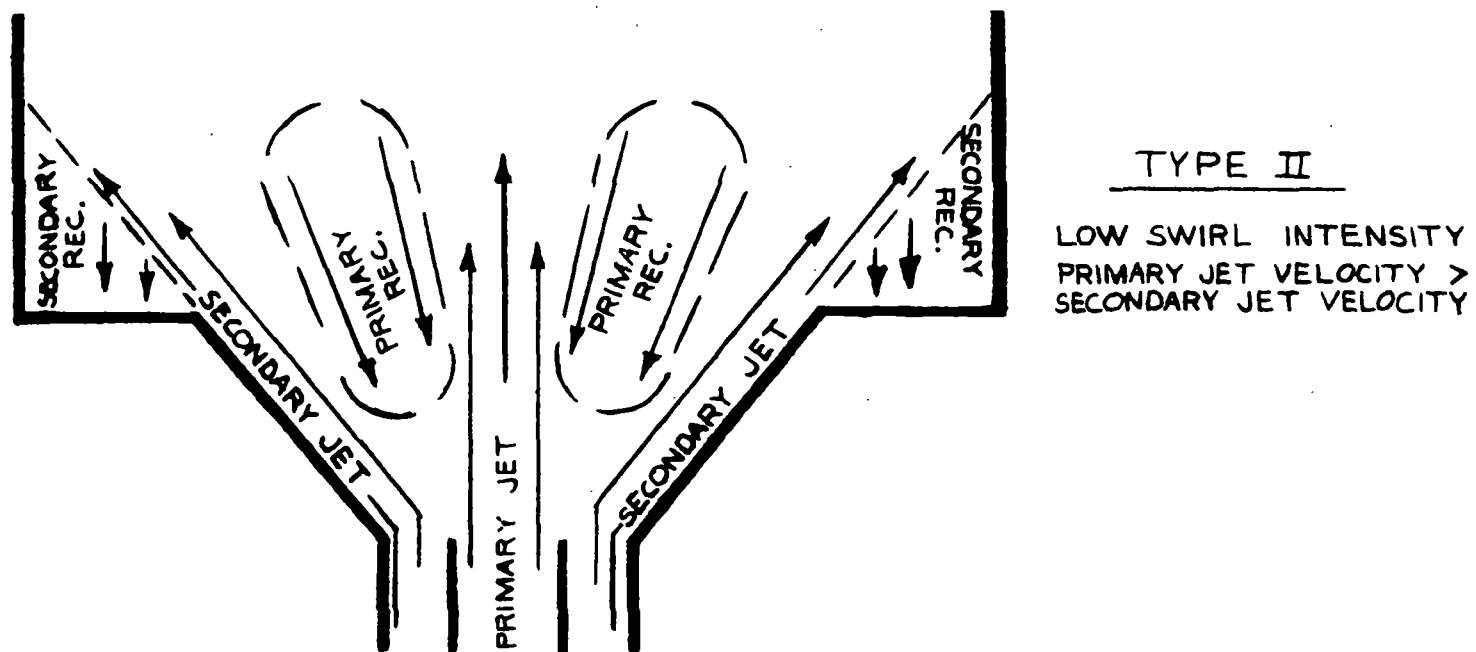


Figure 52. Flame flow pattern tested

measured for natural gas combustion (Figure 46), where the measured emissivity at the front of the furnace is different for each vane angle tested; toward the end of the combustion chamber, however, all the values converged to approximately 0.177.

The variation of emissivity near the furnace front wall as a function of vane angle occurs due to the tangential velocity component of the secondary air – that is, how fast the vortex of combustion air will spread upon leaving the burner block. The larger the tangential velocity component, the higher the rate of post burner-block expansion and the smaller the contribution of the secondary recirculation zone to the measured emissivity.

Another possibility is that a_f (which is the value measured) increases for some distance into the furnace as a consequence of the presence of either soot or cold pockets of absorbing gas.

Emissivities were calculated using the measured flue-gas temperatures and compositions for a 45-degree vane-angle rotation. Two methods of calculating emissivities were used. Emissivities were calculated using the method given by Hottel and Sarofim² in Radiative Transfer and that developed by Leckner³ using NASA data. For all the test gases except one, the measured emissivities fell between the two calculated values. The exception is the Lurgi oxygen medium-Btu gas, where the measured value was lower than both the calculated emissivities. These calculated values are listed in Table 5. They range from a minimum of 0.150 for Winkler air to a maximum of 0.194 for Lurgi oxygen. These calculated values are independent of burner operating conditions, and the furnace geometry is considered only when evaluating the mean beam length. Because the radiometer viewed a collimated beam, the furnace width corresponds to the beam length.

Lurgi oxygen measured emissivities are illustrated in Figure 47. The emissivity measured at the furnace flue was 0.185, which is 5% lower than the value

2. Hottel, H. C. and Sarofim, A. F., Radiative Transfer, 300, New York: McGraw-Hill, 1967.

3. Leckner, B., Combust. Flame 19:33, 1972.

calculated by the Hottel method and 25% lower than the emissivity calculated by the Leckner method.

Table 5. CALCULATED AND MEASURED EMISSIVITIES

$$\begin{aligned}\epsilon_{\text{calc}} &= \text{calculated emissivity} \\ a'_{\text{meas}} &= \text{measured absorptivity} \\ \epsilon_{\text{meas}} &= \text{measured emissivity} \\ \text{Difference} &= \frac{|\epsilon_{\text{calc}} - \epsilon_{\text{meas}}|}{\epsilon_{\text{calc}}}\end{aligned}$$

Fuel	P_{CO_2}	$P_{\text{H}_2\text{O}}$	Gas temp. °R	a'_{meas}	ϵ_{meas}	Hottel-Sarofim		Leckner	
						Emissivity	% $\Delta\epsilon$	Emissivity	% $\Delta\epsilon$
Natural gas	0.083	0.167	3013	0.131	0.177	0.159	+11	0.215	-18
Lurgi oxygen	0.169	0.179	2902	0.158	0.185	0.194	-5	0.246	-25
Koppers-Totzek oxygen	0.204	0.121	3014	0.145	0.190	0.174	+9	0.211	-10
Winkler oxygen	0.183	0.161	2983	0.153	0.218	0.189	+15	0.232	-6
Wellman-Galusha air	0.159	0.092	2894	0.115	0.190	0.154	+23	0.195	-3
Winkler air	0.147	0.081	2795	0.112	0.170	0.150	+13	0.193	-12
Winkler oxygen plus 15% FGR	0.183	0.161	2955	0.182	0.238	0.193	+23	0.237	0

The average emissivity measured at the flue for Koppers-Totzek oxygen was 0.190, compared with 0.174 from the Hottel calculation and 0.211 from the Leckner calculation. Thus the measured value was 9% high or 10% low, respectively. The profiles of the measured emissivities for Koppers-Totzek oxygen are presented in Figure 48.

The Winkler oxygen fuel measured emissivity was 15% higher than the Hottel and 6% lower than the Leckner emissivity. The emissivity profiles measured down the furnace axis are presented in Figure 49.

Emissivity profiles measured for Wellman-Galusha air are presented in Figure 50. These measured emissivities converged to a value of 0.190, which is 23% higher than the Hottel calculated value, but only 3% lower than the Leckner value.

Winkler air measured emissivities are presented in Figure 51. The post-flame emissivity value was measured at 0.170, which is 13% greater than the Hottel and 12% less than the Leckner calculated values.

The agreement between the calculated and measured emissivities is amazingly good considering the fact that the measurements were made on an operating furnace with nonuniform temperatures and compositions. From reviewing the synopsis of calculated and measured emissivities presented in Table 5, the following observations can be made:

- The measured emissivities, with the exception of Lurgi oxygen, were higher than the Hottel calculated values and lower than the Leckner, indicating a bias in the measurements or calculations rather than random experimental error.
- The average deviation of the measured emissivities was 11% with respect to the Hottel calculated emissivities and -12% with respect to the Leckner calculated emissivities.

These experimental data thus provide a basis for recommending the use of calculated emissivities for extrapolating to the dimensions of commercial boilers. As Table 5 shows, the Hottel calculation method gives the more conservative estimate, while the Leckner calculation method is more optimistic.

At least part of the 11% error between measured emissivity and that calculated from the Hottel and Sarofim method occurs in the correction due to spectral overlap of CO_2 and H_2O in a mixture. The highest temperature at which correction data are currently available is 1700°F. However, it can be inferred from emissivity charts of CO_2 and H_2O that the overlap correction will decrease with temperatures above 1700°F. Because the values were calculated using the 1700°F overlap correction, they are smaller in magnitude than if they had been calculated with a 2500°F overlap correction. It is estimated that this correction could lead to an increase of 5% to 10% in the calculated emissivities.

Figure 53 is a plot of emissivity versus furnace length for a furnace fired with coke-oven gas.¹ These data help to quantify the differences in emissivity between the "clean" medium- and low-Btu gases tested in this program and those contain-

1. Land, T., Instrum. Autom. 29, (No. 7): 1956.

ing tars, oils, and particulates, which could be expected from a coal gasifier. The data in Figure 53 were collected on the International Flame Research Foundation furnace, and the firing density was higher than that used in our experiments (10,000 Btu/CF-m versus 6,000 Btu/CF-m). The coke-oven gas gave a calculated gas emissivity of 0.2. The measured emissivity, however, was 0.38. The large difference between the calculated and the measured values is due mainly to the tars and particulates carried by the coke-oven gas.

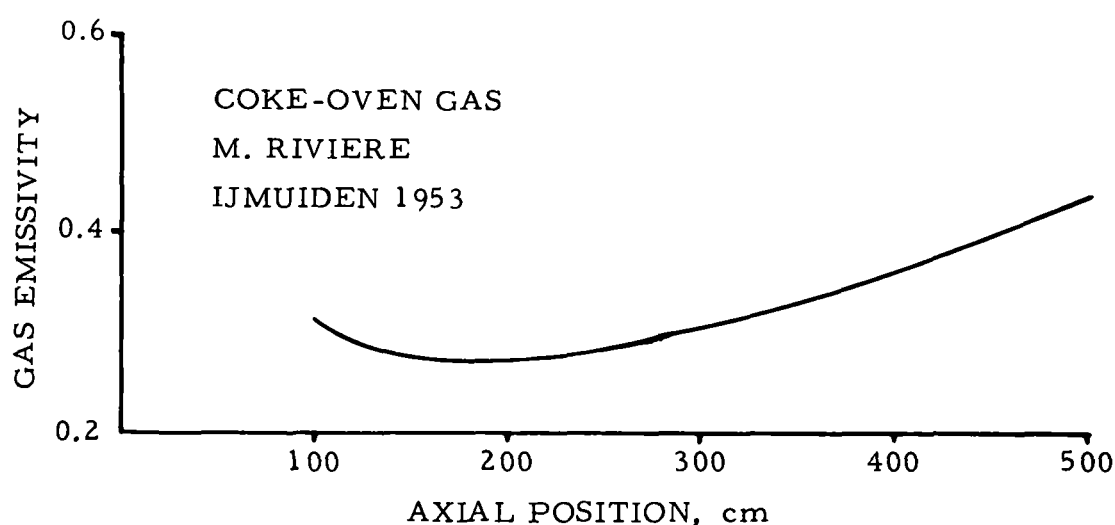


Figure 53. Emissivity profile for coke-oven gas

NITRIC OXIDE EMISSIONS

To determine the environmental impact of retrofitting utility boilers with medium- and low-Btu gases, NO emissions levels were measured as a function of secondary air-preheat temperature for each of the test fuel gases. Baseline NO emission data were collected using natural gas. The combustion-air temperature was varied from ambient to 800°F. Graphs of the experimental results are presented in Figure 54. For the vane orientations studied, the measured NO levels remained relatively constant up to 400°F, above which dramatic increases occurred for the 45-degree and 60-degree angles.

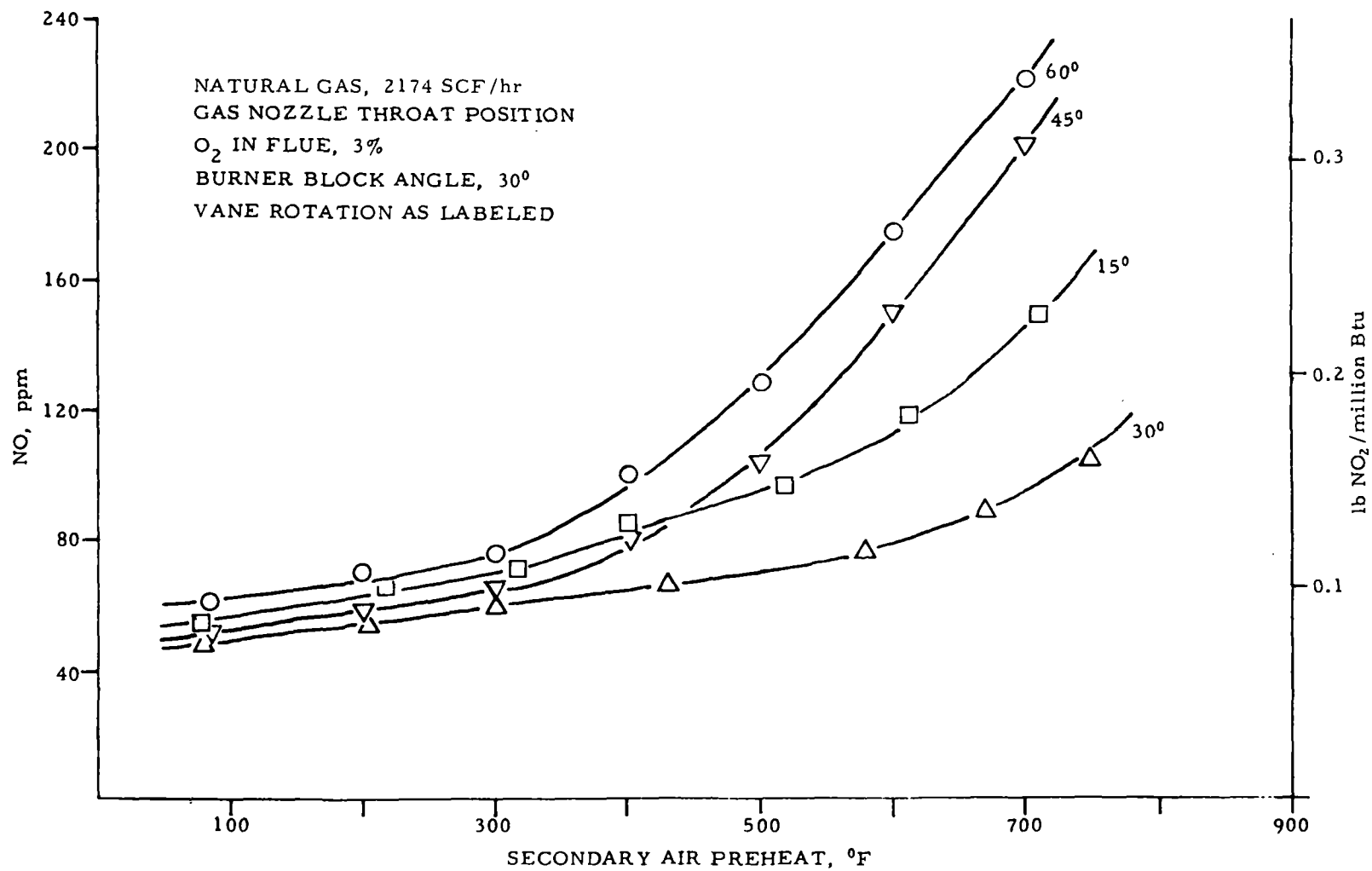


Figure 54. NO versus secondary air preheat with natural gas

Figure 55 presents NO versus secondary air-preheat temperature test results using Lurgi oxygen gas. The flue concentrations of NO are approximately 50% less than with natural gas for all test conditions. For the detailed burner operating conditions (15-degree vane angle, 325°F air-preheat temperature), the NO level was reduced from 65 ppm (natural gas) to 32 ppm (Lurgi oxygen gas). These emission reductions were expected based on an adiabatic flame temperature comparison, because Lurgi oxygen has a 173°F lower temperature than natural gas.

Flue levels of NO measured as a function of combustion-air temperature with Koppers-Totzek oxygen gas are shown in Figure 56. For all conditions tested, the Koppers-Totzek gas resulted in higher NO emission levels than did natural gas. Again, by comparing the adiabatic flame temperatures listed in Table 2, this result was anticipated because Koppers-Totzek gas has a 241°F higher adiabatic flame temperature than natural gas. For the 45-degree vane angle with a 325°F secondary air-preheat temperature, this is translated into a 60% increase in the NO emission level.

Comparing the adiabatic flame temperatures of Winkler oxygen gas with natural gas shows that the former is 9°F lower. Thus, based only on adiabatic flame temperature considerations, the NO emission levels should be comparable. The NO test results with Winkler oxygen gas are presented in Figure 57. These measured levels were lower than those measured for natural gas, except for the 60-degree vane rotation with secondary air-preheat temperatures below 560°F and the 45-degree vane rotation with preheat temperatures below 400°F. These results indicate that NO formation strongly depends on combustion aerodynamics because the peak flame temperature and the time that the gas is subjected to this temperature are controlled by aerodynamic turbulence. Although average temperatures may be the same in two cases, the NO_x formation can be different if the turbulent temperature fluctuations are different. The temperature dependence of the chemical reaction rate constant can be expressed by the Arrhenius rate law:

$$k(T) = k_o \exp \left[-E/RT(t) \right]$$

The time-averaged value would be:

$$\overline{k(T)} = \frac{k_o}{\tau} \int_{t_o}^{(t_o + \tau)} \exp \left[-E/RT(t) \right] dt$$

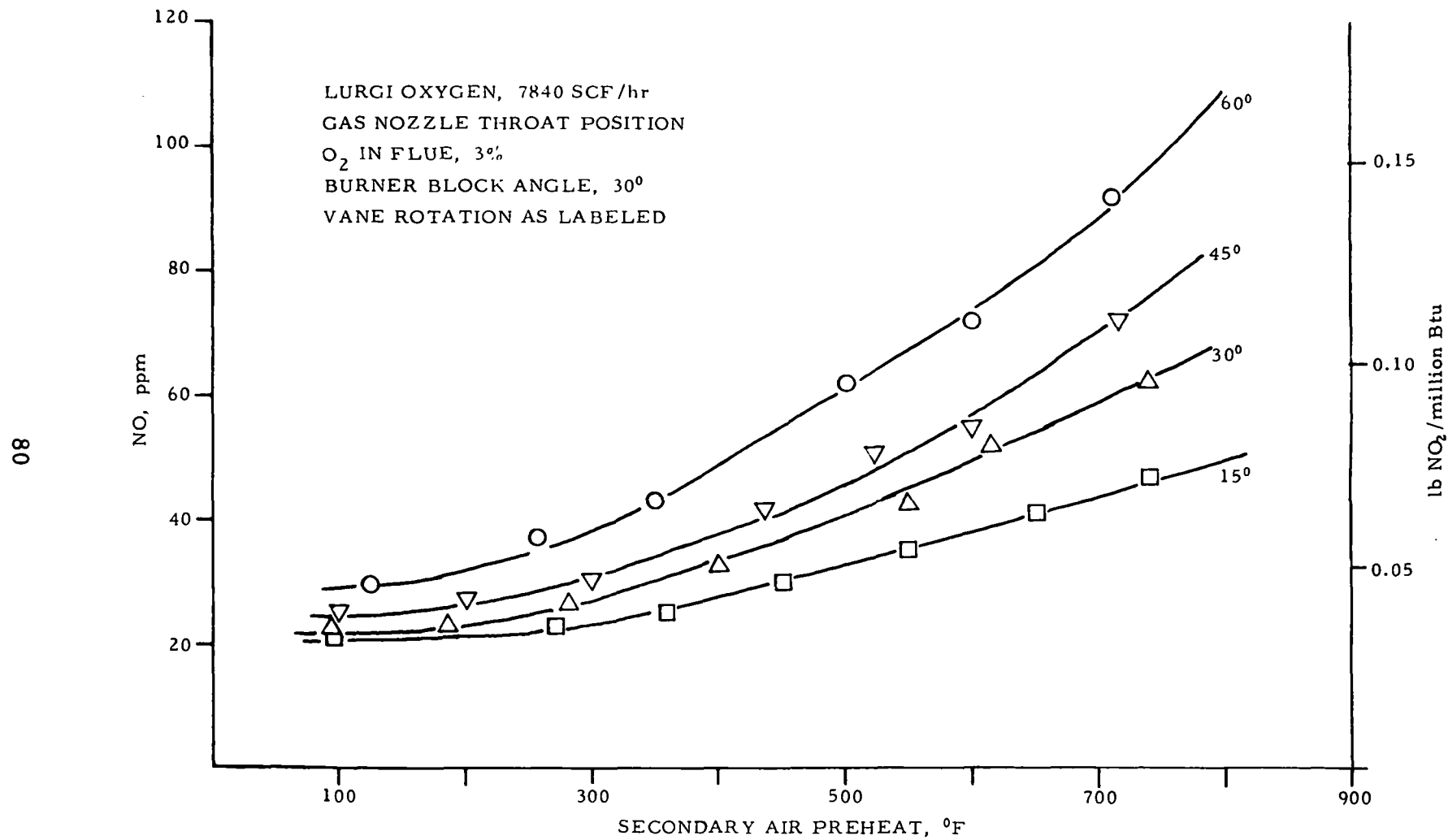


Figure 55. NO versus secondary air preheat with Lurgi oxygen gas

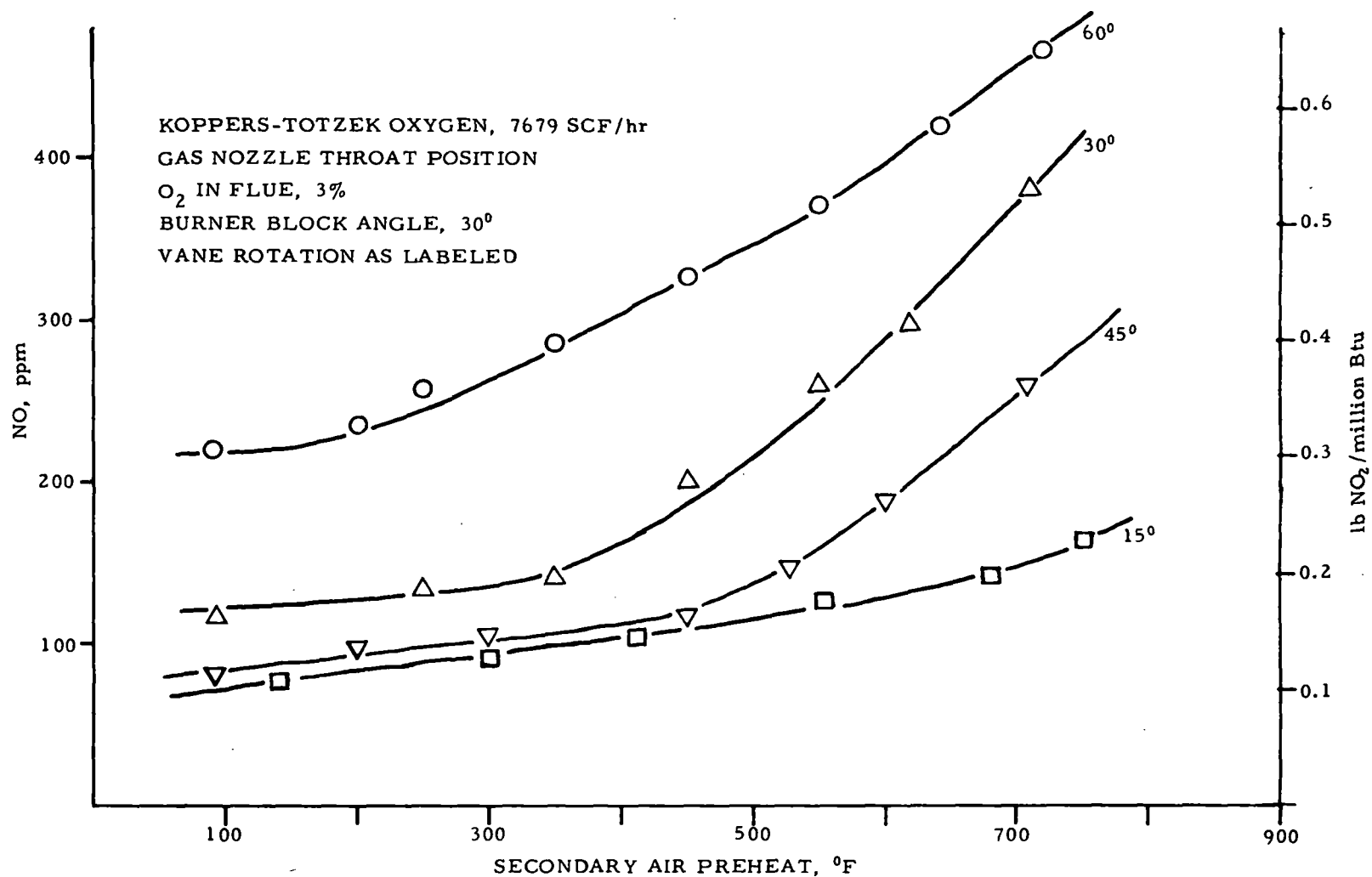


Figure 56. NO versus secondary air preheat with Koppers-Totzek oxygen gas

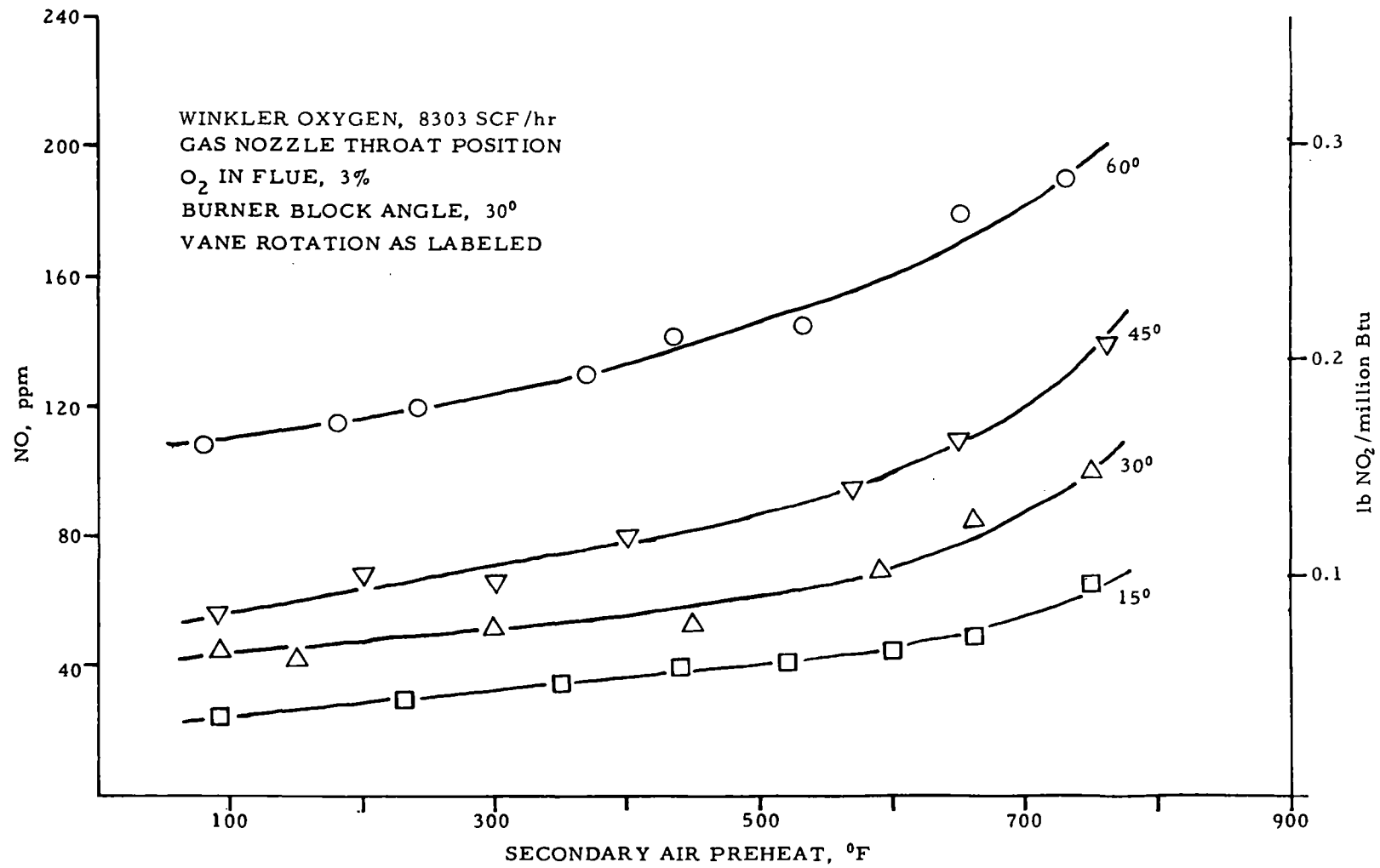


Figure 57. NO versus secondary air preheat with Winkler oxygen gas

for an interval of time, τ , while the rate constant given by the time-averaged temperature would be:

$$k(\overline{T}) = \frac{k_o}{\tau} \exp [-E/R\overline{T}].$$

The ratio –

$$K = \frac{\overline{k(T)}}{k(\overline{T})}$$

This ratio is always greater than 1 because the exponential nature of the temperature dependence means that the rate constant increase for an increase in temperature above the average exceeds considerably the decrease for a similar reduction in temperature. The value of the ratio, K , depends on the extent and the nature of the temperature fluctuations. Thus, observing that the average temperature (the temperature given by a suction pyrometer) is similar in two cases does not necessarily mean that the NO_x emissions will be similar if the turbulent fluctuations are different. Unfortunately, the technology is not sufficiently advanced to allow measurement of the extreme turbulent temperature pulsations. An additional indication of combustion aerodynamic differences is the reordering of the NO concentration levels as a function of vane angle, which can be seen by comparing Figure 56 with Figure 57.

Figure 58 shows the NO emission data collected for Wellman-Galusha air. The flue concentrations of NO are about 70% lower than those measured for natural gas at the lower air-preheat temperatures. They show an almost linear rise with air temperature. The lack of a dramatic increase in emissions with temperature results in up to a 90% lower NO concentration at elevated combustion-air temperatures for Wellman-Galusha air than for natural gas. Some reduction of NO emissions could be anticipated because of the lower adiabatic flame temperature (2948° versus 3337°F).

The NO emission data for Winkler air are presented in Figure 59. As the low adiabatic flame temperature would predict, the NO concentrations in the flue are the lowest of all the gases. The emissions are 82% to 97% lower than those measured

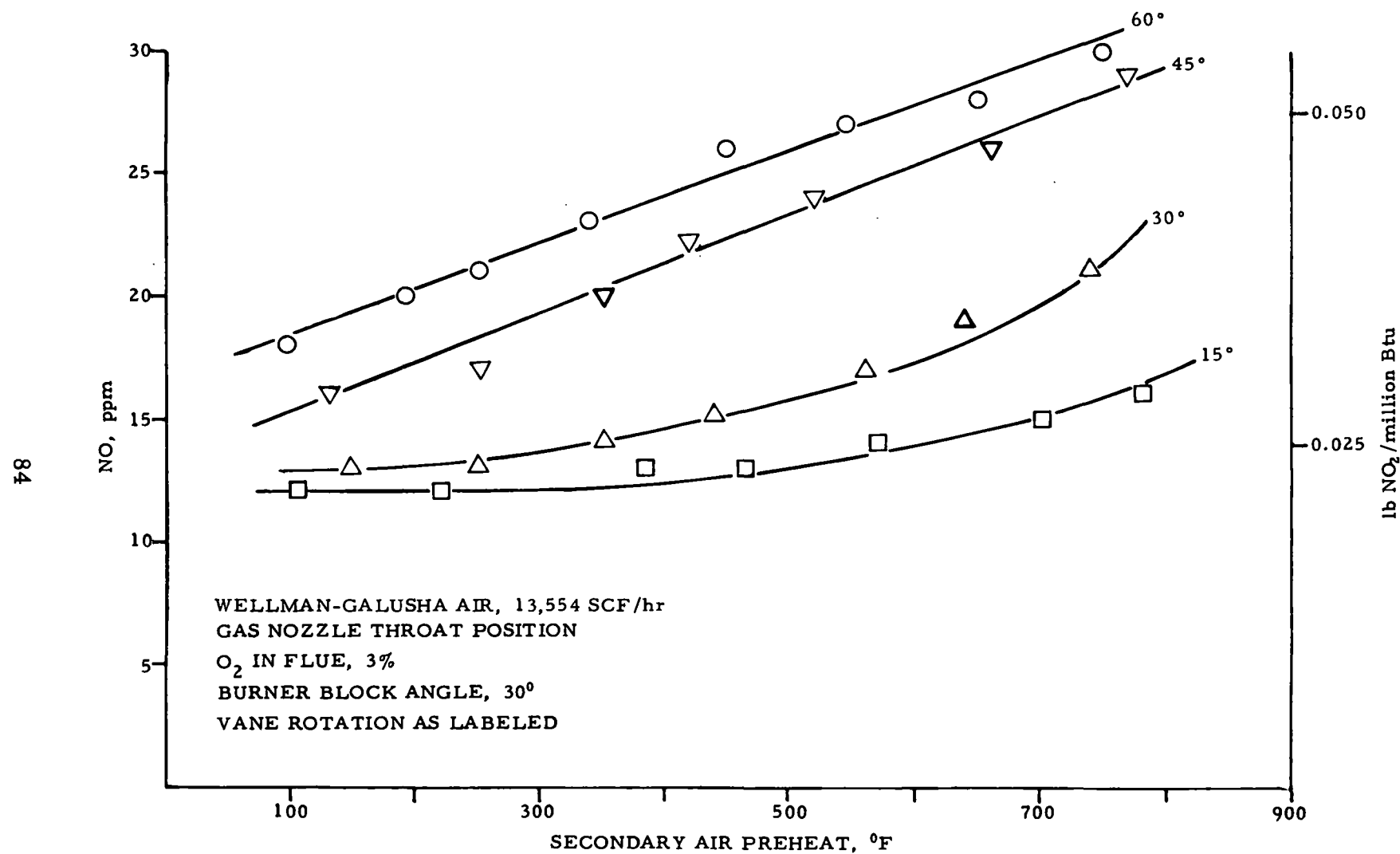


Figure 58. NO versus secondary air preheat with Wellman-Galusha air gas

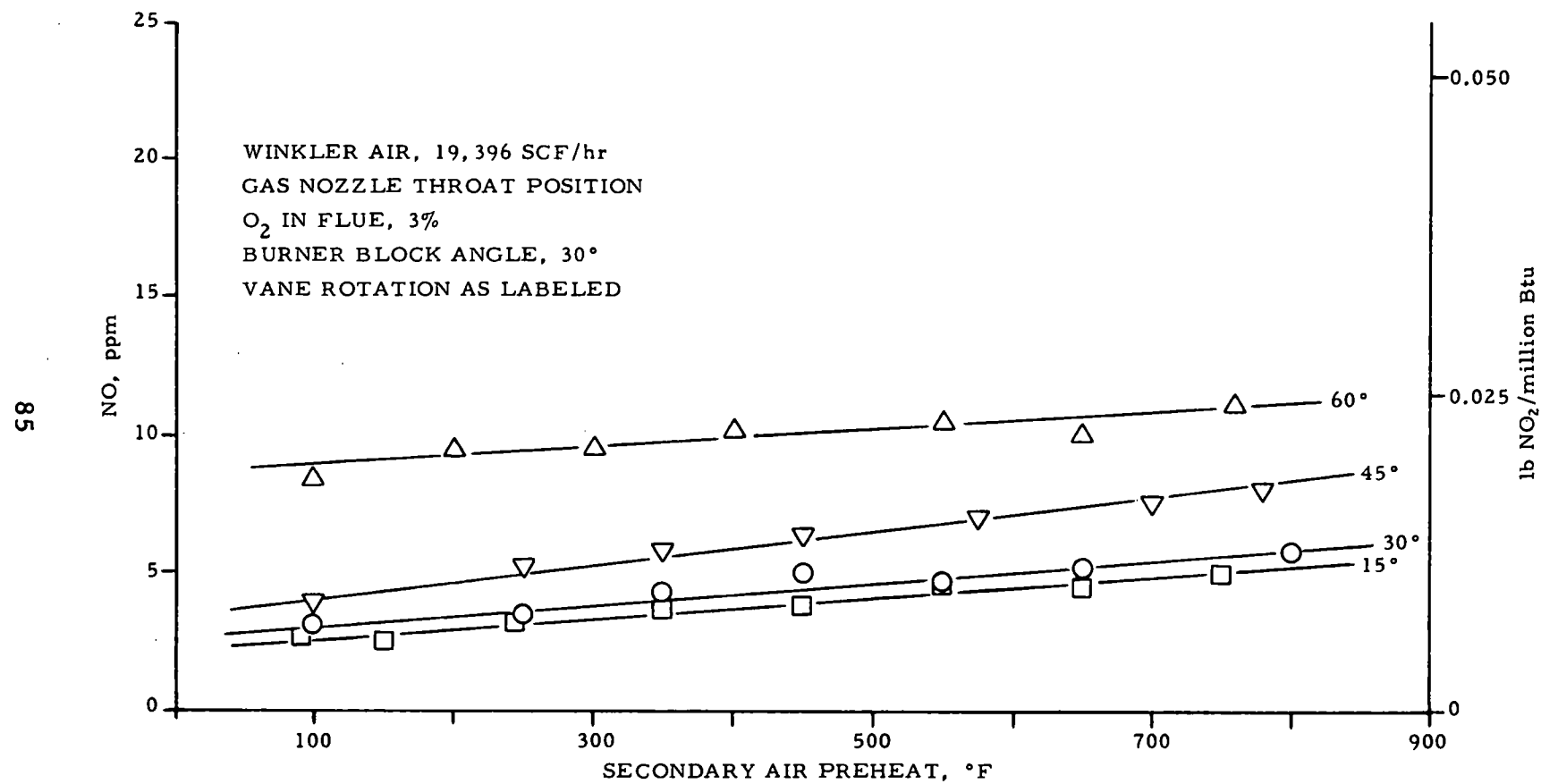


Figure 59. NO versus secondary air preheat with Winkler air gas

for natural gas and show an even more gradual, nearly linear increase with combustion-air temperature.

The NO data for Wellman-Galusha air show a systematic increase in emissions with increased vane angle. This same relationship is not seen with Winkler air. The 15, 45, and 60-degree angle data are all within 2 to 3 ppm of each other but are 5 to 6 ppm lower than the 30-degree angle data.

Figure 60 is an Arrhenius plot for the fuel gases tested with the utility burner at a 45-degree vane rotation. The plot, $\ln(\text{NO})$ versus reciprocal of the adiabatic flame, yields a linear relationship. Correlating these data to a relationship suggested by Thompson, Brown, and Beer⁴ on the formation rate of NO which is of the form:

$$\frac{d(\text{NO})}{dt} = A \exp(-134.7/RT)$$

yields an activation energy of 153 kcal/mol compared with their 134.7. This good agreement suggests that peak temperatures approaching the adiabatic flame temperatures are controlling the rate of NO formation and suggests that the use of adiabatic flame temperature is a good empirical method of predicting NO emissions.

4. Thompson, Brown and Beer, Combust. Flame, 19, 69 (1972).

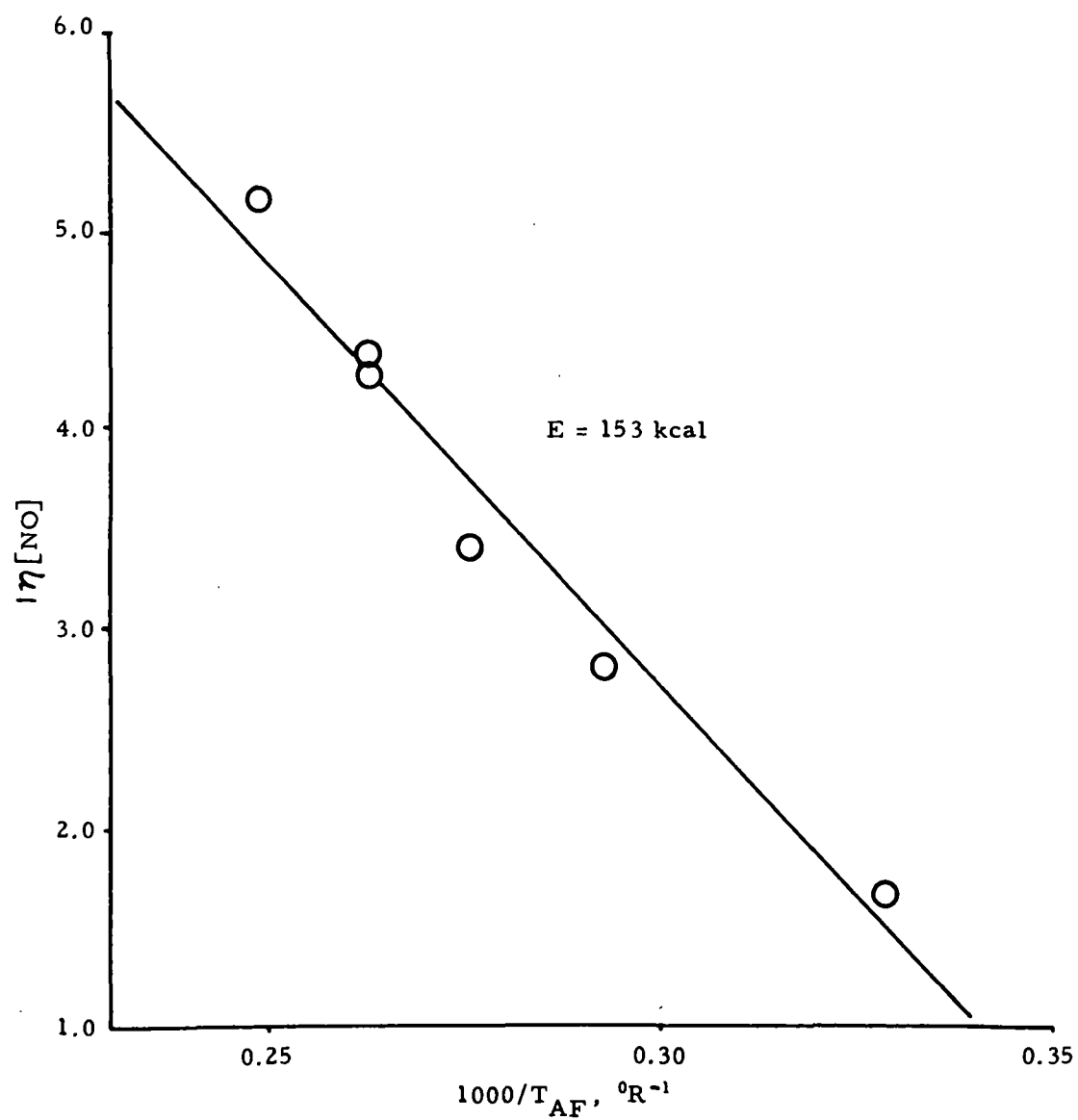


Figure 60. Arrhenius plot of NO versus inverse "pseudo-adiabatic" flame temperature

DATA CORRELATION

NO_x EMISSIONS

Due to the size of the gas-generating system for synthesizing the medium- and low-Btu test gases, the firing density of the pilot-scale test furnace could not exceed 6923 Btu/ft³·hr. To permit a better correlation as to the level of emissions that could be anticipated from a utility boiler, natural gas was fired with inputs up to 3.75 million Btu/hr. This corresponds to a firing density of 11,538 Btu/ft³·hr, which produced a NO emission level of 225 ppm compared with the New Source Performance Standard for natural gas at 1000 Btu/SCF of 168 ppm (0.2 pounds NO₂/million Btu heat input). These data are graphed in Figure 61.

A 300-MW utility boiler with a radiant chamber 30 x 60 feet in cross section and 80 feet high is fired with 2.86×10^9 Btu/hr. The firing density for a boiler of this size at this firing rate is 19,860 Btu/ft³·hr. Extrapolating the data of Figure 61 yields a NO emission level for the 19,860 Btu/ft³·hr firing density of 458 ppm. To quantify the anticipated NO emission levels from this 300-MW boiler for each of the fuel gases tested, it is assumed that an identical firing density-to-NO emission level relationship would occur for each medium- and low-Btu gas as is represented for natural gas in Figure 61. From this assumption, the NO emission levels presented in Table 6 were projected.

Thus, there were only two fuel gases tested that could comply with the 168-ppm performance standard with the burner system operating normally. Both of the fuel gases (Wellman-Galusha air and Winkler air) that comply with the standard do so because of their low adiabatic flame temperatures, 389° and 758°F, respectively, below the natural gas adiabatic flame temperature. All medium-Btu gases that have adiabatic flame temperatures near that of natural gas would require modifications to the burner/boiler system in order to comply with the performance standards.

CORRELATING FURNACE PERFORMANCE

The efficiencies evaluated on the pilot-scale furnace for each of the fuels tested are listed in Table 7. These efficiencies (defined the same as previously for the boiler, that is, the fraction of the total input enthalpy given up in the furnace by the combustion products) can be evaluated using the flue gas temperatures in

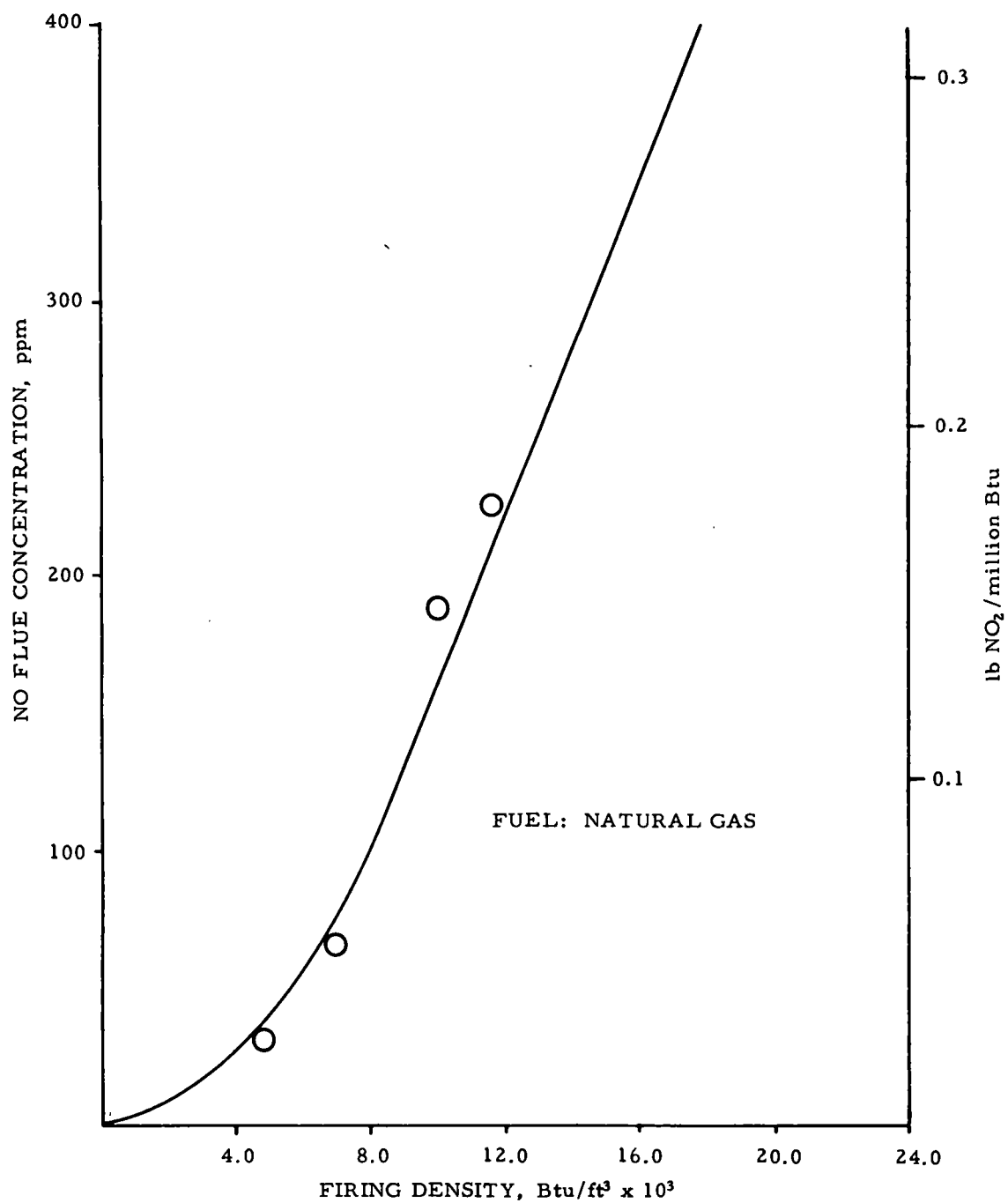


Figure 61. NO flue concentration versus firing density

**Table 6. PROJECTED NO_x EMISSION
LEVELS FOR A UTILITY BOILER**

Fuel	NO _x , ppm	lb NO ₂ /10 ⁶ Btu
Natural gas	458	0.714
Lurgi oxygen	225	0.353
Koppers-Totzek oxygen	733	1.019
Winkler oxygen	514	0.766
Wellman-Galusha air	106	0.198
Winkler air	28	0.061

**Table 7. TEST FURNACE EFFICIENCIES AND COMBUSTION
PRODUCT PROPERTIES AT THE FLUE**

Fuel	n ^a	T _{flue} , °F ^b	\dot{m} , SCF ^c	\dot{Q} , Btu/hr ^d
Natural gas	28.6	2553	26,639	1,693,083
Lurgi oxygen	25.2	2442	26,883	1,762,337
Winkler oxygen	26.4	2523	25,481	1,730,291
Koppers-Totzek oxygen	33.1	2554	24,236	1,570,836
Wellman-Galusha air	19.0	2434	32,889	1,910,009
Winkler air	10.8	2335	37,919	2,104,174

^a Efficiency measured for pilot-scale test furnace.

^b Temperature of combustion products at the flue.

^c Volume of combustion products at 60°F.

^d Heat content of combustion products at listed temperature.

Table 7 and the combustion products in Table 1. Subtracting the flue gas enthalpy from the total enthalpy input gives the amount of heat transferred in the furnace, and dividing by the total enthalpy input gives the efficiency. The efficiencies evaluated for natural gas and the oxygen produced low-Btu test gases (Winkler oxygen, Koppers-Totzek oxygen, and Lurgi oxygen) are comparable within a range of 25% to 33%. For Wellman-Galusha air with a 160 Btu/ft³ heating value, the efficiency decreased to 19.0%. The lowest efficiency measured was 10.8%, for Winkler air with a 116 Btu/ft³ heating value.

In addition to changes in the furnace efficiency when natural gas is replaced with a low-Btu gas, the temperature and volume of combustion gas products entering the convective section will determine the amount of heat absorbed. Using Table 7 to compare the volume of combustion products for the test fuels reveals that Koppers-Totzek oxygen has a 9% smaller volume of combustion products than natural gas, while Winkler air produces a 42% greater volume of combustion products than natural gas. These changes in combustion-product volume will result in changes in gas velocities and will shift the heat absorption patterns within the convective section.

To evaluate a shift in heat absorption when retrofitting a boiler with low-Btu gas requires a method of calculation. Babcock and Wilcox Co. (B&W) agreed to take our experimental data and use them for the input conditions to the convective section to predict differences in overall boiler efficiency (radiant plus convective) between natural gas and low-Btu gases. The method of calculation employed by B&W was to use their design computer program to forecast changes in boiler performance when retrofit with a low-Btu fuel gas.

The particular boiler selected for their calculations was a standard design with a maximum rated steam flow of 2,430,500 lb/hr at 2620 psig/1005°F at the superheater outlet when fired with natural gas. The unit (B&W Contract RB-455) is installed at the Teche Station of the Central Louisiana Electric Co. and supplies steam to a Westinghouse turbine having a maximum capacity of 361 MW. This same unit was reported on by B&W for EPRI Project 265-2, entitled "Low Btu Gas Study," a program designed to look at retrofitting boilers using only existing design information.

To update these results, the flue gas temperatures and gas compositions measured on the IGT furnace were used as input data. These temperatures and gas compositions were assumed to be identical to those entering the convective section of the boiler. Using these experimental results, B&W calculated unit efficiencies for natural gas, Winkler oxygen, and Winkler air fuel gases. The total required output of Unit RB-455 based on a 2,198,000 lb/hr main steam flow is 2652.5×10^6 Btu/hr. Based on the experimental data and fuel analysis presented in Table 1, B&W generated the information in Table 8. The first line shows natural gas firing with the amount of excess air that the unit was designed for at this load. The second line shows natural gas firing with input conditions (325°F air preheat and 3% excess oxygen) identical to those used for the pilot-scale test furnace. The actual output from firing natural gas with the increased level of excess air is in excess of 2652.5×10^6 Btu/hr. This is because higher gas weights result from the increased volume of combustion air creating an overabsorption in the reheater. Similar reheat overabsorption occurs in the output for Winkler air, which is also greater than 2652.5×10^6 Btu.

Table 8. B&W CALCULATED BOILER EFFICIENCIES USING IGT DATA

Fuel	IGT flue-gas temp, °F	Actual unit output, 10^6 Btu/hr	Unit efficiency, %	O₂ in flue gas, % by vol	B&W furnace exit-gas temp, °F
Natural gas	--	2652.5	85.1	1.1	2702
Natural gas	2553	>2652.5	84.8	3.0	2633
Winkler oxygen	2523	2652.5	84.4	3.0	2583
Winkler air	2335	>2652.5	80.4	3.0	2397

It should be noted that these calculations in no way imply that this, or any other unit, could economically be retrofitted to burn these test fuels. Several other factors in addition to unit efficiency must be considered in an actual retrofit study. Two of these important factors are: 1) redistribution of heat absorption between boiler, primary and secondary superheater, and reheat and economizer surface (a significant redistribution of which will affect metal temperatures,

spray flows, and circulation); and 2) changes in combustion-air and flue gas weight from the original design quantities, which will affect fan and air heater performance. Both of these factors can have a significant influence on the feasibility of retrofitting existing units designed for conventional fossil fuel firing.

To aid in determining the value of the experimental data, B&W reran their design calculation without using the experimental results as input. The new inputs required for the computer program were the fuel composition and the desired temperature of combustion products leaving the air heater. The results of these calculations for the gas temperature and emissivity at the exit of the radiant furnace section are listed in Table 9. The combustion-products temperature leaving the radiant section show excellent agreement with the experimental values. This provides substantiation on how realistically the pilot-scale test furnace was able to model the radiant section of a utility boiler.

Table 9. CALCULATED AND MEASURED EFFICIENCIES AND GAS EMISSIVITIES

Fuel	IGT ^a		B&W ^b	
	T _g	ε _g	T _g	ε _g
Natural gas	2553	0.18	2633	0.29
Lurgi oxygen	2442	0.19	--	--
Winkler oxygen	2523	0.22	2583	0.35
Koppers-Totzek oxygen	2554	0.19	--	--
Wellman-Galusha air	2434	0.19	--	--
Winkler air	2335	0.17	2397	0.31

^a Experimental data collected on pilot-scale test furnace.

^b Calculated values based on normal design technique.

Comparing the gas emissivities of the combustion products at the radiant section exit as measured by IGT to those calculated by B&W reveals a large difference. This difference can be understood by looking at the emissivities dependent variables. These variables are the partial pressure of the radiating gas, the temperature of the gas mixture, and the distance across (beam length) the radiating gas. The temperature and partial pressure of the radiating gases are similar for the

IGT test data and the B&W calculated values. Therefore the difference between the pilot-scale furnace and the 360-MW boiler is due to the different beam lengths, 4 feet and 22 feet, respectively. To directly compare the experimental to the calculated emissivity would require knowing the dependence of emissivity on path length. Adjusting the B&W calculated emissivity to the beam length of the test furnace was not practical because B&W does not use a publicized calculation technique for evaluating emissivities but has developed a semi-empirical method based on years of building and measuring heat absorption rates within the radiant boiler section. On the other hand, the width of the test furnace was fixed, thus negating the possibility of experimentally quantifying the dependence of emissivity on beam length. However, since the only difference between the IGT measured and B&W calculated emissivities is the beam length (products of combustion and furnace exit temperatures are similar), a graphical development of the relationship between emissivity and beam length is possible. This relationship is generated using the zero-zero data point (zero emissivity at zero path length), the IGT measured emissivity, and the semi-empirical emissivity of B&W. The resulting curve for natural gas is presented in Figure 62 and is labeled experimental. Also shown in this figure are relationships between the calculation technique of Hottel and Sarofim and the technique of Leckner.

As the plot shows, the calculated values are approximately proportional to the square root of the mean beam length. Leckner developed a statistical model based on existing spectral data to evaluate total emissivities of carbon dioxide and water vapor in homogeneous gases. For carbon dioxide emissivity, there is good agreement with Hottel's emissivities; however, for water vapor, Leckner's emissivities at temperatures above 1650°F are consistently higher and show that the partial pressure correction factor is temperature-dependent. The measured emissivity lies between the two theoretical curves presented. At the larger path lengths comparable to utility boilers, the experimental curve drops below both theoretical curves.

Similar graphs have been developed showing the relationship of emissivity and the square root of mean beam path length for Winkler oxygen and Winkler air fuel gases. These graphs are presented in Figures 63 and 64. Conclusions similar to those with natural gas can be drawn; the measured emissivity lies between the theoretical curves, while the semi-empirical data point lies below both theoretical

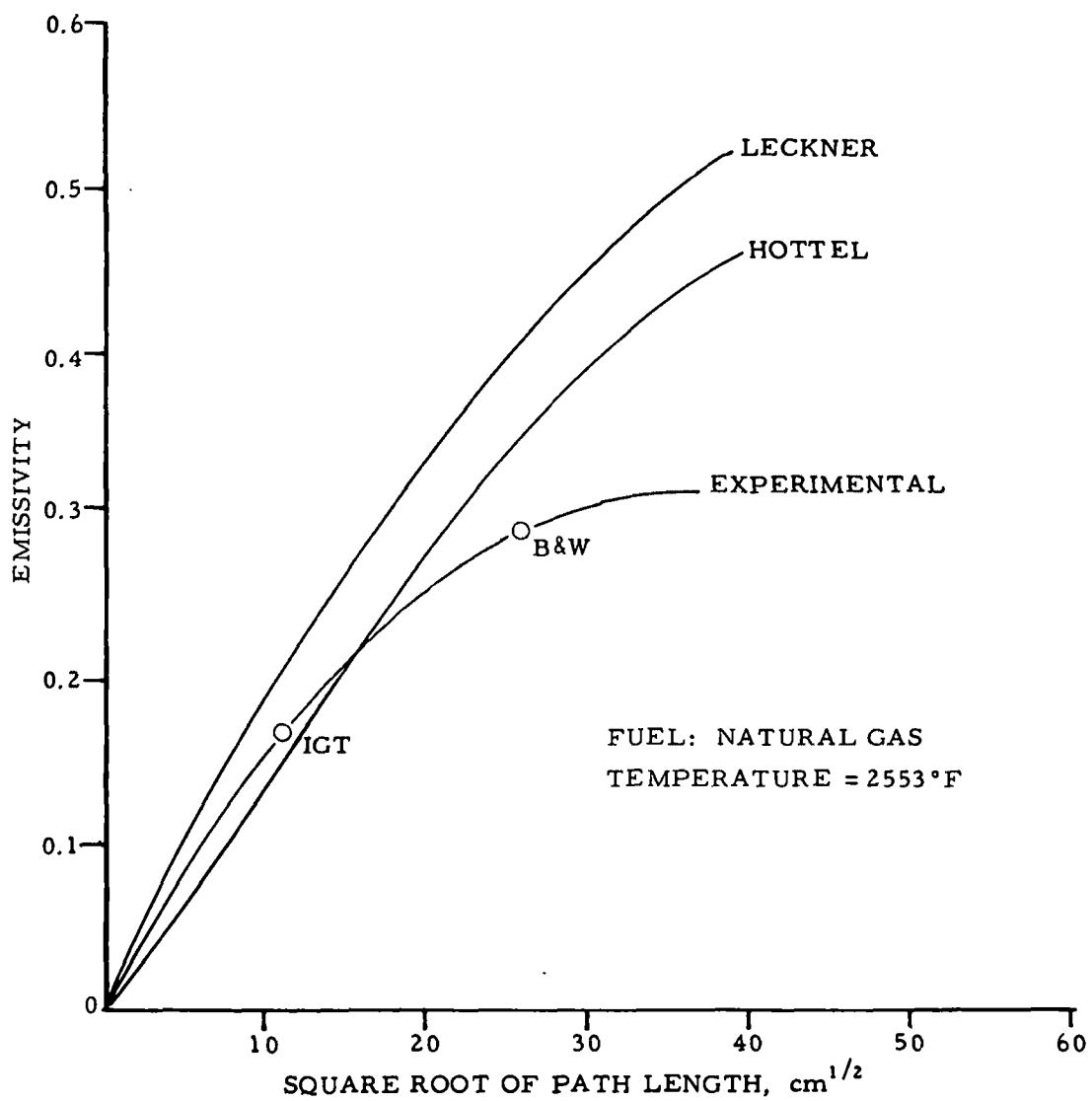


Figure 62. Emissivity versus square root of path length for natural gas

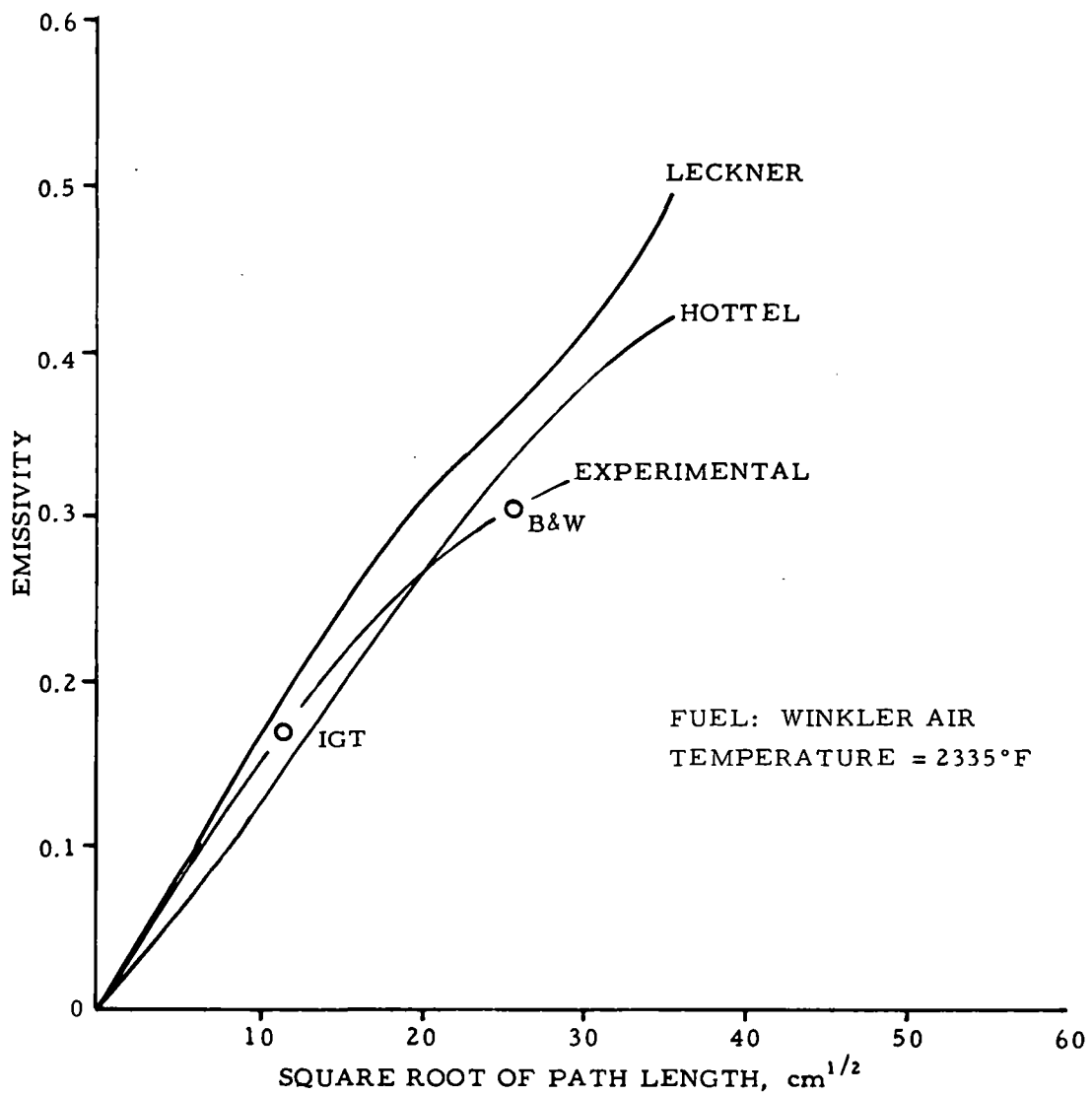


Figure 63. Emissivity versus square root of path length for Winkler air

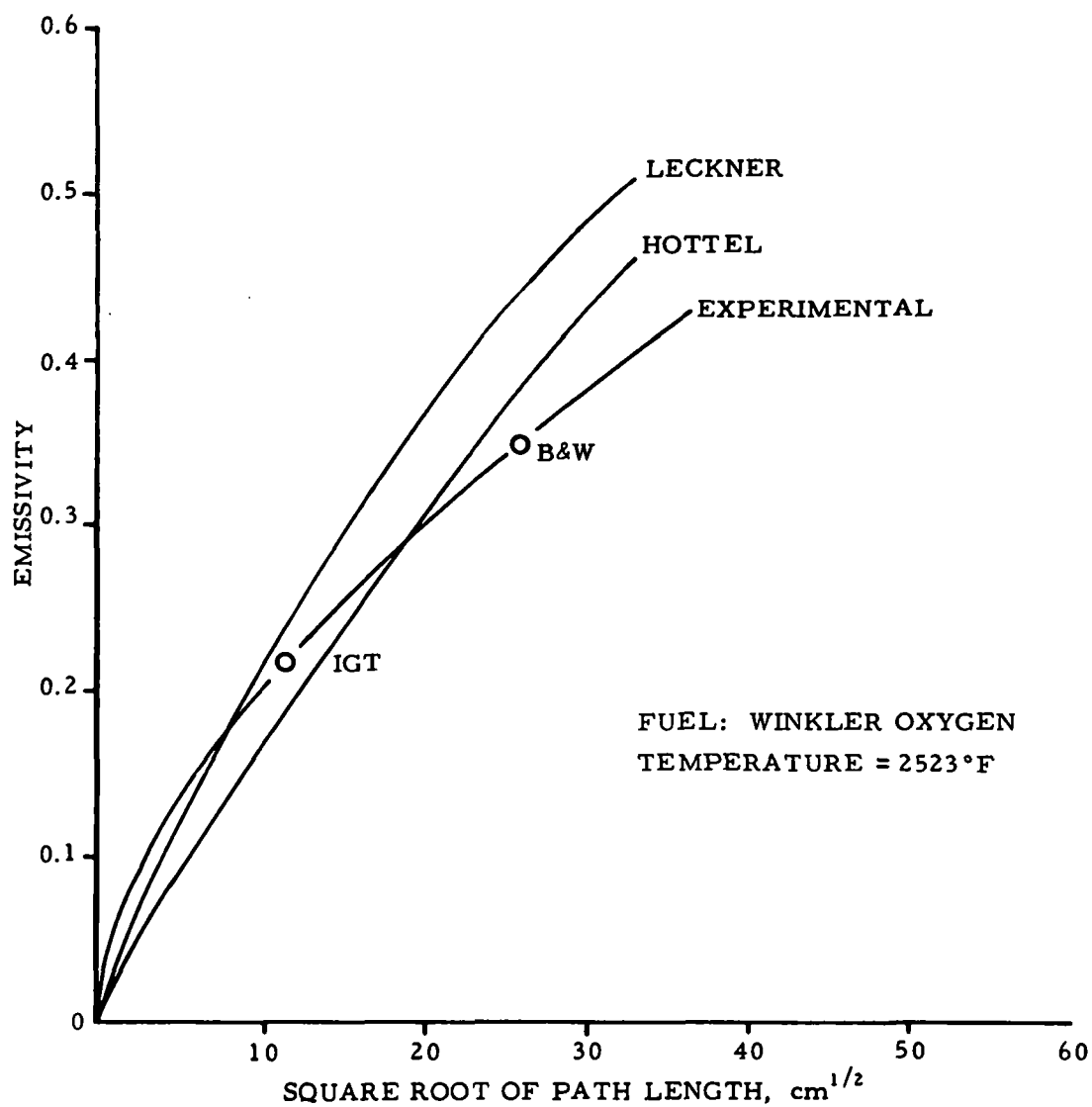


Figure 64. Emissivity versus square root of path length for Winkler oxygen

curves. These curves provide a means of estimating the emissivity of nonluminous combustion products with $\text{CO}_2/\text{H}_2\text{O}$ ratios between 0.5 and 1.8. However, these results are very restrictive because they apply only to the temperatures for which the calculations were made. However, as stated previously, these temperatures, approximately 2500°F, are comparable with those found at the exit of the furnace (radiant section) in a utility boiler.

MATHEMATICAL MODEL OF FURNACE PERFORMANCE

To allow the experimental data to be accurately extrapolated, a mathematical model was sought that would provide estimates of temperature and emissivity in agreement with the experimental results. In addition, the model had to be easy to use (not requiring a high-speed computer) yet provide reliable estimates. The method selected to compare the experimental results with those calculated by B&W is the "speckled-wall" model (SWM) developed by Hottel.⁵ This model makes use of the following assumptions:

1. The combustion products and flame in the combustion chamber are assigned a single mean temperature; this means that the furnace is treated as a well stirred reactor,
2. The gas is gray,
3. The heat sink surface area is gray and can be assigned a single temperature,
4. External losses through the furnace walls are negligible, and internal convection to the refractory furnace walls can be neglected, and
5. The arrangement of heat sink and refractory surfaces is such that any point on the furnace walls has the same view-factor to sink surfaces as any other point. This occurs only when the sink and refractory surfaces are intimately mixed. The walls are speckled.

The items of information needed to use the model applying the iterative method described below are the adiabatic flame temperature, the total enthalpy, the total surface area of the furnace, the ratio of sink surface area to refractory surface area, and the emissivity of the sink.

5. Hottel, H. C., J. Inst. Fuel 34: 220, 1961.

The model has the capability to:

1. Account for convective heat flux to the sink,
2. Allow for heat losses through the furnace walls, and
3. Allow for the difference in flue gas temperature and effective gas radiating temperatures, because an industrial furnace does not have perfect stirring.

The model gives substantially correct predictions of furnace performance for a wide variety of furnaces and can be expected to give a good comparison between fuels in a particular furnace.

A flame-to-sink energy exchange factor, $(\overline{GS})_R$, for radiation heat transfer can be defined by:

$$(\overline{GS})_R = A_T \left[\frac{A_T}{\epsilon_s A_s} + \frac{1}{\epsilon_g} - 1 \right]^{-1} \quad (2)$$

for the case where the heat sink is well distributed. Here A_T is the total furnace area, A_s is the heat sink area, and ϵ_s and ϵ_g are the sink and flame emissivities, respectively. Then a total energy exchange factor can be defined to include radiative and convective heat transfer by:

$$(\overline{GS})_{R,C} = (\overline{GS})_R + h_s A_s / 4\sigma T_{gs}^3 \quad (3)$$

where h_s is the convective heat transfer coefficient, σ is the Stefan-Boltzman constant, and T_{gs} is the mean temperature between the sink and the flame.

A "reduced firing density" can be defined by:

$$D' = H_F / [\sigma (\overline{GS})_{R,C} T_{AF}^4 (1 - T_o / T_{AF})] \quad (4)$$

where H_F is the total enthalpy input to the furnace and T_{AF} is a "pseudo-adiabatic" flame temperature defined as the temperature that the combustion products would attain if the total enthalpy input were used to heat the combustion products from ambient, T_o , at the mean heat capacity between T_o and the flame temperature. Combining the equation above with an energy balance and denoting the fraction of the input enthalpy transferred to the sink by η , we obtain:

$$\eta' D' + \tau^4 = (1 + D' - \eta')^4 \quad (5)$$

where $\eta' = \eta(T_{AF} - T_o)/T_{AF}$

$$\tau = T_s/T_{AF}$$

$$\text{and } \Delta' = \Delta/T_{AF} \quad (6)$$

where Δ accounts for departures of the furnace from the well stirred approximation. The effective radiating temperature of the gas will differ from the mean enthalpy temperature of the gases at the flue of the furnace by an amount Δ which depends on the firing density and furnace geometry.

The first attempt at using the well stirred speckled-wall model ($\Delta^1 = 0$) was to evaluate how it would agree with the IGT experimental data and the values calculated by B&W. The measured and calculated efficiencies are plotted in Figure 65 versus adiabatic radiance. Adiabatic radiance is defined as the total radiant energy that would be emitted from the combustion products of a test fuel at the test fuel's adiabatic temperature. Figure 65 again illustrates how accurately the pilot-scale test furnace was able to model the radiant section of a utility boiler. Thus to get efficiencies calculated with the well stirred speckled-wall model to agree with the IGT test data would demonstrate the model's ability to predict performance of a utility boiler radiant section.

To allow the speckled-wall model to be used from a completely theoretical position with no experimental data needed, an iterative method was devised. A combustion-products gas temperature is estimated at the exit of the radiant section. From this temperature an emissivity is calculated using the Hottel-Sarofim charts. (Any technique for calculating emissivities can be used. The Hottel-Sarofim method was chosen based on the ease of calculation and the universal availability of the gas emissivity charts.) This emissivity is plugged into Equation 2 to evaluate the flame-to-sink energy exchange factor. This permits the total energy exchange factor, Equation 3, and the reduced firing density, Equation 4, to be calculated. A reduced furnace efficiency can then be determined by Equation 5. This reduced efficiency can be turned into a true furnace efficiency using

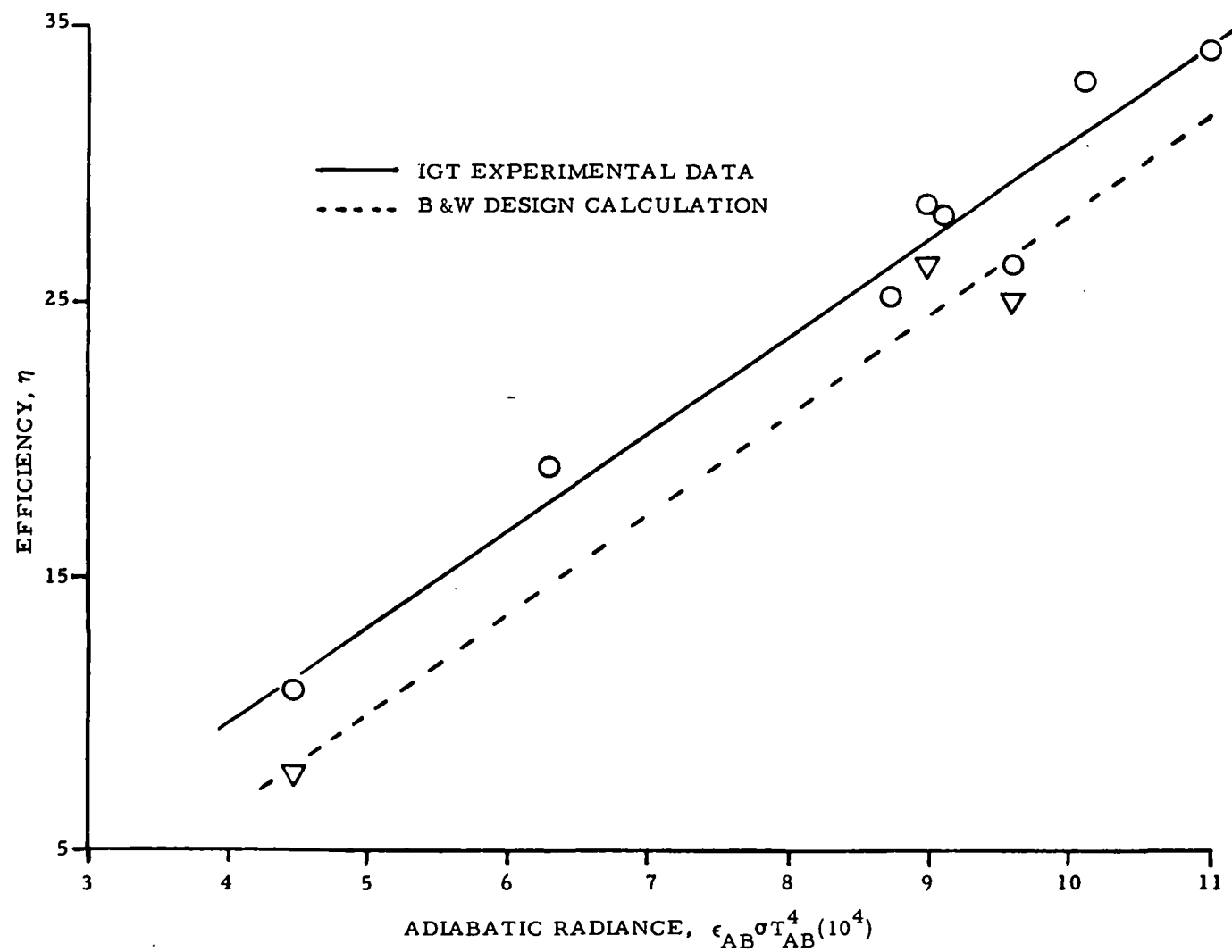


Figure 65. Comparison of IGT experimental and B & W calculated furnace efficiencies

Equation 6. Having the true furnace efficiency, the exit-gas temperature can be determined using the heat content of the combustion-product gases. If the exit-gas temperature derived from the speckled-wall model agrees with the temperature used to calculate the emissivity, then the solution is finalized. If the temperature does not agree, then the estimated temperature is incremented, a new emissivity is calculated and plugged into the speckled-wall model, and the iteration continues. This procedure is followed until a satisfactory agreement between estimated and calculated temperatures is achieved, that is, until the calculated and estimated temperatures are sufficiently close that the emissivity is constant over the temperature range between them.

Figure 66 compares the efficiencies calculated with the well stirred speckled-wall model determined using the iterative method discussed above to the IGT measured efficiencies as a function of adiabatic radiance. These calculated efficiencies are proportional to the adiabatic radiance. The slope of this linear relationship of calculated efficiencies to adiabatic radiance is smaller than the slope of the line relating measured efficiency to adiabatic radiance, indicating that the pilot-scale test furnace deviated from a well stirred reactor. If the slopes of the experimental and theoretical lines were equal, then the deviation from a well stirred reactor would be independent of adiabatic flame temperature and emissivity. However, the slopes of the relationships illustrated in Figure 66 are not equal, meaning that as the adiabatic radiance of the fuel gas becomes larger the deviation of the furnace being modeled will get farther from a well stirred reactor. The speckled-wall model can make allowances for this deviation by assigning Δ an appropriate value. (Refer to Equation 5.) From reviewing the extreme left (Winkler air) and right (Koppers-Totzek preheated to 425°C) data points of the theoretical curve of Figure 66, it can be concluded that no connection need be made for Winkler air ($\Delta = 0$); however, a value for Δ must be determined that will raise the 425°C preheated Koppers-Totzek oxygen fuel gas efficiency from 22.9% to 34.2%. The value of Δ needed to get the calculated and measured efficiencies to agree can be determined by evaluating the exit-gas temperature that would result in a furnace efficiency of 34.2%. Having determined this temperature, 2592°F, it is used to find the combustion-product gas emissivity, 0.359. The speckled-wall model is then solved for Δ , 605°R. A linear relationship can now be developed between Δ

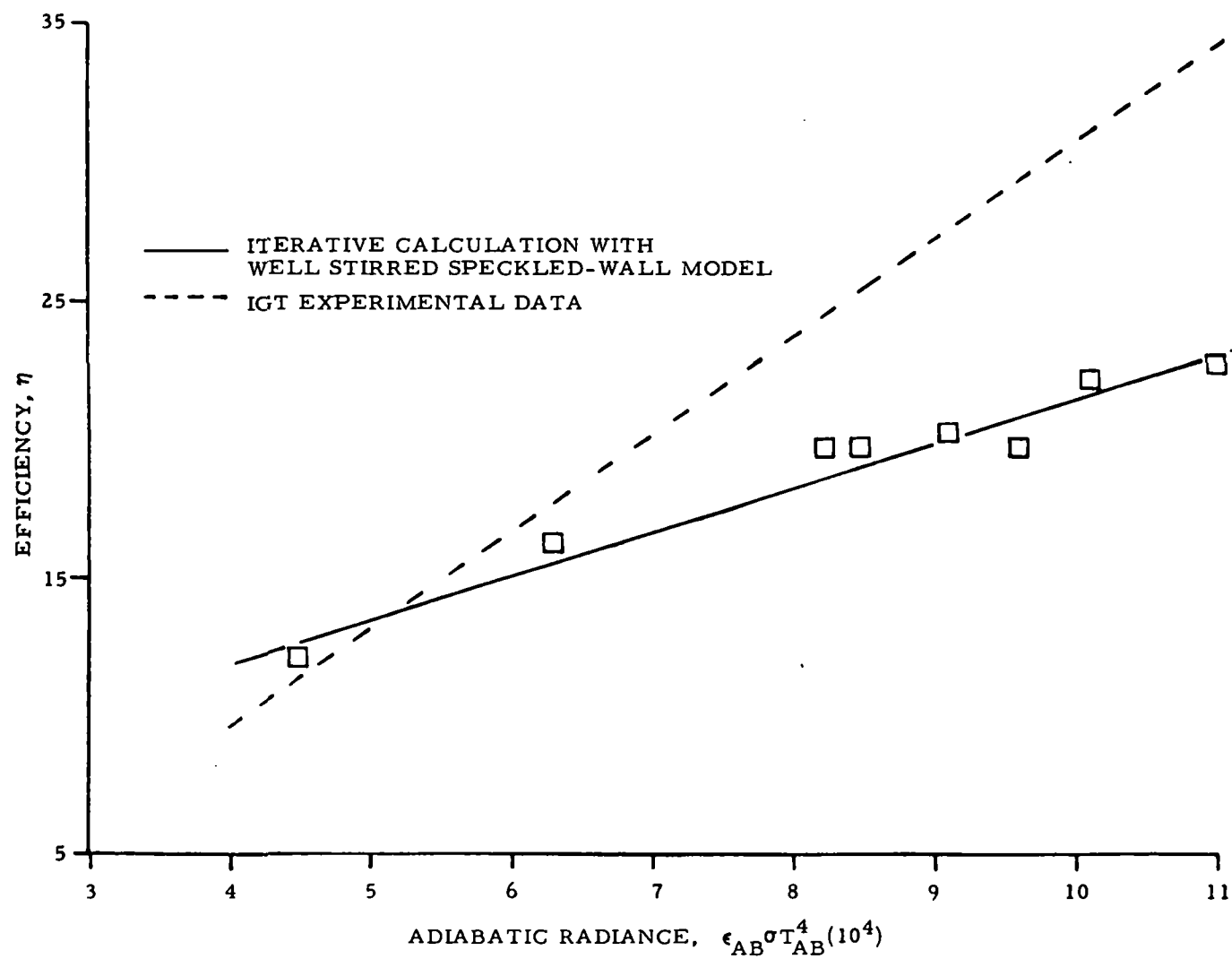


Figure 66. Comparison of experimental and well stirred speckled-wall model calculated efficiencies

and adiabatic radiance. This relationship is shown in Figure 67. This figure illustrates that the departure of the furnace from a well stirred reactor is dependent on the adiabatic radiance of the fuel gas. Using Figure 67, can be determined for each of the fuel gases tested. This allows the efficiency for each fuel gas to be reevaluated using this non-well stirred speckled-wall model. As with the well stirred model, the iterative procedure is followed. The results of this calculation are shown in Figure 68 and are listed in Table 10. The figure illustrates that the iterative speckled-wall calculation can give results in good agreement with experiment when properly modified to allow for deviation of the furnace from perfect stirring. Table 11 lists the iteratively evaluated emissivities as well as those calculated by B&W. To evaluate the effect emissivity has on efficiency, the emissivity calculated by B&W for Winkler oxygen fuel gas was substituted in the non-well stirred speckled-wall model to determine an exit-gas temperature. The non-well stirred speckled-wall model using the B&W computed emissivity yields an exit-gas temperature of 2463°F, or 33°F above that determined using the iterative technique. Thus a 7.9% change in gas emissivity will produce only a 1.4% change in exit-gas temperature.

The non-well stirred speckled-wall model provides a calculation tool that yields good agreement with the more sophisticated techniques employed by B&W. Using the iterative technique, accurate predictions of furnace performance can be made for nonluminous fuels.

IN-THE-FLAME ANALYSIS

Detailed in-the-flame data were collected for natural gas and Winkler oxygen gas. These data are to aid in quantitative modeling of large-scale turbulent diffusion flames and to provide a qualitative guide in understanding and controlling NO emission levels. The measurements included gas species concentrations and temperature profiles. The detailed in-the-flame data are available upon request from the EPA Project Officer (919)549-8411, extension 2236.

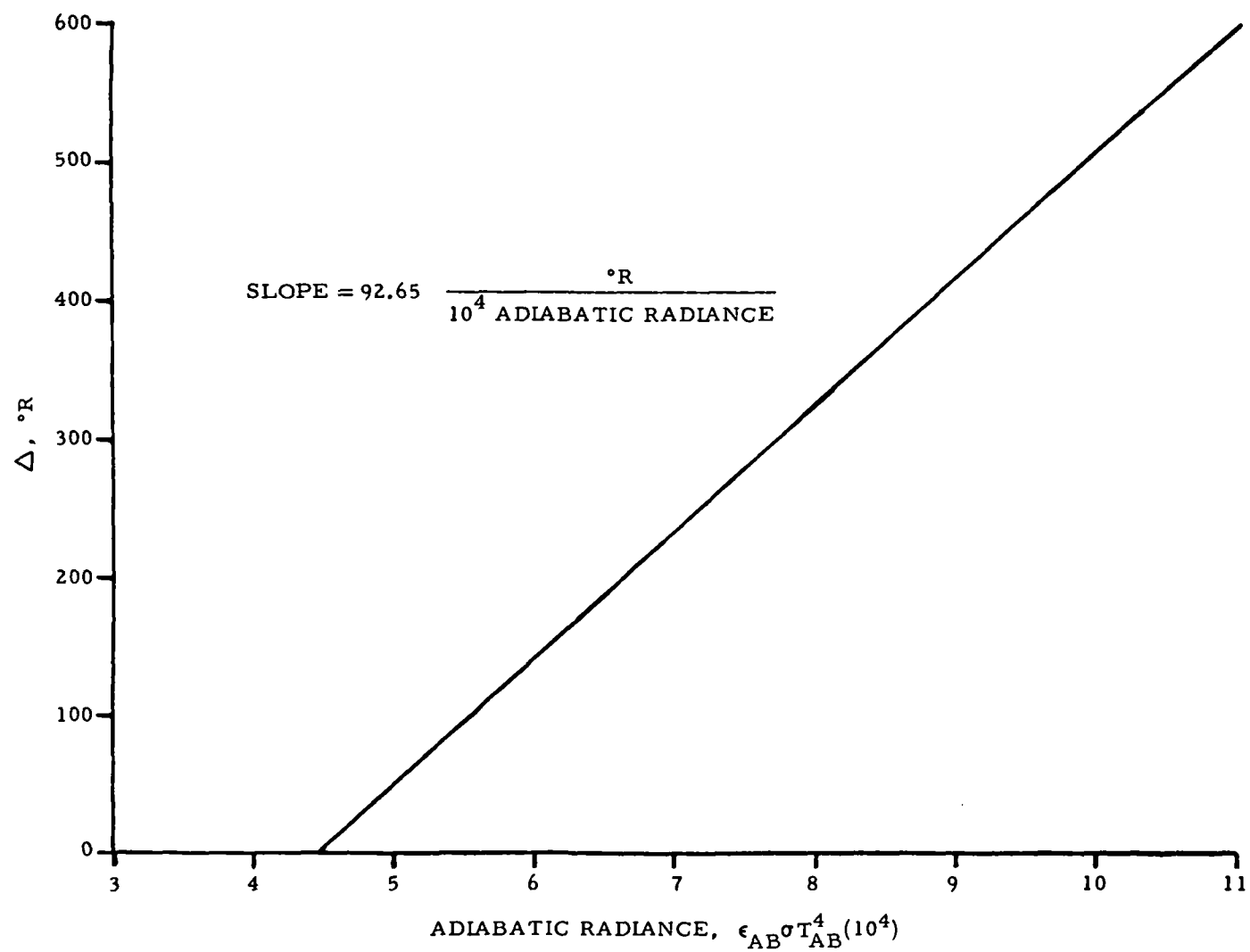


Figure 67. Variation of well stirred approximation with adiabatic radiance

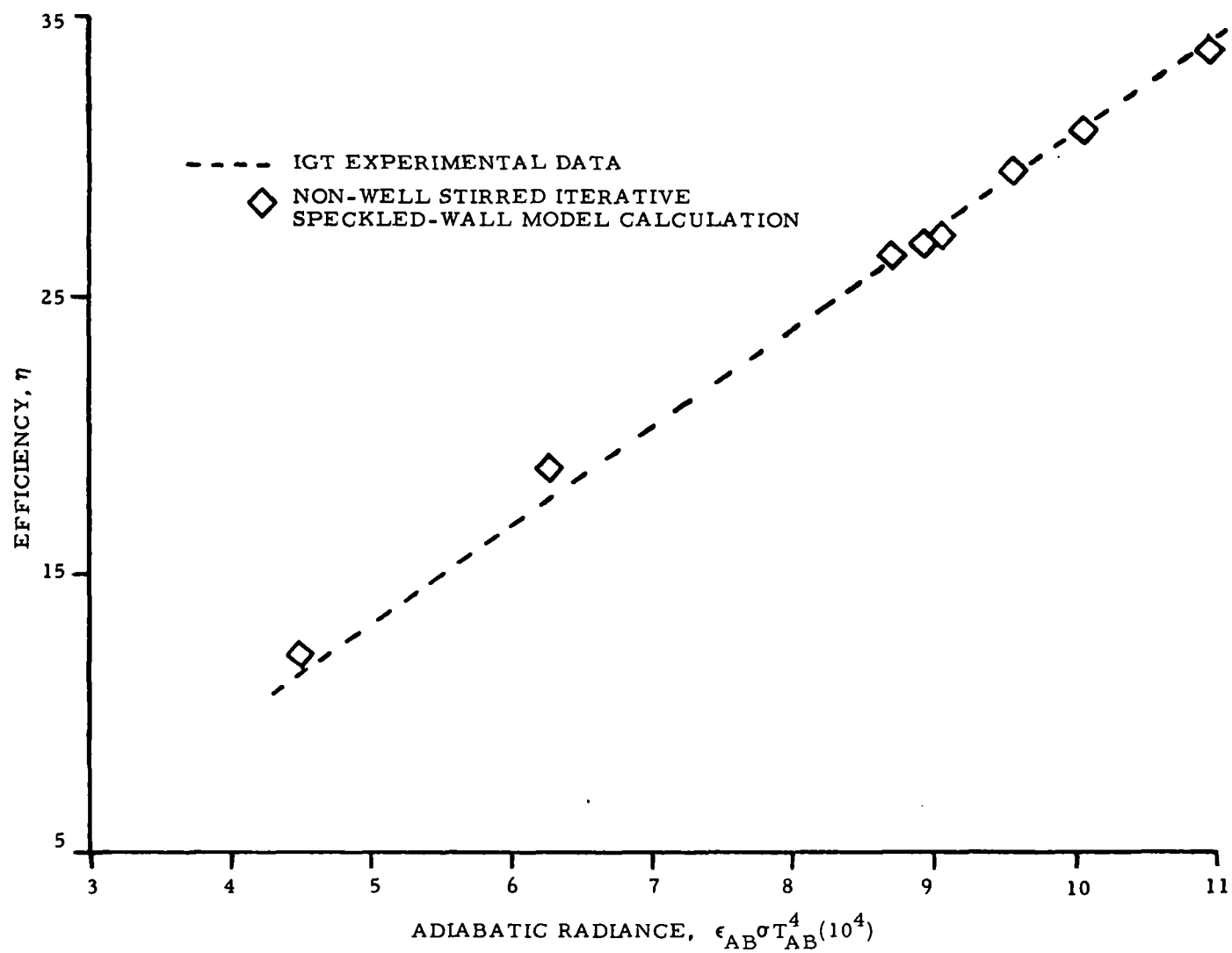


Figure 68. Comparison of experimental and non-well stirred speckled-wall model calculated efficiencies

**Table 10. COMPARISON OF MEASURED AND CALCULATED
FURNACE EFFICIENCIES**

Fuel	$\epsilon_A \sigma T_A^4 (10^4)$	IGT^a	B&W^b	SWM^c	NSWM^d
Natural gas	8.98	28.6	26.3	19.8	27.0
Lurgi oxygen	8.72	25.2	--	19.8	26.6
Winkler oxygen	9.61	26.4	25.1	19.9	29.6
Koppers-Totzek oxygen	10.12	33.1	--	22.4	31.4
Wellman-Galusha air	6.31	19.0	--	16.3	18.9
Winkler air	4.47	10.8	7.8	12.2	12.2
Koppers-Totzek oxygen, 425°C	11.00	34.2	--	22.9	34.2
Koppers-Totzek oxygen, 425°C plus 15% FGR	9.10	28.2	--	20.4	27.4

^a Measured on IGT pilot-scale test furnace.

^b Calculated by B&W for Teche Station Boiler (RB-455) using design calculation technique.

^c Calculated using the well stirred iterative speckled-wall model ($\Delta = 0^\circ\text{R}$).

^d Calculated using the non-well stirred iterative speckled-wall model (Δ evaluated using Figure 67).

Table 11. COMPARISON OF CALCULATED EMISSIVITIES

Fuel	B&W^a	SWM^b	NSWM^c
Natural gas	0.29	0.30	0.33
Winkler oxygen	0.35	0.35	0.38
Winkler air	0.31	0.34	0.34

^a Calculated by B&W for Teche Station Boiler (RB-455) using design calculation technique.

^b Calculated using the well stirred iterative speckled-wall model technique ($\Delta = 0^\circ\text{R}$).

^c Calculated using the non-well stirred iterative speckled-wall model technique (Δ evaluated using Figure 67).

CONVERSION TABLE

ENGLISH TO SI METRIC CONVERSION FACTORS

<u>To Convert From</u>	<u>To</u>	<u>Multiply By</u>
lb/10 ⁶ Btu	ng/J	4.299 E + 02
10 ⁶ Btu/hr	MWt	2.928751 E - 01
Btu	J	1.055 E E + 03
psi	Pa	6.894757 E + 03
SCFH	m ³ /s	7.865790 E - 06
ft/s	m/s	3.048000 E - 01
Inch	m	2.540000 E - 02
Feet	m	3.048000 E - 01
Feet ²	m ²	9.290304 E - 02
Inches of water (pressure)	Pa	2.4884 E + 01
lb/ft ³	kg/m ³	1.601846 E + 01
gpm	m ³ /s	6.309020 E - 05
Inch ²	m ²	6.451600 E - 04
°F	°C	t°C = (t°F - 32)/1.8
°R	°C	t°C = [(5/9)t°R] - 273.15

J = Joule

g = gram

s = second

MWt = megawatts thermal

gpm = gallons (U. S. liquid)/minute

Pa = Pascal

m = metre

k = kilo (10³)

n = nano (10⁻⁹)

M = mega (10⁶)

C = Celsius

F = Fahrenheit

R = Rankine

psi = pounds per square inch

SCFH = standard cubic feet per hour

TECHNICAL REPORT DATA (Please read Instructions on the reverse before completing)			
1. REPORT NO. EPA-600/7-77-094a		2.	
4. TITLE AND SUBTITLE Burner Design Criteria for NOx Control from Low-Btu Gas Combustion; Volume I. Ambient Fuel Temperature		3. RECIPIENT'S ACCESSION NO.	
7. AUTHOR(S) Donald R. Shoffstall		5. REPORT DATE August 1977	
9. PERFORMING ORGANIZATION NAME AND ADDRESS Applied Combustion Research Institute of Gas Technology IIT Center, 3424 South State Street Chicago, Illinois 60616		6. PERFORMING ORGANIZATION CODE	
12. SPONSORING AGENCY NAME AND ADDRESS EPA, Office of Research and Development Industrial Environmental Research Laboratory Research Triangle Park, NC 27711		8. PERFORMING ORGANIZATION REPORT NO.	
15. SUPPLEMENTARY NOTES IERL-RTP project officer for this report is David G. Lachapelle, Mail Drop 65, 919/514-2236.		10. PROGRAM ELEMENT NO. EHE624a	
16. ABSTRACT The report gives results of a research program initiated to characterize problems associated with retrofitting existing utility boilers with low- and medium-Btu gases produced using commercially available coal conversion processes. All experimental results were gathered from a pilot-scale furnace fired with a movable-vane boiler burner at a heat input of 0.66 MW (2.25 million Btu/h). The synthetic gases tested, ranging in heating value from 3.7 to 11.2 MJ/cu m (100 to 300 Btu/SCF), were produced using a natural gas reformer system. Data were collected to permit a comparison between natural gas and the synthetic gases in the areas of flame stability, flame length, flame emissivity, furnace efficiency, and NOx emissions. Flame stability was found to be very sensitive to fuel jet velocity. An injection velocity of 30.5 m/s (100 ft/s) was found to be optimum. Flame length decreased with increasing movable-vane angle (swirl of the combustion air): flames of the synthetic gases tested generally were shorter than those of natural gas. Good agreement was obtained between measured and calculated flame emissivities. Some boiler modifications would be necessary to maintain rating when burning gases of less than 7.5 MJ/cu m (200 Btu/SCF) heating value. NO emissions were ordered by adiabatic flame temperature. The NO emissions data yielded an activation energy of 153 kcal/mole compared to kinetic model predictions of 135 kcal/mole.		11. CONTRACT/GRANT NO. 68-02-1360	
17. KEY WORDS AND DOCUMENT ANALYSIS		13. TYPE OF REPORT AND PERIOD COVERED Final; 9/75-10/76	
a. DESCRIPTORS		14. SPONSORING AGENCY CODE EPA/600/13	
b. IDENTIFIERS/OPEN ENDED TERMS		15. SUPPLEMENTARY NOTES	
c. COSATI Field/Group		16. ABSTRACT	
Air Pollution		The report gives results of a research program initiated to characterize	
Design		problems associated with retrofitting existing utility boilers with low- and medium-Btu	
Nitrogen Oxides		gases produced using commercially available coal conversion processes. All experi-	
Temperature		mental results were gathered from a pilot-scale furnace fired with a movable-vane	
Coal Gasification		boiler burner at a heat input of 0.66 MW (2.25 million Btu/h). The synthetic gases	
Natural Gas		tested, ranging in heating value from 3.7 to 11.2 MJ/cu m (100 to 300 Btu/SCF), were	
Flames		produced using a natural gas reformer system. Data were collected to permit a	
Swirling		comparison between natural gas and the synthetic gases in the areas of flame stability,	
Emissivity		flame length, flame emissivity, furnace efficiency, and NOx emissions. Flame sta-	
Burners		bility was found to be very sensitive to fuel jet velocity. An injection velocity of 30.5	
Unlimited		m/s (100 ft/s) was found to be optimum. Flame length decreased with increasing	
18. DISTRIBUTION STATEMENT		movable-vane angle (swirl of the combustion air): flames of the synthetic gases tested	
19. SECURITY CLASS (This Report)		generally were shorter than those of natural gas. Good agreement was obtained be-	
Unclassified		tween measured and calculated flame emissivities. Some boiler modifications would be	
20. SECURITY CLASS (This page)		necessary to maintain rating when burning gases of less than 7.5 MJ/cu m (200 Btu/	
Unclassified		SCF) heating value. NO emissions were ordered by adiabatic flame temperature. The	
21. NO. OF PAGES		NO emissions data yielded an activation energy of 153 kcal/mole compared to kinetic	
119		model predictions of 135 kcal/mole.	
22. PRICE		17.	